

The Controlled Diffusion Solidification Process:  
Fundamentals and Principles

by

Kimon Symeonidis

A Dissertation

Submitted to the Faculty

of the

WORCESTER POLYTECHNIC INSTITUTE

in partial fulfillment of the requirements for the

Degree of Doctor of Philosophy

In

Mechanical Engineering

April 2009

APPROVED by:

---

Dr. Diran Apelian, Advisor

---

Dr. Makhlouf M. Makhlouf, Committee Member

---

Dr. Richard D. Sisson Jr, Committee Member

---

John L. Jorstad, Committee Member

---

Dr. Nikolaos Gatsonis, Graduate Committee Representative

## Abstract

Aluminum based alloys can be broadly classified into two groups: casting alloys and wrought alloys. Wrought Al-based alloys exhibit superior physical and mechanical properties compared to the conventional shaped casting alloys. The wrought alloys cannot be cast into near net shapes, because they develop hot tears or hot cracks during the solidification process. For this reason these alloys are cast into ingots and are subsequently brought to final shape by mechanical processes like rolling, extrusion, drawing and forging. Invariably these processes significantly increase the cost of the final part up to 50%, and have restrained the application of the wrought alloys in applications where the cost is not a major factor. The CDS (**Controlled Diffusion Solidification**) is a novel process that bypasses the intermediate steps by casting the wrought alloy directly into final shape, free of hot tears, and eliminating additional deformation steps. The CDS process follows a different route from conventional casting methods. In CDS, two liquid metals of predetermined composition and temperature are mixed producing a globular microstructure instead of a dendritic one. The nondendritic microstructure minimizes the hot-tearing tendency and makes the wrought alloys more suitable to casting operations.

The underlying principles and mechanisms of the CDS process have been established through both experimental work and the development of a mathematical model. The operating window of the process has been defined, and guidelines are proposed to enable application of the CDS process to various alloy systems. The reduction of the hot-tearing tendency in Al wrought alloys was experimentally verified.

## Acknowledgments

First of all, I would like to sincerely thank Prof. Diran Apelian, for supervising my work throughout these years. He has not only guided me in the professional field, but also encouraged me and has given me valuable support. Thank you for letting me participate in decisions regarding the direction of my PhD work which enabled me to work in fields that interested me the most.

My deep gratitude goes to Prof. Makhoul M. Makhoul for his guidance and the numerous insightful conversations on a variety of topics. His input has been invaluable to this work and is gratefully acknowledged.

It has been a great opportunity and experience to present my work to the MPI's conferences. The close contact with the consortium members and their direct input brought this work valuable perspective. I treasure all the discussions I have had during these events.

My PhD was supported by WPI's ME department as a Teaching Assistant and at the late stages as a Research Assistant from MPI. I would like to extend my gratitude to all the professors that I have worked with as a TA at WPI, especially Prof. Michael Demetriou and Prof. Nikolaos Gatsonis, for their cooperation and support.

In the first year of my PhD I had the opportunity and pleasure to visit Prof. Sumanth Shankar and his research group at McMaster University in Canada. Thank you for sharing your knowledge on this work.

As anyone at MPI knows, there are a few practical obstacles that can be overcome by Dr. Libo Wang and Carl Raatikainen. Their continuous support and insight is highly appreciated.

I have spent most of my time at WPI back to back with my good friend and colleague Brian Dewhirst. Our office has been the place of many interesting and fruitful discussions. It has been a great pleasure.

I would also like to thank the staff at MPI and especially Carol Garofoli and Maureen Plunkett. Your support greatly facilitated my work in all aspects. Also thank you for our little discussions.

I would also like to thank following persons for sharing all the ups and downs of a PhD student: Pat Hogan, Leigh Duren, Shimin Li, Lance Wu, Eva Ikonomu and Anastasios Gavras.

Last but not least I would like to thank my parents Chrysoleon and Maria and my sister Antonia who supported me throughout the years and who always has had faith in me. This would have not been possible without you.

## Contents

Abstract .....	ii
Acknowledgments .....	iii
List of Figures .....	viii
List of Tables .....	xiii
1. Introduction .....	- 9 -
1.1 The Controlled Diffusion Solidification Process .....	- 9 -
1.2 Impact and Benefits of CDS.....	- 13 -
2. Objectives .....	- 17 -
3. Hypothesis.....	- 18 -
3.1 Mixing .....	- 21 -
3.2 Nucleation.....	- 24 -
3.3 Growth .....	- 25 -
4. Experimental.....	- 26 -
4.1 Materials and Procedures .....	- 26 -
4.2 Mixing of Two Liquid Melts – <i>procedures and measures</i> .....	- 27 -
4.3 Visualization of the $L_1/L_2$ interface: <i>formation of striations</i> .....	- 33 -
4.4 Addition of Synthetic Nuclei: procedures and measures .....	- 38 -
4.5 Globular Stability vs. Cooling Rate .....	- 41 -

4.6	Hot Tearing in CDS castings: <i>procedures and measures</i> .....	- 44 -
5.	Theory .....	- 50 -
5.1	Introduction .....	- 50 -
5.2	Thermodynamic Considerations .....	- 51 -
5.3	Mixing .....	- 56 -
5.4	Thermal and Mass Transport Phenomena .....	- 59 -
5.5	Numerical model: <i>Evolution of solute and temperature fields</i> .....	- 60 -
5.6	Nucleation.....	- 70 -
5.6.1	Classical Nucleation Theory .....	- 70 -
5.6.2	Nucleation Rate in CDS.....	- 73 -
5.7	Interface Stability .....	- 76 -
5.7.1	Mullins Sekerka Stability Criterion .....	- 77 -
5.7.2	Undercooling Considerations .....	- 81 -
5.8	Globular Growth .....	- 86 -
5.8.1	Globular Stability Analysis.....	- 89 -
5.8.2	Discussion.....	- 93 -
6.	Conclusions .....	- 98 -
7.	Suggestions for Future Work .....	- 100 -
8.	References.....	- 101 -

9. Appendices .....	- 106 -
9.1 Appendix I: Published Work .....	- 106 -
9.2 Appendix II: Diffusion Solidification .....	- 122 -
9.3 Appendix III: Numerical Simulation Algorithm .....	- 128 -

## List of Figures

Fig. 1: Hypothetical phase diagram of a binary alloy illustrating (a) conventional solidification and (b) diffusion solidification. In (a) the liquid alloy of composition  $X$  is cast from a temperature  $T_1$ ; partitioning occurs during solidification leading to segregation of the solute. In (b) an amount  $f_s$  of a solid alloy of composition  $C_s$  and at temperature  $T_2$  is mixed with an amount  $f_L$  of a liquid of composition  $C_L$  held at the same temperature  $T_2$  such that  $f_s C_s + f_L C_L = X$ ..... - 9 -

Fig. 2: CDS Investment mold logic where (A) - (F) indicate the sequence of events. In (B) the mold is filled with the shot; in (C) the particle valve is inserted; in (D) the infiltrant is emplaced; (E) the setup is evacuated and heated to process temperature; (F) infiltration takes place [1]..... - 10 -

Fig. 3: The Iron-Iron carbide phase diagram [2]. The precursor alloys are depicted, a solute rich liquid phase which infiltrates isothermally a solute depleted  $\gamma$  phase. - 11 -

Fig. 4: Schematic description of the CDS applied to a liquid-liquid system. Pure Al is mixed with an Al-33wt%Cu eutectic liquid to form a target alloy of composition: Al-4.5wt%Cu..... - 12 -

Fig. 5: Left: Conventional solidification – Dendritic microstructure, Right: CDS liquid-liquid system – Globular microstructure. .... - 12 -

Fig. 6: Schematic representation of Al-Cu phase diagram..... - 18 -

Fig. 7: Schematic description of the CDS. Pure Al is mixed with an Al-33wt%Cu eutectic liquid to form a target alloy of composition: Al-4.5wt%Cu. .... - 19 -

Fig. 8: (a) Pure Al is mixed with the eutectic liquid forming striations. (b) Undercooling in the Pure Al striations forces rapid nucleation while at the same time

solute diffuses from the eutectic liquid in the Pure Al striations. (c) The Al nuclei grow in a solute rich matrix.....	- 20 -
Fig. 9: Generic binary phase diagram depicting different mixing modes. ....	- 21 -
Fig. 10: Phenomena that occur during the mixing of two liquids [3].....	- 23 -
Fig. 11: SiC crucible dimensions.....	- 27 -
Fig. 12: Schematic diagram of the CDS.....	- 27 -
Fig.13: From left to right a) Homogeneous liquid solidifying (dendritic microstructure) b) Reaction mixing, (globular) c) Quenching (severe segregation).....	- 28 -
Fig. 14: Schematic diagram of mixing process. ....	- 29 -
Fig. 15: Thermal Curves 671 – 682. ....	- 31 -
Fig. 16: Representative microstructures obtained with CDS under different Al Superheats.....	- 32 -
Fig. 17: Steel mold dimensions. ....	- 33 -
Fig. 18: Schematic representation of quenching experiment. (a): The two liquids are being held at controlled temperatures in the steel mold. (b): As the gate is lifted the two liquids mix freely. The heavier eutectic will displace the Pure Al. Striations are formed across the interface and reaction mixing occurs. (c): The striations freeze due to governing heat conduction.....	- 35 -
Fig. 19: Developing striations across the interface. (The reflection in the background is the camera lens).....	- 36 -
Fig. 20: Striations and microstructure. ....	- 36 -

Fig. 21: High magnification SEM image of the globular microstructure. ....	- 37 -
Fig. 22: EDX line scan across $\alpha$ -Al grains – Concentration profile.....	- 38 -
Fig. 23: From Left to right: Grain refiner added to: 1) Pure Al 2) Al-33wt%Cu 3) Al-4.5%Cu. ....	- 40 -
Fig. 24: Representative microstructures obtained with different cooling rates. ..	- 43 -
Fig. 25: Ring mold schematics. ....	- 44 -
Fig. 26: 206 – Conventional casting without superheat – separation.....	- 46 -
Fig. 27: 206 – Conventional casting at 670°C – Hot tear. ....	- 46 -
Fig. 28: 206 Cast via CDS - No hot tearing.....	- 47 -
Fig. 29: 206 Conventional casting – Dendritic microstructure (bar: 100 $\mu$ m).....	- 48 -
Fig. 30: 206 Cast via CDS– Predominantly globular microstructure. (bar: 100 $\mu$ m)....	- 48 -
Fig.31: Experimental data for initial liquids and final alloy temperatures. The final alloy temperature is a significant indication of the solidification mechanism. ....	- 52 -
Fig. 32: CDS cooling curve. Al at 670°C mixed with Al-33%Cu at 550°C.....	- 53 -
Fig. 33: S (t) Evolution of Striation thickness S on different strain rates.....	- 61 -
Fig. 34: Initial temperature distribution $T_x$ at $t = 0$ . $S_0$ is the initial thickness of the Al striation. ....	- 63 -
Fig. 35: Initial composition distribution $C_x$ at $t = 0$ . $S_0$ is the initial thickness of the Al striation. ....	- 63 -

Fig. 36: Temperature evolution at the center of the Al striation at  $x = 0$  and at  $x = 0.55$ . The equilibration of temperatures is rapid due to the high heat transfer coefficient. Equilibration is attained at 0.05sec..... - 66 -

Fig. 37: Concentration evolution at the center of the Al striation at  $x = 0$  and at  $x = 0.55$ . The equilibration of concentration is much slower than the temperature equilibration due to the lower diffusion coefficient. Equilibration is attained in 0.5sec. .... - 67 -

Fig. 38: Comparison of the actual temperature at  $x = 0$  and  $x = 0.55$  and the respective liquidus temperature. The aluminum is undercooled right when the simulation begins. After a short time the solute is diffusing from  $x = 0.55$  towards the center of the aluminum striation. As a result the liquidus temperature is increasing and the melt finds itself in an undercooled state. .... - 68 -

Fig. 39: Nucleation rate and fraction solid at different degrees of undercooling. - 74 -

Fig. 40: Critical nuclei size of Al vs degree of undercooling. .... - 74 -

Fig. 41: Critical radius for globular stability of an aluminum crystal related to the degree of undercooling based on the M-S stability criterion. .... - 80 -

Fig. 42: Comparison of diffusion boundary layer for growth of a particle under traditional partitioning solidification and under CDS. .... - 83 -

Fig. 43: Liquid composition vs. radial distance. When the cooling rate increases at  $r = 20\mu\text{m}$  the solute starts to build up at the interface. But when  $r = 40\mu\text{m}$  the solute concentration at  $r = 50\mu\text{m}$  starts increasing and this marks the onset of solute field overlap. Martinez [10]. .... - 87 -

Fig. 44: Typical Al-4.5wt%Cu microstructure cast via CDS. .... - 87 -

Fig. 45: Liquid composition and grain density vs initial grain size. .... - 89 -

Fig. 46: The graph shows the stability region for an Al-4.5wt%Cu alloy under cast via CDS under different cooling rates. The left of the curve denotes stability and the right indicates instability of the front. From the above graph the combinations of fraction solid and maximum cooling rate can be extracted that ensure stable globular growth..... - 91 -

Fig. 47: The graph compares the stability region of the Al-4.5wt%Cu alloy for different fraction solid and cooling rate combinations. The higher the solid fraction and the grain density, the higher the maximum cooling rate is. .... - 91 -

Fig. 48: 2014 - Regularly cast - Hairline Hot Tear..... - 96 -

Fig. 49: 2014 - Regularly cast - Moderate crack. .... - 97 -

Fig. 50: 2014 - Cast via CDS - No crack..... - 97 -

Fig. 51: Paths of conventional casting, Rheocasting and of CDS. In Rheocasting alloy X is cooled to T2 and isothermally agitated. The solid - liquid mixture consists of liquid phase of composition CL and solid phase of composition CS. In CDS fs amount of solid particles of composition CS\* and at temperature T1 are infiltrated by fL amount of liquid of composition CL\* such that  $f_sCS^* + f_LCL^* = X$ . .... - 124 -

## List of Tables

Table I: Properties of some wrought and casting alloys. ....	- 14 -
Table II: Processing parameters for the three mixing paths. ....	- 28 -
Table III: Mixing parameters. ....	- 29 -
Table IV: Quenching experiment – Initial liquids parameters. ....	- 33 -
Table V: Processing parameters. ....	- 39 -
Table VI: Cooling rates and data from thermal curves.....	- 41 -
Table VII: Composition of 206. ....	- 44 -
Table VIII: Initial compositions of liquids melts mixed via CDS.....	- 47 -
Table IX: Steps of the CDS mechanism and processing parameters calculated at each step.....	- 50 -
Table X: Experimental parameters.....	- 53 -
Table XI: Material constants [10]. ....	- 65 -
Table XII: Thermochemical and physical properties of solid and liquid aluminum at <b>T<sub>m</sub></b> [10]. ....	- 73 -
Table XIII: Thermochemical and physical properties of Al-4.5%Cu alloy.....	- 90 -
Table XIV: 2014 Chemical composition. ....	- 95 -
Table XV: Chemical Analysis, Weight Fraction, and Temperature of the Initial Alloys Used in Casting 2014 Alloy <i>via</i> CDS. ....	- 96 -

# 1. Introduction

## 1.1 The Controlled Diffusion Solidification Process

### The Controlled Diffusion Solidification concept

The Controlled Diffusion Solidification process, which circumvents the problem of hot-tearing is based on the concept of Diffusion Solidification, which was first introduced by Langford and Apelian in 1980 [1].

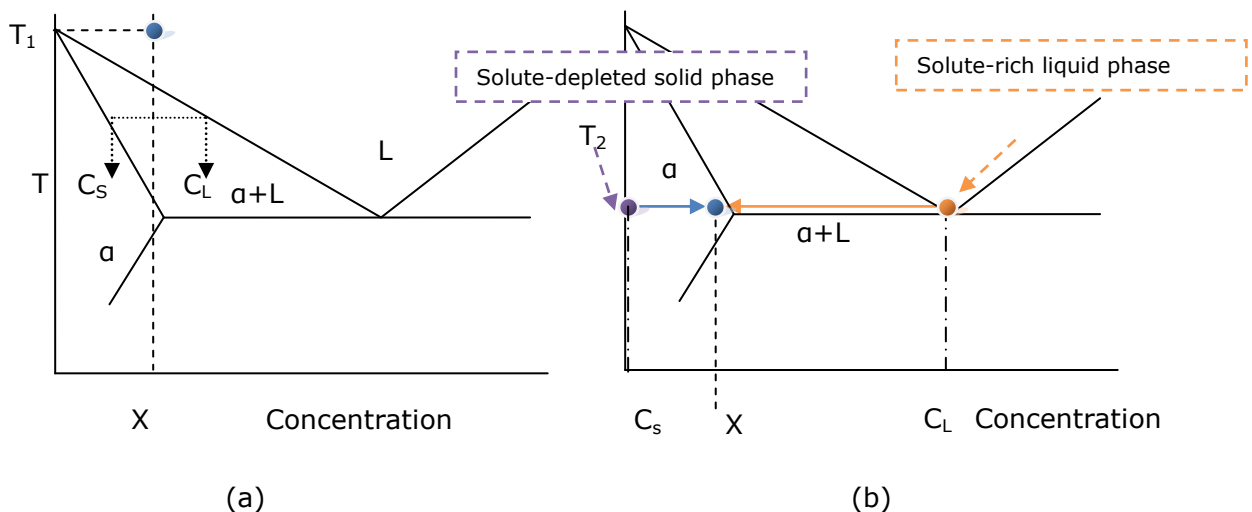


**Fig. 1: Hypothetical phase diagram of a binary alloy illustrating (a) conventional solidification and (b) diffusion solidification. In (a) the liquid alloy of composition X is cast from a temperature  $T_1$ ; partitioning occurs during solidification leading to segregation of the solute. In (b) an amount  $f_s$  of a solid alloy of composition  $C_s$  and at temperature  $T_2$  is mixed with an amount  $f_l$  of a liquid of composition  $C_l$  held at the same temperature  $T_2$  such that  $f_s C_s + f_l C_l = X$ .**

During conventional solidification, (Fig. 1 a), as the alloy solidifies and its temperature drops, its composition changes down the iso-concentration line. Entering the semisolid region ( $\alpha+L$ ), partitioning occurs and two phases form: a solute-depleted  $\alpha$  phase and a solute-rich liquid phase. In this case, solidification time depends on the rate of heat extraction from the liquid phase.

In the CDS process (Fig. 1 b), two phases are also present: a solute-rich liquid phase and a solute-depleted solid phase. However both of these phases are held at the same temperature on the same isothermal line of the phase diagram. After the two precursor alloys mix with one another, the solute diffuses down the solute concentration gradient from the liquid to the solid phase. Solidification proceeds as the liquid loses solute. In this case solidification depends on the rate of diffusion of the solute atoms from the liquid phase to the solid phase, thus making the solidification time independent of the casting's size.

### Diffusion Solidification applied to a solid-liquid system

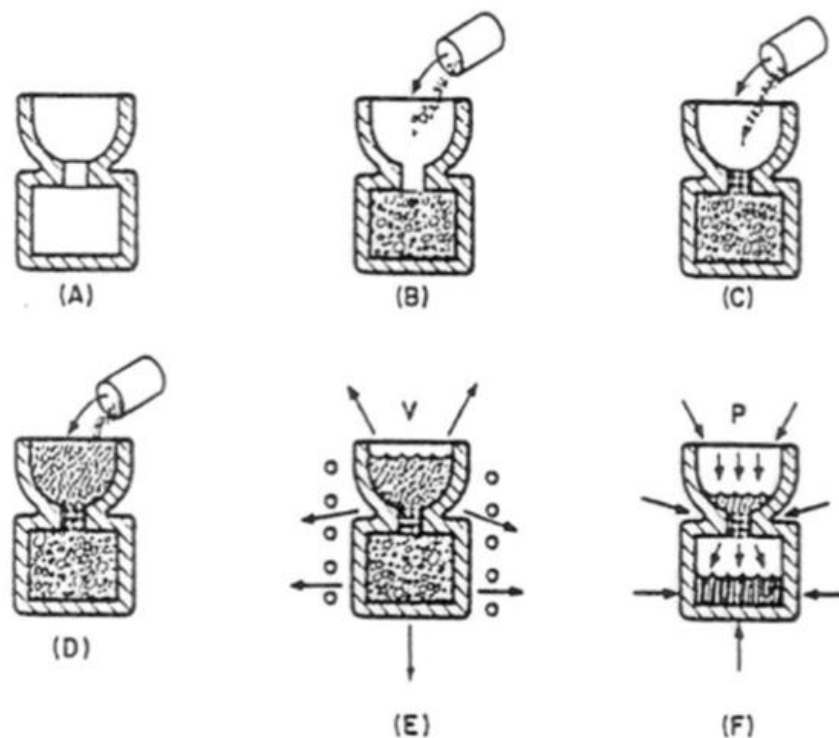


**Fig. 2: CDS Investment mold logic where (A) - (F) indicate the sequence of events. In (B) the mold is filled with the shot; in (C) the particle valve is inserted; in (D) the infiltrant is emplaced; (E) the setup is evacuated and heated to process temperature; (F) infiltration takes place [1].**

The first application of CDS was in the development of a rapid-cycle casting process for steel [1]. In this process, liquid iron with relatively high carbon content is brought into contact with solid iron of relatively low carbon content and held isothermally so that the liquid solidifies by rejecting carbon to the surrounding solid. In practice, the mold is first filled with uniform-sized low carbon steel shot, then heated and subsequently infiltrated with liquid cast iron (2 to 4% C) under moderate pressure as shown in Fig. 2.

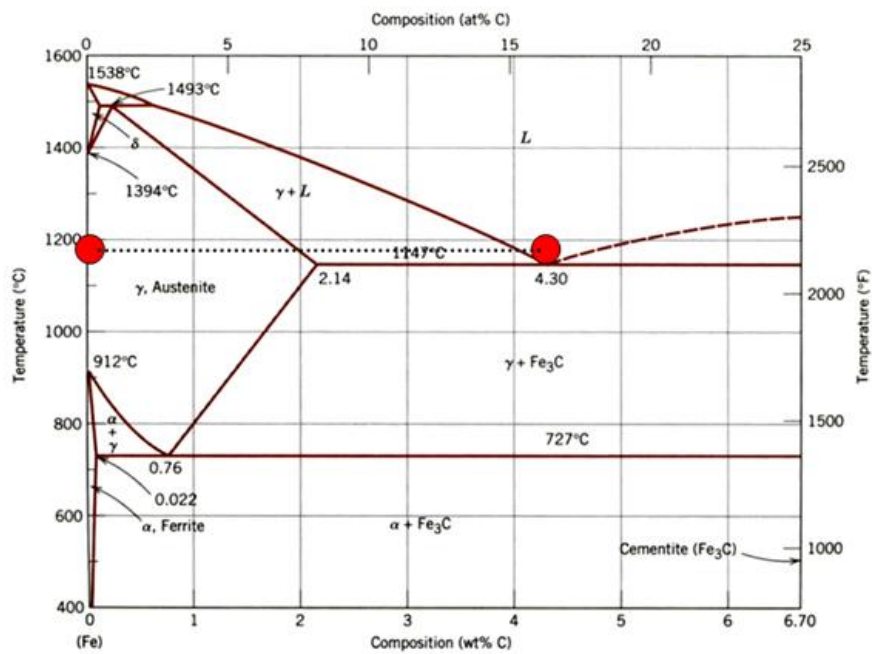


**Fig. 3: The Iron-Iron carbide phase diagram [2]. The precursor alloys are depicted, a solute rich liquid phase which infiltrates isothermally a solute depleted  $\gamma$  phase.**

Fig. 3 shows the position of the precursor liquid and solid alloys on the iron-iron carbide binary phase diagram. More details on the solid-liquid system are given in the Appendix II.

## The Controlled Diffusion Solidification applied to a liquid - liquid system

Recently Saha et al. [3,4] investigated the application of the CDS principles to a liquid-liquid system. They mixed two liquid melts with predetermined temperatures, volumetrics, and composition.

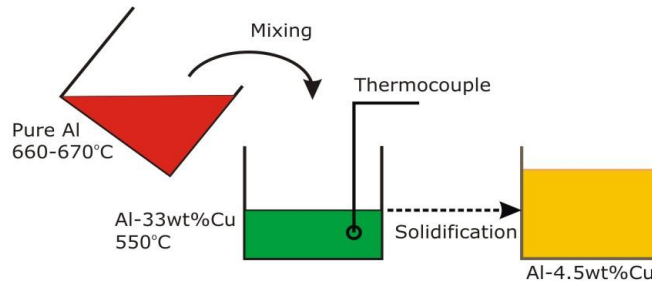


**Fig. 4: Schematic description of the CDS applied to a liquid-liquid system. Pure Al is mixed with an Al-33wt%Cu eutectic liquid to form a target alloy of composition: Al-4.5wt%Cu.**

Fig. 4 shows a schematic drawing of CDS applied to the Al-Cu system. The lower-temperature eutectic liquid is held near its liquidus temperature. Note that both pure Al and the eutectic solidify isothermally. Their melting point will be referred to in this Thesis as their liquidus.

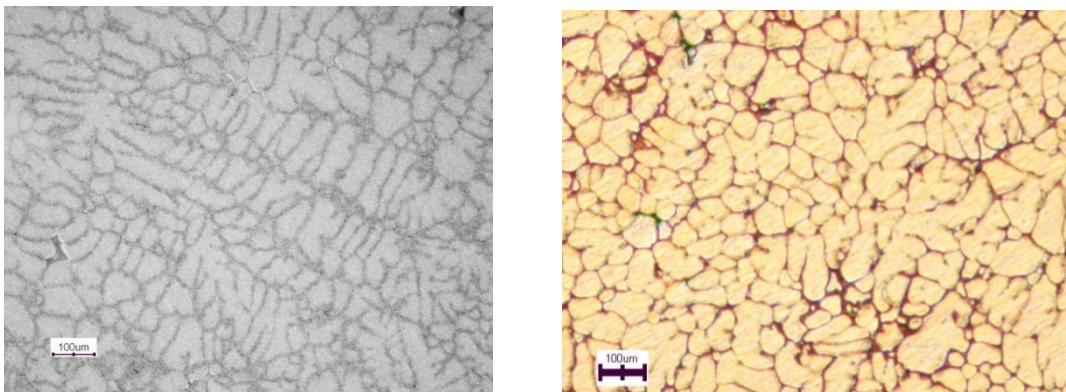


**Fig. 5: Left: Conventional solidification – Dendritic microstructure, Right: CDS liquid-liquid system – Globular microstructure.**

The higher- temperature Pure Aluminum is also held near its liquidus temperature and then it is introduced into the eutectic liquid. The goal is to produce an alloy of composition Al-4.5%Cu. The mixture is left to solidify without any mechanical mixing or forced cooling. The final microstructure of the resultant alloy is globular. Normally with conventional solidification, the alloy would have solidified by forming dendrites. However the mechanism of solidification in CDS is such that the formation of dendritic protrusions during the growth of the grains is restricted. Representative microstructures of Al-4.5wt% Cu alloy cast conventionally and via CDS are presented in Fig. 5.

## 1.2 Impact and Benefits of CDS

Aluminum-based alloys can be broadly classified into two groups: casting and wrought alloys. Wrought aluminum-based alloys have superior physical and mechanical properties compared to conventional casting alloys. These wrought alloys typically cannot be cast into near net shapes because they develop hot tears or hot cracks during solidification. Therefore, these alloys are cast into ingots that are subsequently made into shapes by inducing plastic deformation through rolling, extruding, forging and drawing. These working processes introduce more shape restrictions than casting. Invariably these processes can add up to approximately 50% to the cost of the manufactured part. This is significant when one considers the size of the market. Consequently, it would be economically advantageous to cast wrought alloys directly into near net-shape components.

The biggest problem in casting wrought alloys is their tendency to form hot tears during solidification. It is generally accepted that hot tears originate due to the inadequate permeability of the dendritic network for the flow of the interdendritic liquid to occur, as well as the lack of strength of the dendritic network during the

early stages of solidification [5-7]. Thus, alloys with long solidification ranges are more prone to hot tearing than others.

Currently structural components requiring the mechanical properties of wrought alloys are fabricated by combining forgings, extrusions, sheets and plates to create built up assemblies. This results in a substantial part count requiring numerous fasteners and joining techniques to create the final assembly. It also requires significant capital investment in the equipment and fixtures necessary to undertake these multiple processes.

		<b>Tensile strength (Mpa)</b>	<b>Yield Strength (Mpa)</b>	<b>Elongation %</b>
<b>Wrought alloys</b>	2XXX	448	379	7
	7XXX	537	469	8
<b>Cast alloys</b>	A356	262	193	4
	A357	345	276	5

**Table I: Properties of some wrought and casting alloys.**

The current casting alloy families, many of which were developed in the early 1950's, have been pushed to their limits, thus limiting new applications and/or cost reductions in current applications. Current cast structures tend to be inconsistent because of their propensity for microshrinkage and porosity. To compensate for this propensity, current casting alloys are conservatively specified. The one alloy family that approaches wrought Al-based alloy properties is the 2XX; however alloys in these series are plagued with the problems of hot tearing and thus see limited use. The published properties achievable for the 2XXX and 7XXX wrought alloys as compared to A356 and A357 cast alloys are shown in Table I.

As is evident from Table I, the wrought alloys are approximately 50% to 75% higher in tensile and yield strength and significantly higher in ductility than the casting alloys. However wrought alloy compositions will not provide typical wrought properties. The wrought properties are developed by working, microstructure modification and heat treatment. The unique microstructure of the CDS will reduce the hot-tearing tendency of wrought composition alloys and will potentially affect the properties. The latter needs to be established experimentally.

The primary users of premium aluminum castings are the automotive and military and commercial aerospace industries. Thus, the inability to use the current wrought alloys in castings and the necessity of using more costly and less reliable, less consistent processes, severely constrains the basic industries that still drive the economy. Motor vehicles manufacture and production of parts are the second largest revenue-producing industry in the world, surpassed only by petroleum and coal products. The car and light truck industries use 33% of all US-produced castings. Military and commercial aircraft use another 30%, with a significant portion of the remainder used in weapons and spacecraft. Furthermore, the use of premium aluminum castings in both the automotive and aerospace industries continues to grow as designers and OEMs pursue lighter weight finished products. In addition, the aircraft industry finds that it can substantially reduce component costs by converting machined components and build-up assemblies to castings when casting technology is feasible.

However, the quality, consistency, strength and toughness of cast Al parts have always been inferior to those of wrought Al fabricated products. Consequently, castings have not been used in many airframe primary structure applications. One reason for this is that casting aluminum alloys generally exhibit lower design allowable than wrought Al alloys because of their wider variability in properties

compared with wrought products. The need for aluminum casting alloys with greater strength and toughness has led to a desire to cast wrought alloys. However casting wrought alloys into near net-shape products is not done because these alloys develop hot tears during solidification. Hot tearing is recognized as one of the most common and serious defects encountered during the casting of wrought alloys. This phenomenon is also referred to as solidification cracking, hot shortness and shrinkage brittleness, which has been the subject of several studies [5,7-9]. In general, hot tearing is defined, as the formation of a macroscopic separation in a casting as a result of distortion due to differential contraction of an ingot or shaped casting during solidification [10]. The hot tear nucleates and propagates interdendritically within the solidifying material. This phenomenon of hot-tearing has prevented the use of higher strength and tougher wrought Aluminum alloys in near net shape castings.

The CDS process addresses the issues of quality consistency in castings and allows the use of higher strength, tougher and more ductile alloys. Some of these alloys are wrought Al-based alloys that are typically used in aircraft construction and could make their way into other areas of the transportation industry.

## 2. Objectives

CDS is a promising process that can enable near net shape casting of wrought Al alloy compositions. With today's casting practices, the metallurgist is limited to the use of specific alloys due to constraints introduced by the shape of the part. Intricate shapes give rise to casting issues such as hot tearing, which has its roots in dendritic solidification and alloy composition. The CDS process may alleviate composition limitations by improving the castability of alloys.

However, in order to take full advantage of the CDS process, it is necessary to understand its fundamental mechanism and principles. Therefore the goal of this work is to develop the mechanisms underlying CDS, and to establish the range of flexibility of the process with respect to possible alloy compositions and processing parameters.

Specifically the objectives are to:

- Identify volumetric and temperature constraints for the two starting liquids.
- Formulate a theory of the nucleation and growth events that occur during CDS
  - Construct a mathematical model that predicts the degree of undercooling for a binary alloy system as a function of mixing conditions
  - Apply the globular stability model to predict instability of the interface at the latter stages of CDS
- Establish the hot tearing tendency of alloys when cast via CDS.

### 3. Hypothesis

A hypothesis for the mechanism underlying controlled diffusion solidification is presented in this Chapter.

Composing the hypothesis begins by breaking the CDS process into steps. This makes it easier to identify the governing factors, the processing parameters, and the boundary conditions of each step.

The general idea of CDS in a liquid-liquid system is simple in concept. It can be described as: The mixing of two melts of predetermined composition and temperature to produce a solid alloy with globular microstructure. Many questions are immediately raised from the above description. These include: What are the two initial liquids? What are the limits to their compositions? How are their temperatures selected? How do they mix? What is the mechanism responsible for formation of the globular microstructure? The hypothesis is formulated around the answers to these questions.

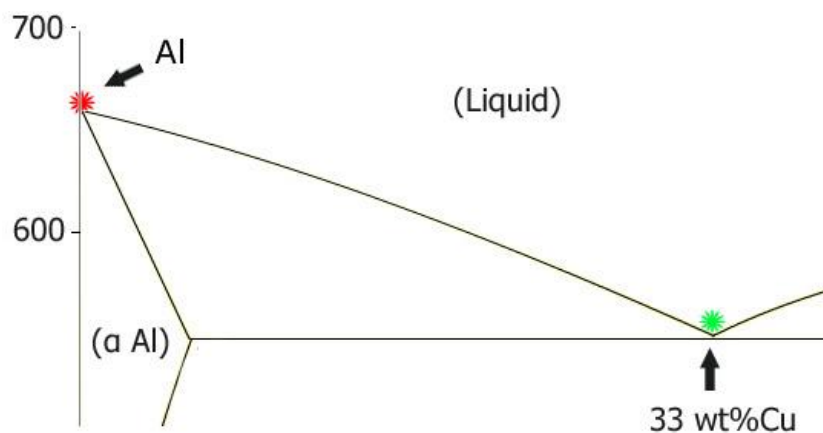


**Fig. 6: Schematic representation of Al-Cu phase diagram.**

In order to answer these questions, consider a simple binary phase diagram like the one shown in Fig. 6. Since the Al-Cu system was studied experimentally, it is used as a reference in the hypothesis.<sup>1</sup>

There are two variables concerning the selection of the two liquids; temperature and composition. For demonstration a simple case is selected: Pure Al liquid and the Al-Cu eutectic liquid that has a composition of Al-33%Cu. The liquidus temperatures are: Pure Al = 660°C, Al-Cu Eutectic = 545°C.

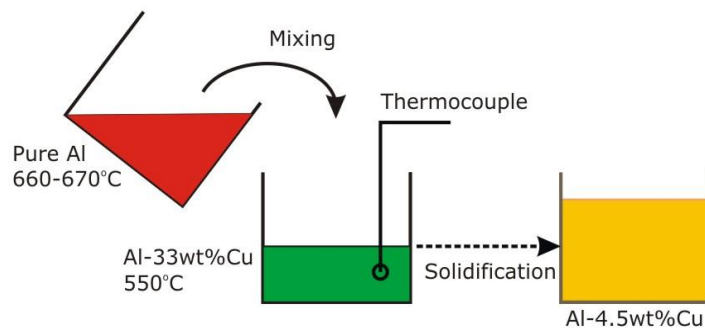


**Fig. 7: Schematic description of the CDS. Pure Al is mixed with an Al-33wt%Cu eutectic liquid to form a target alloy of composition: Al-4.5wt%Cu.**

The mixing procedure is the following: The eutectic liquid is held near its liquidus temperature. The Pure Al is then poured into the crucible that holds the eutectic liquid and the final mixture solidifies inside the crucible holding the eutectic as shown schematically in Fig. 7.

---

<sup>1</sup> Note that the same principles apply to other phase diagrams with certain considerations and guidelines which will be identified in Chapter 5.

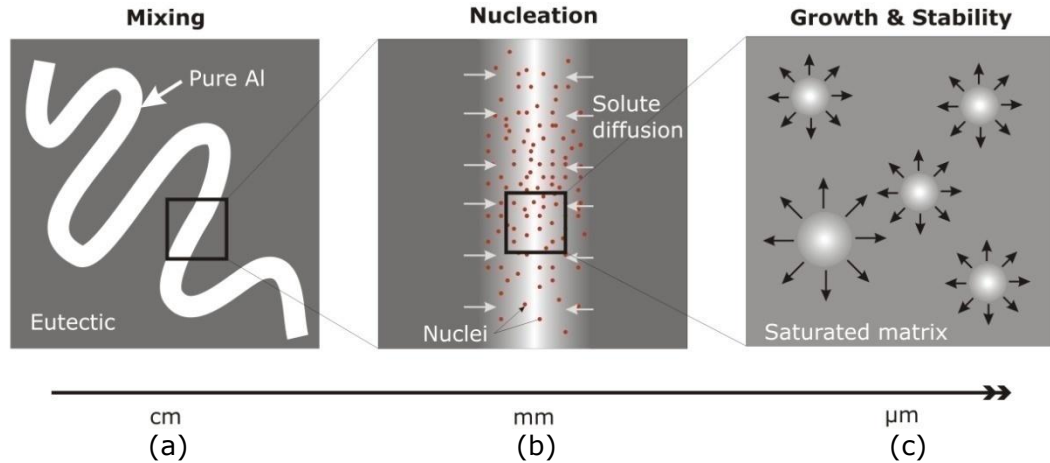


**Fig. 8: (a) Pure Al is mixed with the eutectic liquid forming striations. (b) Undercooling in the Pure Al striations forces rapid nucleation while at the same time solute diffuses from the eutectic liquid in the Pure Al striations. (c) The Al nuclei grow in a solute rich matrix.**

For a better insight into what happens during CDS, we break down the process into 3 steps. These are:

1. Mixing
2. Nucleation
3. Growth

Fig. 8 is a schematic representation of these steps.

The first step concerns fluid flow when the two liquids mix. The mixing procedure is critical because incomplete mixing can lead to segregation issues. The initial melt temperatures are also important as they determine the process window.

The study of the mixing mechanism provides information as to where nucleation of the solid occurs inside the mixture. Due to the nature of the mixing process, the liquid Al becomes highly undercooled, which results in rapid nucleation of solid Al particles. Rapid nucleation creates a high nuclei density of solid Al nuclei, which favors globular stability.

While nucleation of the solid Al particles is occurring Cu diffuses in the Al liquid. As a result the environment where the nuclei grow during CDS is different compared to that during conventional solidification. In CDS, the nucleated particles grow in a solute rich matrix. It is known that when a metal front grows into a liquid that has a high concentration of solute the growth is slow and a planar solid-liquid front is favored. However, if the cooling rate is relatively high, the front can become unstable and break down into a cellular or dendritic one.

### 3.1 Mixing

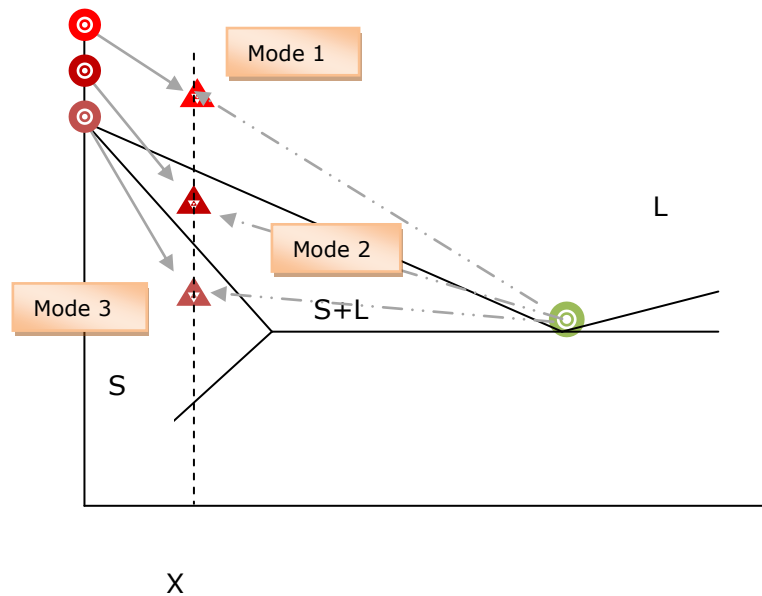


**Fig. 9: Generic binary phase diagram depicting different mixing modes.**

Both liquids have thermal energies. When they mix, the resultant liquid has the sum of these energies plus a small quantity that is called the heat of mixing. Consider the binary phase diagram shown in Fig. 9. Two liquids are selected: a pure substance and a eutectic liquid. X is the target composition.

When these two liquids are brought together, one of the following three mixing modes is possible:

### 1. **Ideal mixing**

This mode of mixing occurs when the superheat of the pure substance is high enough that the resultant mixture finds itself in the liquid region of the phase diagram (Fig. 9). This situation is the same as alloying in the liquid state. The two liquids combine to form a homogeneous liquid of composition X that solidifies with the conventional solidification mechanism.

### 2. **Reaction mixing**

In this mode of mixing, partial solidification of the pure liquid occurs as it comes into contact with the lower temperature eutectic liquid. In the CDS process, the initial temperatures and compositions of the starting liquids are such that the resultant mixture is in the two-phase region of the phase diagram.(Fig. 8)

### 3. **Quenching**

The third mode of mixing occurs when the superheat of the pure liquid is too low and/or the target composition is high in solute. This means that the weight ratio of the pure substance to the eutectic is low. If this is the case, then heat transfer will be the governing mechanism and the pure liquid becomes quenched before it is allowed to mix with the eutectic liquid. This extreme path will lead to considerable segregation. (Fig. 8)

The operative mixing mode in CDS is Reaction-Mixing and its boundary conditions dictate the range of castable alloys via CDS.

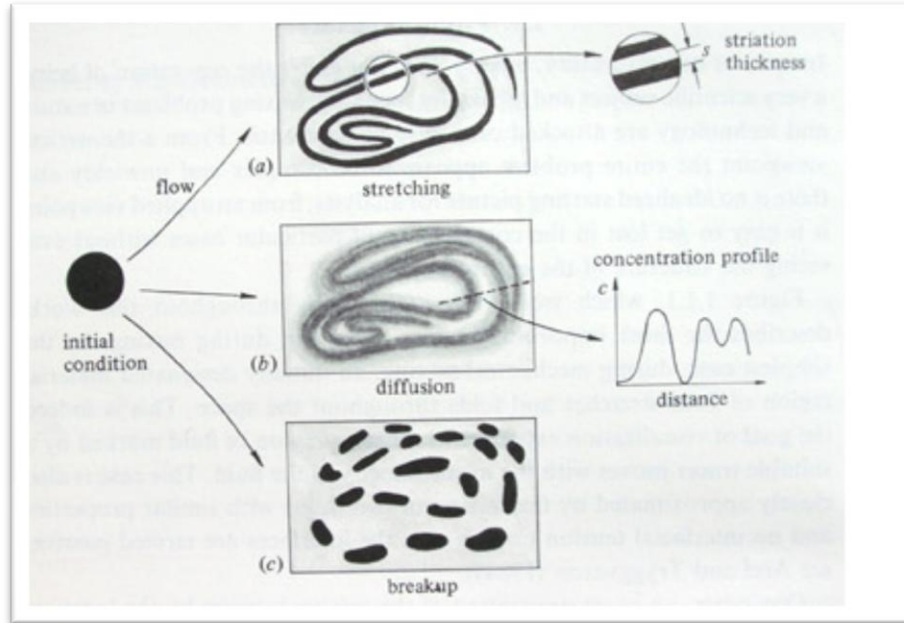


**Fig. 10: Phenomena that occur during the mixing of two liquids [3].**

Fig. 10 is a schematic representation depicting the phenomena that occur when two liquids mix [3]. The black circle on the left represents the pure liquid that will mix with a eutectic liquid (white). Mixing starts with the pure liquid stretching inside the eutectic liquid forming striations that are driven by buoyancy, gravity and momentum. At the same time diffusion of solute occurs from the eutectic liquid into the pure liquid. The driving force for diffusion is the concentration difference between the pure substance and the solute rich eutectic liquid. The striations may break up, depending on the surface energies of the liquids and the flow conditions. The thickness of the striation, which is defined in Fig. 10 as the distance between the centers of two adjacent striations is very important because the smaller the striation thickness is, the shorter the diffusion length.

## 3.2 Nucleation

At the moment when the two liquids come together, there is a large difference between their temperatures, in addition to the difference in their solute content. Hence, thermal diffusion will occur simultaneously with solute diffusion. Compared to the solute, heat diffuses about 3 orders of magnitude faster for most metals. This creates a high degree of undercooling of the pure liquid before the final mixture becomes compositionally homogeneous. This sudden undercooling can be in the range of 20 to 60°C, depending on the initial temperatures and volumetrics of the two liquids.

Such high undercooling enables rapid nucleation of particles of the pure liquid. The particles that form during this partial solidification of the pure substance are thermodynamically stable as long as they lie within the two-phase region of the phase diagram. The critical nucleus size is inversely proportional to the degree of undercooling. This means that the higher the undercooling the smaller the nuclei size will be. It is well understood today that a high nuclei density is favorable for a globular microstructure [12,13].

### 3.3 Growth

After rapid nucleation of the solid, the nuclei find themselves in a solute-rich liquid and the temperature of the casting is higher than the temperature of the eutectic liquid. The absence of dendritic protrusions can thus be explained by the absence of constitutional undercooling which is one of the main reasons of undercooling for the breakdown of the interface and formation of dendrites [14,15].

Based on the preceding, the hypothesis for formation of globular microstructure via CDS can be summarized as follows:

- As the liquids mix by the Reaction mixing mode, striations of one liquid are formed in the second liquid.
- Within these striations, rapid nucleation of the pure liquid occurs due to the high undercooling created by the difference in temperature between the two liquidus.
- The pure solid nuclei are dispersed in the eutectic liquid matrix and so they grow in a solute rich environment.
- The solid particles grow by diffusion of solute and the shape of the interface is a function of the cooling rate.

## 4. Experimental

### 4.1 Materials and Procedures

The following experiments were designed and performed in order to validate the proposed hypothesis with experimental evidence. The experiments focus on the Al-Cu binary system. This system is suitable for experimentation as it has two significant characteristics: (i) There is a large temperature difference between the melting point of Pure Al and the Al-Cu eutectic temperature enabling high undercooling, and (ii) it has a high eutectic concentration which increases the rate of diffusion of the solute (Cu). Both of these characteristics are favorable for CDS since it is based on solute and temperature diffusion phenomena.

Pure Al and an Al-50%Cu master alloy were used to prepare the different alloys; chemical composition was checked using a spark emission spectrometer<sup>2</sup>. The solidification curves were obtained with calibrated K-type thermocouples and the thermocouple data were recorded with a data acquisition system<sup>3</sup>.

Microstructure analysis was performed with standard metallographic procedures on vertical cross-sections that were cut from cast samples. The samples were ground and finally polished using 1  $\mu\text{m}$  alumina suspension in water. Between the polishing steps the samples were thoroughly cleaned. A Nikon inverted type metallurgical microscope with a digital camera was used for optical microscopy.

---

<sup>2</sup> Spectromax Spark Spectrometer LMXM3, Spectro Analytical Instruments, Boschstr. 10, 47533 Kleve, Germany.

<sup>3</sup> Daisy Lab 6 © National Instruments 11500 N Mopac Expwy Austin, TX 78759-3504

## 4.2 Mixing of Two Liquid Melts – *procedures and measures*

The objective of this experiment is to identify the modes of mixing of the two liquids and analyze the resultant solid microstructure.

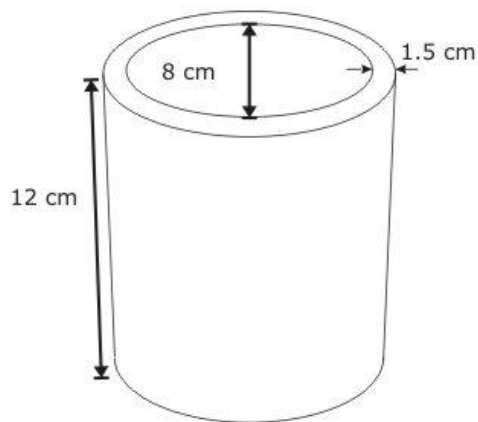


**Fig. 11: SiC crucible dimensions.**

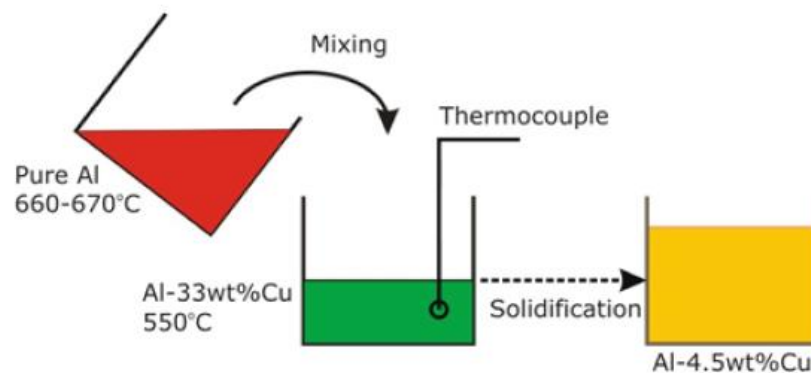


**Fig. 12: Schematic diagram of the CDS.**

The present procedure precursor liquids are: (i) Pure Al and (ii) Al-Cu eutectic. The procedure is presented schematically in Fig. 12, and the chemical compositions and initial weight of the liquids are shown in Table II. All crucibles used were SiC with

dimensions shown in Fig. 11 coated with Boron Nitride. The process took place in room temperature atmosphere. The cooling rate was 0.7 °C/sec.

Mixing Path	Pure Al		Eutectic		Target alloy
	T(C°)	weight (gr)	T(C°)	weight (gr)	
Alloying in the liquid state	680	300	570	48	Al-4.5%Cu
CDS – Reaction Mixing	660	300	550	48	Al-4.5%Cu
Quenching	660	175	550	175	Al-17%Cu

**Table II: Processing parameters for the three mixing paths.**



**Fig.13: From left to right a) Homogeneous liquid solidifying (dendritic microstructure) b) Reaction mixing, (globular) c) Quenching (severe segregation).**

Three distinct experiments were performed:

(1) The two liquids were mixed with relatively high superheats (Al 680°C, Al-33wt%Cu 570°C) and left to solidify in a SiC mold in room temperature air. Using precursor liquids with high superheats leads to the creation of a homogeneous liquid alloy with the target concentration. The resulting microstructure is shown in (Fig.13 a) and is clearly dendritic.

(2) By lowering the superheat of the Pure Al liquid to 10°C, the process enters the reaction mixing mode and the microstructure which is shown in (Fig.13 b) becomes globular.

(3) A relatively smaller quantity of liquid aluminum (175gr) was mixed with equal quantity of eutectic liquid (175gr). The result was immediate quenching of the Al as it entered the crucible and minimal mixing between the two liquids as shown in (Fig.13 c). In this Figure, the dark area on the top is the eutectic and the white area on the bottom is the Pure Al. The two liquids are hardly mixed. The Pure Al displaced the eutectic and the system was quenched. Air entrapment is due to rapid solidification.

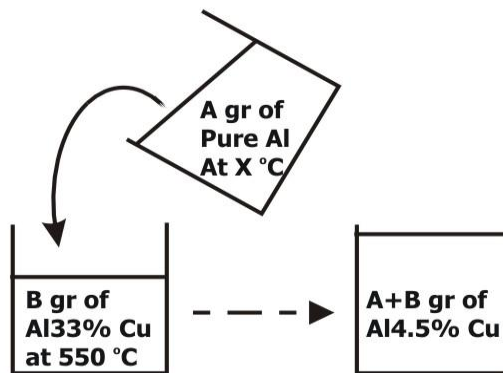


**Fig. 14: Schematic diagram of mixing process.**

Al Pouring	Al33wt%Cu
T (°C)	T(°C)
662	<b>549</b>
670	<b>550</b>
682	<b>550</b>

**Table III: Mixing parameters.**

This experiment shows that the amount and temperature of the two precursor liquids should be chosen so that reaction mixing prevails. If these two parameters are not chosen correctly, either mixing in the liquid state or quenching will prevail and will not lead to a globular microstructure in the solid. In order to understand the effect of the initial temperatures three experiments were performed. At all experiments the eutectic liquid temperature was held constant while the aluminum temperature was increased successively by 10°C. The initial temperature data is shown in Table III.

As shown in Fig. 14, 300g of Pure Al liquid is kept at a controlled temperature in the resistance furnace. A thermocouple placed in the center of the melt monitors the melt temperature. In the induction furnace, 50gr of Liquid Al-33wt%Cu is maintained at a temperature of 550°C.

The standard mixing procedure presented in 4.2 is followed in each experiment. Each time the liquid Al-33wt%Cu is taken out of the furnace and placed on a refractory material. A thermocouple is inserted at the center of the melt and the temperature is monitored. When the temperature drops to 550°C the Pure Al is poured in the Al-33wt%Cu crucible as shown in Fig. 14. The crucible dimensions are shown in Fig. 11. The alloy is left to solidify at room temperature and atmosphere. Samples were cut in half vertically with a SiC cutting wheel and one side was ground and polished with Struers SiC papers using water as a coolant. Subsequently, the samples have been etched using Keller's Reagent (2.5 % HNO<sub>3</sub>, 1.5 % HCl, 0.5 % HF, balance H<sub>2</sub>O) for approximately 7-8 sec.

Thermal curves were recorded with Daisy Lab<sup>4</sup>.

---

<sup>4</sup> **Daisy Lab®** National Instruments 11500 N Mopac Expwy Austin, TX 78759-3504

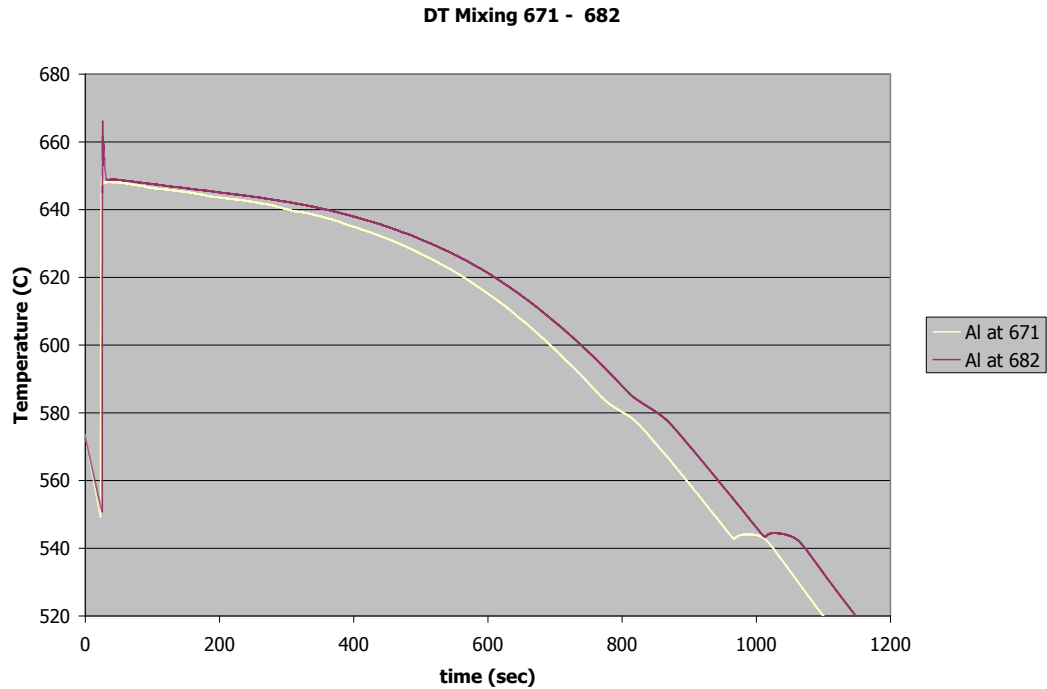


**Fig. 15: Thermal Curves 671 – 682.**

On the very left of Fig. 15 the linear temperature drop is the temperature of the Al33wt%Cu liquid (Fig. 14). When the Al33wt%Cu reaches 550°C, then the Pure Al is introduced. When the two liquids mix, there is a sudden rise of temperature.

The microstructures up to 672°C exhibit non-dendritic morphology – see Fig. 16. However a breakdown of the non-dendritic morphology is evident, that occurs between 672 and 682°C. At that temperature range dilution occurs before solidification begins and the solid microstructure is dendritic as would be expected with a regular casting approach. With the present setup, (Al33%Cu at 550°C and non pre-heated mold) one can safely state that there is at least a 13°C operation window from 658°C (Al melting point) to 671°C. This is an encouraging fact, as it provides flexibility over the control of the process. The microstructures of the samples as well as the composition were homogeneous throughout the sample, which proves that there is adequate mixing even without any mechanical means.

---

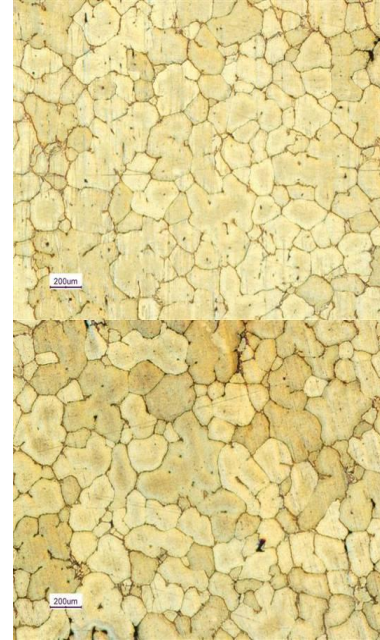
Al at 662°C

Al at 672°C

Middle

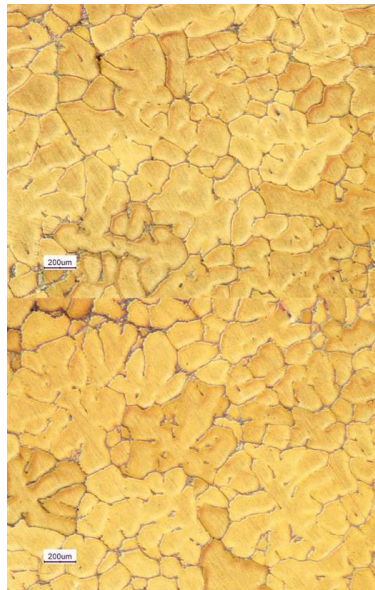


Bottom



Al at 682°C

Middle



Bottom

---

**Fig. 16: Representative microstructures obtained with CDS under different Al Superheats.**

### 4.3 Visualization of the $L_1/L_2$ interface: *formation of striations*

	Temp (°C)	Weight (gr)
<b>Pure Al</b>	660	500
<b>Eutectic</b>	545	500

**Table IV: Quenching experiment – Initial liquids parameters.**

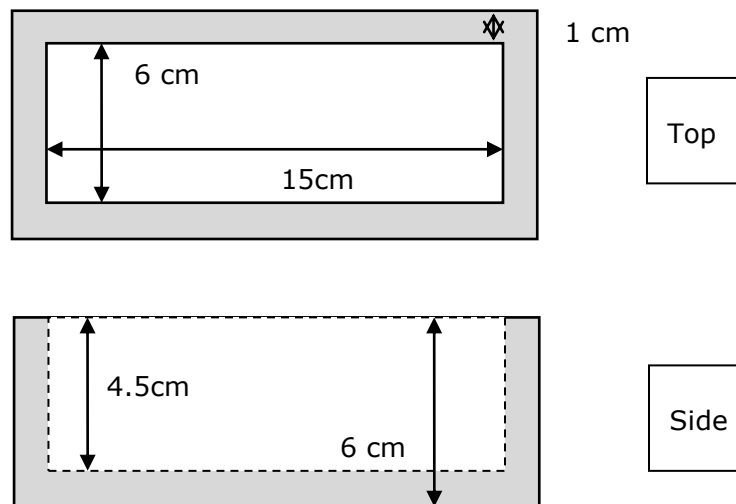


**Fig. 17: Steel mold dimensions.**

Experiments were performed in order to visualize the evolution of the interface between the two liquids before mixing is complete. The goal is to quench the two liquid melts while they mix. Because mixing is very rapid and happens in less than a second it is difficult to quench the mixture by using conventional means. In the present experimental setup the idea is to take advantage of the ideal quenching mode (3<sup>rd</sup> path) and force the liquids to freeze before mixing is completed. However, the reaction mixing process will take place locally along the interface. Note that this experiment doesn't aim in producing a homogeneous alloy. The initial liquids and

volumes were selected as should be such that the system would solidify before the mixing was complete. Also before any conclusions concerning the actual method of applying the CDS can be drawn, one has to take into account that the actual flow should be less laminar.

For the visualization experiments a steel rectangular mold with the dimensions shown in Fig. 17 was constructed. A thin steel gate divides the mold cavity into two compartments. Each compartment contains the two liquids as shown in Fig. 18. The steel mold is preheated to the same temperature as the eutectic liquid. The liquids are then added to each compartment, the gate is lifted and the two liquids mix freely. The relevant parameters are given in Table IV.

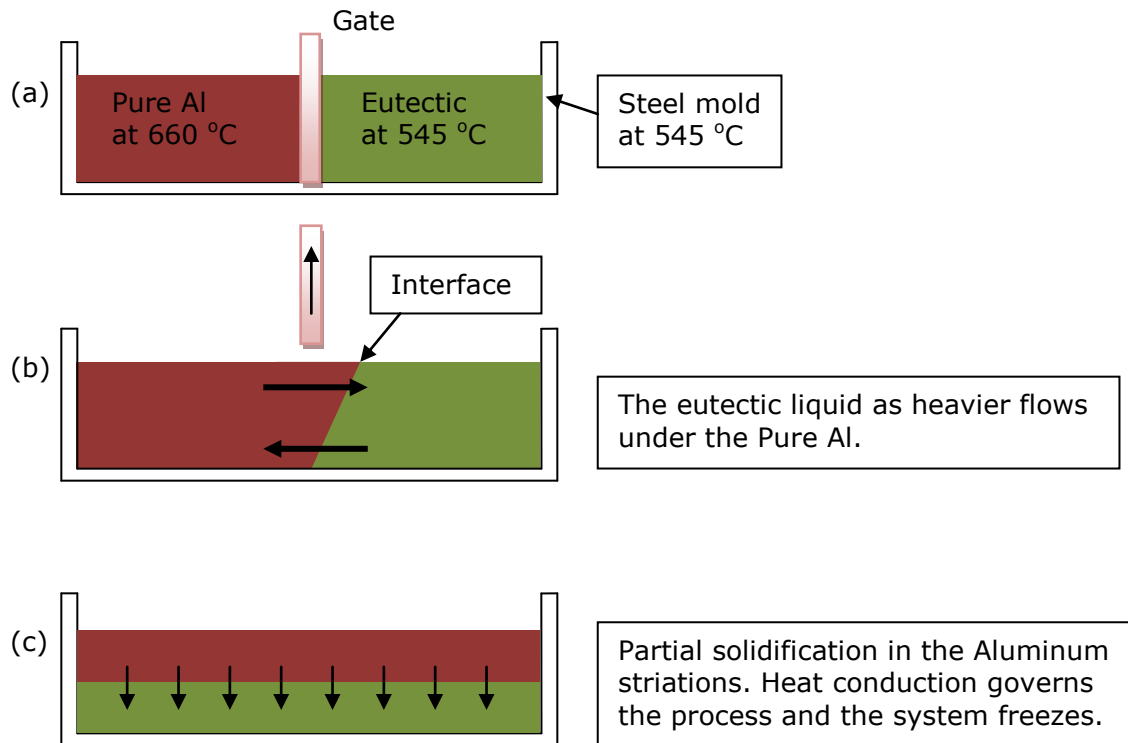


**Fig. 18: Schematic representation of quenching experiment. (a): The two liquids are being held at controlled temperatures in the steel mold. (b): As the gate is lifted the two liquids mix freely. The heavier eutectic will displace the Pure Al. Striations are formed across the interface and reaction mixing occurs. (c): The striations freeze due to governing heat conduction.**

The casting was cut vertically in half along the long axis of the mold. It was subsequently polished and etched using Keller's reagent in order to reveal the macrostructure shown in Fig. 19. Three regions can be clearly distinguished. In the microstructure the top white region is predominantly quenched Pure Al. The bottom darker region is the eutectic liquid. The developing interface and the protruding striations can be seen in the middle zone. The average size of the striations was measured to an average of 1mm.

The detailed microstructure of the striations is shown in Fig. 20. Inside the striations, partial solidification has occurred and the globular particle morphology is evident.

The way this experiment was designed forced the liquids to freeze abruptly. If the temperatures of the two liquids were higher, these particles would have more time to disperse inside the solute rich matrix and the casting would have had a homogeneous globular microstructure.



**Fig. 19: Developing striations across the interface. (The reflection in the background is the camera lens).**

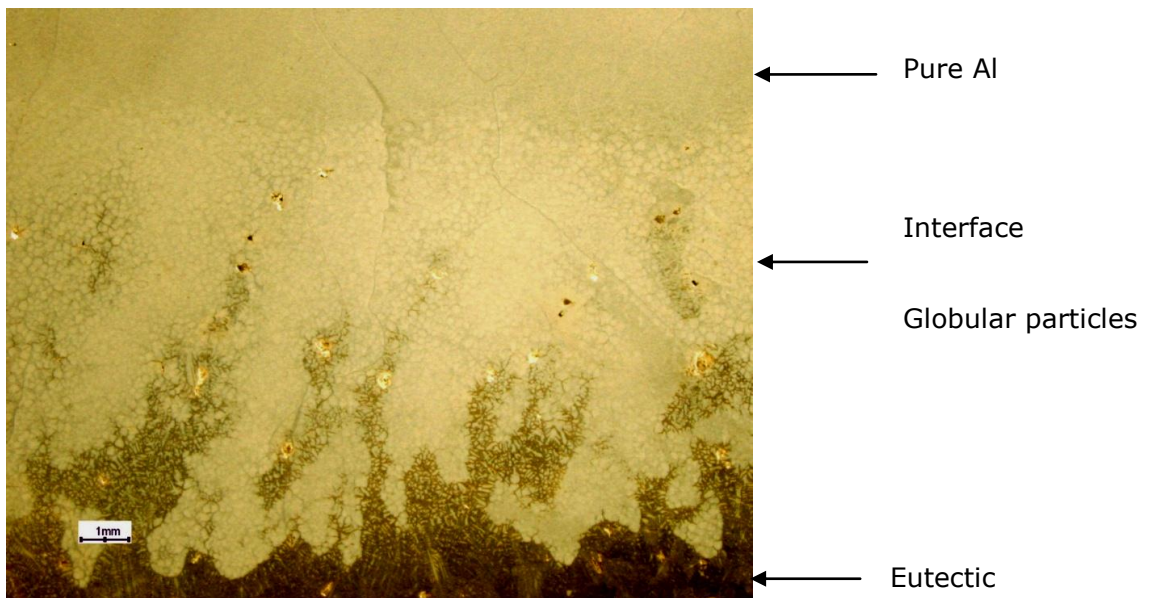


**Fig. 20: Striations and microstructure.**

This experiment shows that striations of one liquid (in this case Al) develop in the second liquid (Al-33%Cu) during reaction mixing and that the average width of a typical striation is 1mm.

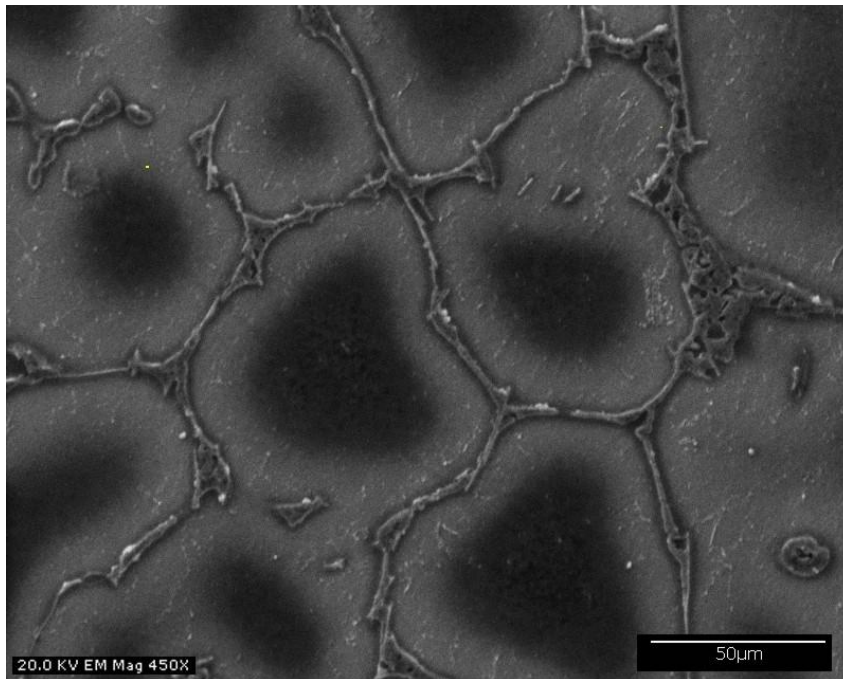


**Fig. 21: High magnification SEM image of the globular microstructure.**

In Fig. 21 the globular grains are shown in greater detail. The grains are  $\alpha$ -Al while the solute is concentrated at the grain boundaries. The concentration profile is shown in Fig. 22.

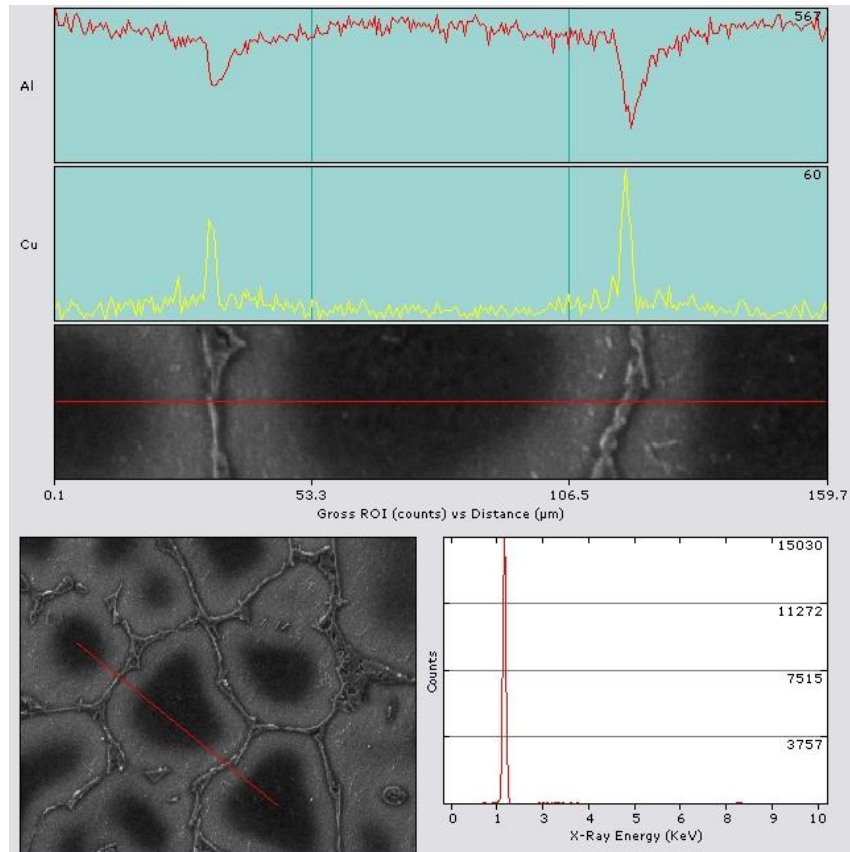


**Fig. 22: EDX line scan across  $\alpha$ -Al grains – Concentration profile.**

By employing an EDX (Energy Dispersive X-ray) line scan across successive grains the composition profile is acquired as shown in Fig. 22. The profile is taken across the red line. The concentration of solute is very small inside the Al grain and there is a sharp increase close to the boundary. This agrees with the initial assumption that states that primary nucleation particles are Pure Al and therefore the low solute concentration inside the grain.

#### 4.4 Addition of Synthetic Nuclei: procedures and measures

It was long well known in the foundry practice that the addition of grain refiner reduces the hot-tearing tendency of Al-Cu alloys [4]. In 1970 the study published by Davies [5] actually proved this by directly showing the proportionality of the hot tear

length to the cast grain size. The best grain refinement in these alloys occurs with a low Ti content and when B is added as Al-5Ti-1B rod [6].

The present experimental series attempts to further strengthen the hypothesis that nucleation takes place inside the undercooled Al. Two sets of experiments were carried out. In the first the grain refiner (GR) Al-5Ti-1B was added to the Pure Al prior to mixing. In the second the GR was added in the eutectic Al<sub>33</sub>Cu prior to mixing. Finally a sample with grain refiner was cast by the traditional alloying method. The resulting microstructures were compared.

What is expected is to see a more uniform and refined microstructure when the grain refiner is added to the Pure Al because it will assist the nucleation that occurs in the rapidly undercooled Al.

	Temp (°C)	Weight (gr)
<b>Pure Al</b>	660	300
<b>Eutectic</b>	545	50

**Table V: Processing parameters.**

The same experimental procedure is employed as in 4.2 and the processing parameters are given in Table V. The grain refiner added was Al<sub>5</sub>Ti<sub>1</sub>B and the quantity was similar to foundry practice [7] (0.05wt% of the total sample weight). The grain refiner was added at 750 °C in all cases.

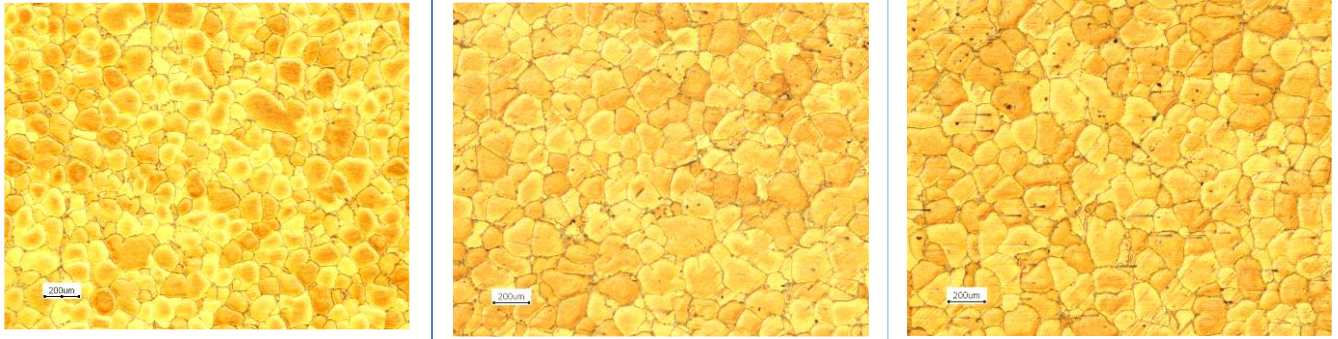


**Fig. 23: From Left to right: Grain refiner added to: 1) Pure Al 2) Al-33wt%Cu  
3) Al-4.5%Cu.**

These experiments confirm the validity of the hypothesis presented in Chapter 3.

Specifically,

- Nucleation rate and microstructure quality increases when the GR; however, this is only so when the GR is added to the Pure Al. If the GR is added to eutectic, nucleation rate is not increased.
- Nucleation theory is applicable to quantitatively describe and analyze the results.
- Numerical simulations presented in section 5.3 show a large undercooling in the bulk of the Al liquid. This undercooling effect augments the presence of the grain refiner.
- A new window for controlling the microstructure has been established. To which of the two melts the alloy constituents are added to plays a significant role, as this may enhance their beneficial effect or hinder any unwanted features.

## 4.5 Globular Stability vs. Cooling Rate

The present series of experiments quantifies the effect of the cooling rate on the resulting microstructure. As expected, at high cooling rates, the evolving globular grains are unstable and result in dendrites.

The system employed is the Al - Al33wt%Cu, with no grain refiner added. The addition of a grain refiner would enhance the nucleation and globular stability, and higher cooling rates would be feasible.

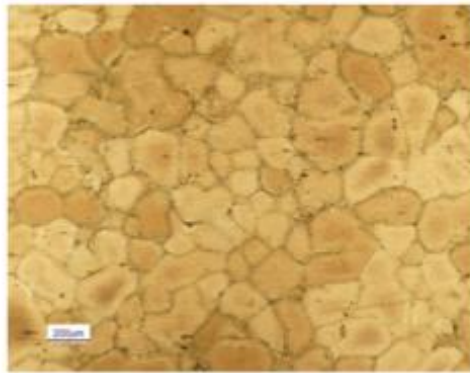
Cooling Rate (°C/sec)	Al Temp (°C)	Al33CuTemp (°C)	Mixing T (°C)
0.25	660	547	<b>647</b>
0.34	661	549	<b>650</b>
0.4	660	552	<b>652</b>
1.3	660	548	<b>648</b>

**Table VI: Cooling rates and data from thermal curves.**

The same experimental setup is employed as in 4.2 with the processing parameters listed in Table VI. After the metals have been mixed, different cooling rates are enforced on the system. The samples are prepared following the same procedures with 4.2.

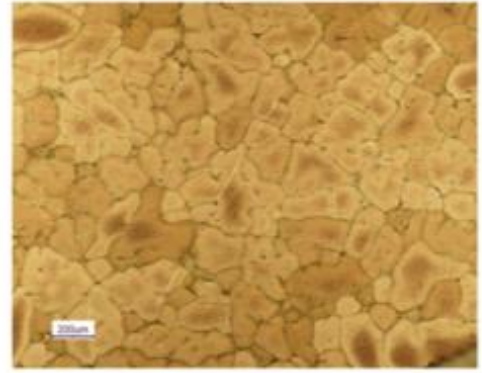
The experimental results validate the hypothesis presented in Chapter 3. Increased cooling rate leads to instability of the globular phase and the microstructure breaks down to dendritic. The lower the cooling rate the more uniform and globular the microstructure is as more time is allowed for diffusion. Stability analysis favors dendritic protrusions when the speed of the solidification front is increasing. This result may seem to constrain the CDS process only to casting processes with a slow

cooling rate. However, the above results are without the presence of any grain refining agent. With the presence of a grain refiner, higher cooling rates will be achievable.



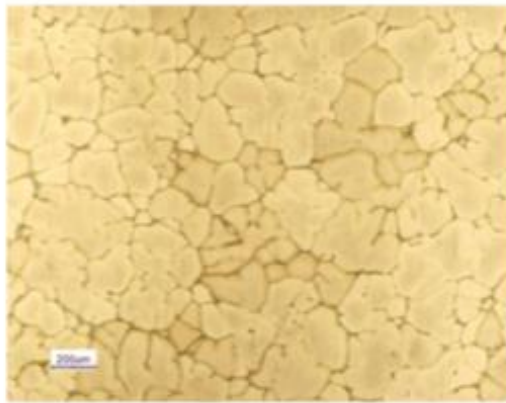
0.25 °C/sec

(Globular-non dendritic)



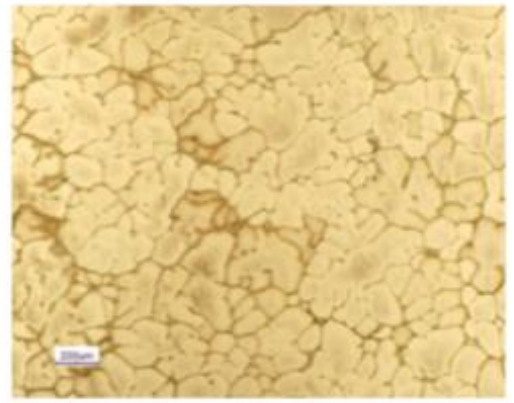
0.34 °C/sec

(Non dendritic)



0.4 °C/sec

(Globular microstructure starts to break down)



1.3 °C/sec

(Coarse dendritic)

**Fig. 24: Representative microstructures obtained with different cooling rates.**

#### 4.6 Hot Tearing in CDS castings: *procedures and measures*

Experiments were conducted to evaluate the hot-tearing tendency of a 206 type alloy when cast conventionally versus cast via the CDS.

Al	Cu	Mg	Mn	Fe	Si	Zn
Balance	4.2-5.0	0.15-0.35	0.2-0.5	0.15 max	0.054	0.014

**Table VII: Composition of 206.**

206 is an important alloy of the Aluminum-Copper family and its copper content varies between 4.2 and 5%. Its nominal composition is given in Table VII.

Aluminum cast alloys are less prone to hot tearing than the wrought alloys. However, commercial alloys such as the 206 are not free of hot tears. The aluminum copper family of alloys is specifically important to the metal casting industry. They are heat treatable and high strength alloys with a wide field of applications ranging from cylinder heads for aircraft and automotive engines, pistons for diesel engines, aircraft structures and similar applications [20,21].

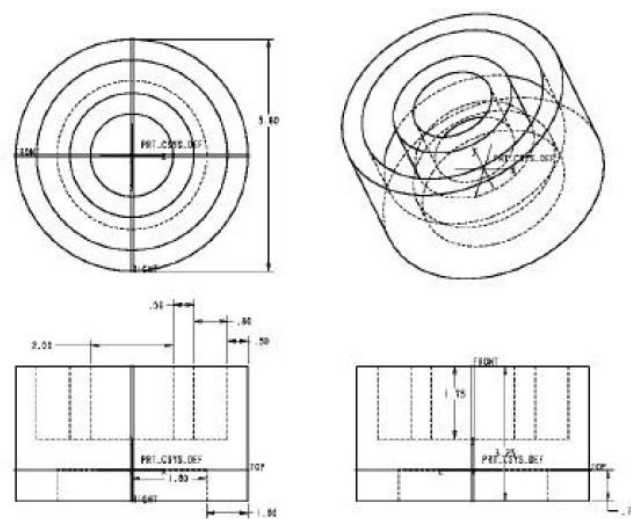


**Fig. 25: Ring mold schematics.**

## **Ring Mold Test**

The ring mold setup is one of the most frequently used tools to assess the hot tearing tendency of aluminum alloys [22-24]. The experimental setup is simple; the mold consists of a ring and a core which are concentric as shown in Fig. 25. The ring and the core are made of materials of higher melting points and with thermal expansion coefficients much lower than the alloys to be tested. The molten alloy is poured radially in the gap between the ring and the core. Attention should be paid in that the height of the poured melt is the same for all experiments in order to avoid the effect of a varying metallostatic head.

The complexity of the ring mold lies in the fact that there are many possible configurations. (cold, preheated mold, different temperature of ring vs. core). The limitation of the ring mold setup lies to the fact that it is difficult to control the solidification rate. Besides that, the test gives only a qualitative value for the hot tearing tendency [8].

In this experiment the mold was at room temperature which renders the alloys more prone to hot tearing. A heated mold reduces the hot-tearing tendency. Another variable considered was the pouring superheat. In the casting practice an alloy is usually cast with superheat. The relationship of the alloy superheat with the HT tendency is as such: The higher the alloy superheat the more prone the alloy is to hot tearing. Because in CDS the final alloy is cast with almost no superheat the 206 alloy was cast under different superheats to see if there is any correlation. The ring mold was always at room temperature in a climate controlled lab foundry.

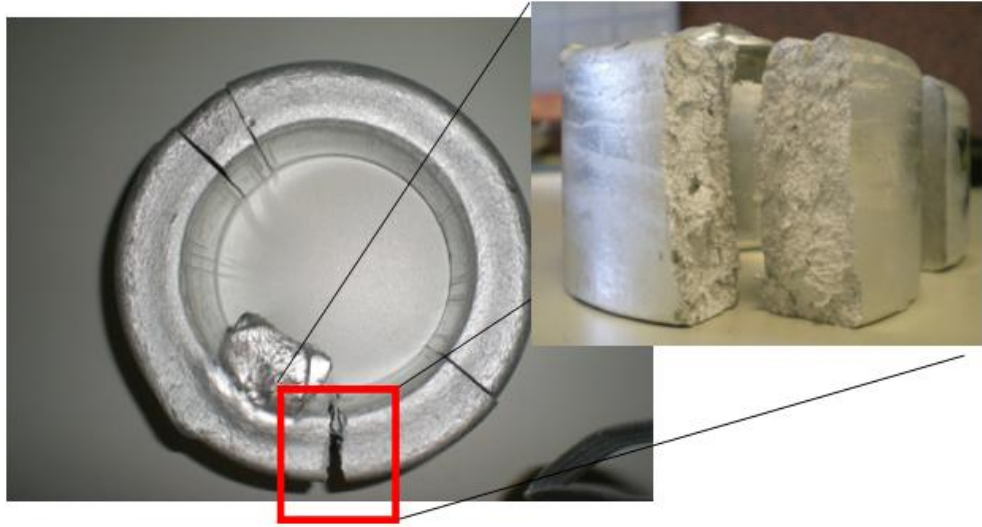


**Fig. 26: 206 – Conventional casting without superheat – separation.**

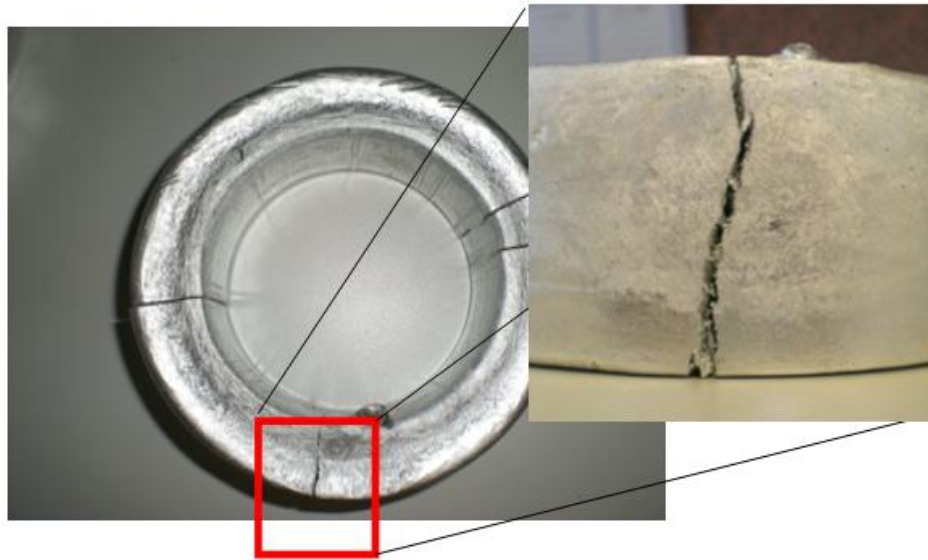


**Fig. 27: 206 – Conventional casting at 670°C – Hot tear.**



**Fig. 28: 206 Cast via CDS - No hot tearing.**

The CDS initial liquids are presented in Table VIII. The resultant alloy has the nominal composition of 206 and other alloys of the 2xx and 2xxx series.

Liquid #1	Liquid #2
<b>600gr Al</b>	<b>110gr Al-33%Cu</b>
<b>35gr Al-52%Mg</b>	
<b>70gr Al-24%Mn</b>	

**Table VIII: Initial compositions of liquids melts mixed via CDS.**

Should someone look into optimizing the process when casting more complex alloys he would attempt to create a higher temperature difference between the two alloys to increase the undercooling in the higher melting point liquid.

Two sets of experiments were performed. In the first set a 206 nominal composition alloy was cast under different superheats in the ring mold. In the second set the same target alloy was made via the CDS method. The two liquids were mixed in a crucible and then immediately poured in the ring mold.

There was separation of the casting when the 206 was conventionally cast as shown in Fig. 26. When the superheat was increased there were always hot tears in multiple sites. A characteristic hot tear is presented in Fig. 27. (the red box marks the hot tear, the rest of the cuts are due to sample removal from the mold. The 206 alloy showed no hot tears when cast via the CDS method Fig. 28.

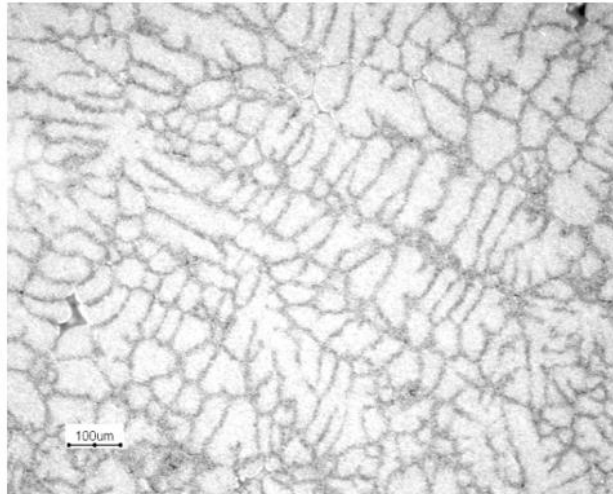


**Fig. 29: 206 Conventional casting – Dendritic microstructure (bar: 100µm).**

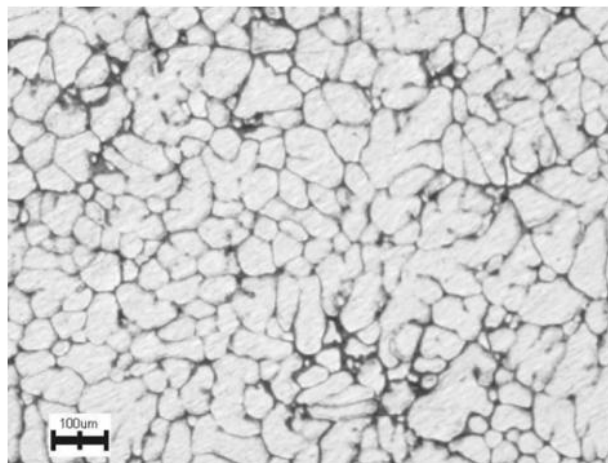


**Fig. 30: 206 Cast via CDS– Predominantly globular microstructure. (bar: 100µm).**

Hot tears originate due to the impermeability of the dendritic network during the latter stage of solidification. The remaining liquid cannot fill the empty space between the dendrites and hot tears form. That is not the case when the alloy is solidifying with a globular microstructure, such as the one produced via the CDS. Samples were cut from different sections of the samples, polished and etched with the Keller's reagent. In all regularly cast 206 the microstructure is dendritic, as can be seen in Fig. 29. In the CDS samples the microstructure was predominantly globular as in Fig. 30.

## 5. Theory

### 5.1 Introduction

The goal is to formulate a general theory of what occurs when two liquid alloys mix during the CDS process. This theory, can then be applied to any alloy system to predict the final microstructure.

The mechanism of globular formation in the CDS process is rather complicated because it incorporates phenomena in different scales. In the following study the theory of the CDS has been divided into five discrete areas as shown in Table IX.

Mechanism of CDS steps	Processing parameters
<b>1. Thermodynamic Considerations</b>	(Suitable initial conditions)
<b>2. Macroscale – Mixing</b>	(Evolution of Striations)
<b>3. Thermal – Mass diffusion</b>	(Degree of Undercooling)
<b>4. Nucleation</b>	(Nucleation Rate)
<b>5. Stability of the interface</b>	(Stability of nuclei and grains)

**Table IX: Steps of the CDS mechanism and processing parameters calculated at each step.**

Each step is capable of calculating the processing parameters for the next one. The end result is a homogeneous casting with globular microstructure. The theory in this dissertation employs as an example the Al-Cu system. It can likewise be applied to any binary system that satisfies the conditions of each processing step.

In summary, each time the castability of an alloy via the CDS needs to be examined, following methodology should be applied.

Suitable initial conditions need to be specified for the experimental variables. These are: composition, volumetrics, and temperatures. Next follows the study of the

mixing of the two liquids. The properties of the two liquids and the intensity of mixing are needed as input to the mixing model. From the model the compositional evolution of the striations and the degree of undercooling can be calculated. The degree of undercooling can provide via the classical nucleation theory the nucleation rate. The final part is the stability of the nucleating and growing particles. The liquid properties and the processing parameters such as cooling rate serve as input. The stability of the nuclei is examined by applying the Mullins-Sekerka stability criterion [9]. The interface stability during the latter stages of solidification is correlated with processing parameters by applying the Martinez stability criterion [10].

## 5.2 Thermodynamic Considerations

The initial processing variables in the CDS process are the initial temperatures, compositions and volumes of the initial liquids. The key for the CDS to work is to ensure a high degree of undercooling in the Pure Al liquid. A high undercooling will lead to a high nuclei density, which will ensure nondendritic growth. In the CDS process the degree of undercooling is dependent on two factors: a) the initial temperatures of the two melts and b) their volume ratios.

It is understood that by increasing the volume ratio of the cold liquid the degree of undercooling will increase as well. This is true, but two scenarios need to be taken in account:

- (i) Considering for example the Al-Cu phase diagram in Fig.31 and predefining for both the Pure Al and the eutectic liquid temperatures close the solidus, the only factor that can affect the undercooling is the *volumetric ratio* between the two liquids. In order for the CDS to achieve

the desired microstructure the resultant mixture should find itself in a metastable condition. As the volumetric ratio varies and the target composition shifts towards the eutectic the CDS is no more effective and the microstructure is not globular.

- (ii) The other scenario is a boundary condition where, due to excess volume of eutectic liquid, conduction will be the governing mechanism and cause the high temperature liquid to freeze rapidly and settle at the bottom of the crucible or mold. At this extreme condition, no mixing will take place, and there will be total segregation of the two liquids. These extreme conditions were verified experimentally in the Al-Cu system in section 4.2

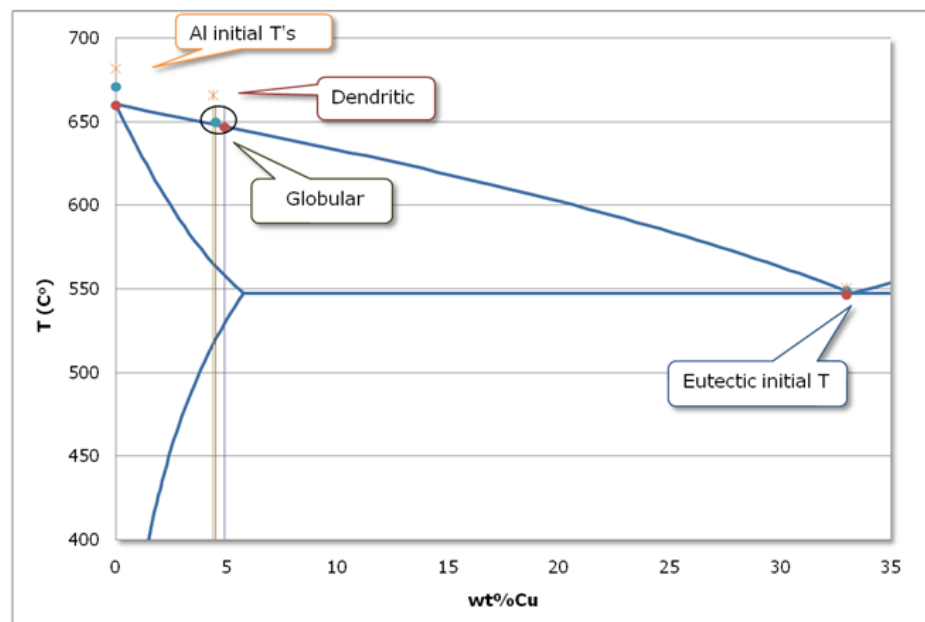


**Fig.31: Experimental data for initial liquids and final alloy temperatures. The final alloy temperature is a significant indication of the solidification mechanism.**

In order for CDS to result in a globular microstructure, one must not only target a final composition but one should also target a final temperature of the mixture. After the two liquids mix the resultant liquid should find itself in a metastable condition.

That is, the final temperature should lie in the semisolid region of the phase diagram. If the resultant mixture's temperature is higher than the target alloys liquidus, then the microstructure will be dendritic.

In Fig.31 the values of experimental results are plotted. These results exhibit favorable and non favorable processing parameters for the reaction mixing path. One can calculate the final mixture temperature thermodynamically or experimentally using a thermocouple.

Initial Temperatures		Initial Weights		Mixture Composition	Mixing T	Mixture Liquidus
Al	Al-33wt%Cu	Al	Al-33wt%Cu			
660	547	300	52	4.9	647	650
671	549	305	47	4.5	650	650
682	550	302	45	4.5	666	647

**Table X: Experimental parameters.**

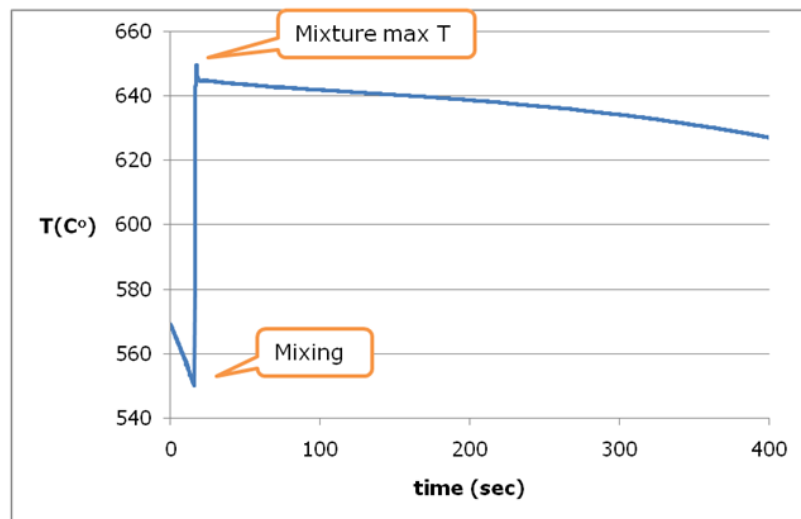


**Fig. 32: CDS cooling curve. Al at 670°C mixed with Al-33%Cu at 550°C.**

The system studied is the binary Al-Cu. The materials and procedures followed are the same as in 4.1. The initial temperature of the eutectic was held constant in all experiments. The initial temperature of the Al was increased by steps of 10 °C. The final alloy compositions ranged from Al-4.5wt%Cu to Al-4.9%Cu.

In Fig.31 the experimental values from three experiments are plotted. Experimental parameters are listed in Table X. The Aluminum temperature was varied in order for the mixture to reach different final temperatures. The experimental data were extracted from cooling curves such as the one in Fig. 32.

Regarding Fig. 32, the thermocouple is positioned in the center of the eutectic liquid and monitors the mixing and solidification process. The first slope on the left is the eutectic's liquid temperature as it cools down. When its temperature reaches ~550°C, the Al is poured inside the eutectic. The aluminum melt has a temperature of 660 to 682°C. That is why when it is introduced in the eutectic liquid there is a rapid increase in the mixture temperature. The peak of the spike in Fig. 32 is the final mixture temperature that is plotted in Fig.31. However the real mixture temperature should be a few degrees lower because of the latent heat created from the partial solidification inside the aluminum.

Nucleation should be occurring in the undercooled region of the melt which is in the Pure Al striations as was shown in section 4.3. The rest of the melt is superheated. The primary Al particles are then distributed in the eutectic melt and solidification is diffusion controlled. Here it is assumed that the heat equilibrates almost instantly compared to the solute diffusion and therefore the nucleation occurs before the equilibration of solute. The aluminum particles should nucleate on the impurities of the melt or on a substrate provided by grain refiner particles. In this case heterogeneous nucleation on impurities is considered.

The intensity of mixing directly affects the striation's size and can thus provide a wide range of undercooling. Different mixing methods might range from simply pouring one liquid into the other to a sophisticated mixing mechanism of two volumetrically controlled streams.

Now that the favorable initial processing variables can be determined experimentally, the next step is the actual mixing process. The next section examines what processes occur when two liquids mix in general, and how these can be applied to the CDS process.

### 5.3 Mixing

As was shown experimentally in section 4.3, when two liquids mix they form striations of one the other. The initial striation thickness and the mixing intensity are quantities that are used in the modeling of the evolution of thermal and diffusion fields. Even though their values can be approximated from relevant literature, interrupted quench methods can also be employed to increase the accuracy of the approximations. An interrupted quench technique that can provide visual results rather than just theoretical calculations was devised and its description and results were presented in section 4.3.

The interrupted quenching technique is unique in that there is no need to use external quenching means such as liquid nitrogen or pouring in copper crucibles. The experimental setup takes advantage of the intermediate mixing mode between the reaction mixing and ideal quenching path. The quenched mixture looks like Fig. 20 and one can calculate the average striation thickness.

Now the underlying processes of mixing of two liquid melts need to be understood and from that a model can be built that calculates the degree of undercooling in the Al striations.

### **Mixing of two liquids**

The theory begins by examining the processes that occur during the mixing of two liquids. The dispersion of one liquid into another is of great importance in many industrial processes. If both liquids are soluble into each other then two things can happen; 1) The liquids form striations and diffusion of solute takes place from the eutectic liquid to the Pure Al. The thickness, elongation and form of these striations depend on the mixing conditions. These striations tend to thin out as mixing is continued or intensified. 2) Diffusion takes place synchronously across the interface of the striations. The diffusion is driven by the difference in concentration in solute between the two liquids and continues even when the mechanical mixing stops [3].

Diffusion will drive the system towards a uniform concentration even when mechanical mixing is minimal; diffusion rate is however proportional to mechanical mixing as the diffusion length increases (or the striations become thicker). Diffusion is the reason that the final mixture will have complete uniformity. If there was only mechanical mixing and no diffusion present, then the system would have discrete compositions at different regions.

Interdiffusion and break-up occur independent of each other. Break-up will tend to reduce the size of the striations and interdiffusion will tend to homogenize neighboring parts of the mixture [11].

### **Mixing of two liquid melts**

When two liquid metals of predetermined composition and temperature mix, then the phenomenon becomes increasingly complex as apart from the mixing processes stated above, crystallization might also occur. The presence or absence of crystallization during mixing will depend on the chemistry of the system, the thermal fields and the local mixing intensity.

In the simplest scenario, mixing of two metal melts will be no different than the mixing of two miscible liquids. The process then is simply alloying in the liquid state. On the other hand, upon manipulation of the concentration of the alloys and their initial temperatures, solidification and-or other reactions may take place. These reactions are controlled by coupled heat and solute diffusion, which are in turn directly related to the local flow pattern [27,28].

The stretching and diffusion processes of mixing are incorporated in the following model.

## 5.4 Thermal and Mass Transport Phenomena

It is critical to understand the thermal and mass transport phenomena that occur when two liquid melts are mixed. The governing equations of heat and mass flow are formed and solved numerically to study the evolution of undercooling in the high temperature melt. The alloy system selected is the Al and Al-33wt%Cu. System selection was based on the high eutectic content of the binary phase diagram and the high temperature difference between the Pure Al and the eutectic.

The following model can calculate the degree of undercooling between the striations of two liquids. This model does not consider latent heat effects so it actually evaluates the solidification potential. It takes into account the thermodynamic properties of the liquids the striation thickness and the mixing intensity. The degree of undercooling can then be used to calculate the nucleation rate as shown in section 5.6.

## 5.5 Numerical model: *Evolution of solute and temperature fields*

A numerical model is presented that investigates the undercooling phenomena of an Al-4.5%Cu alloy being cast via CDS. The model describes the evolution of the temperature and solute diffusion fields upon mixing of two liquid melts of predetermined composition and temperature. When two liquid melts that are near their respective liquidus temperatures come into intimate contact the following processes occur: stretching, breakup and diffusion. The present model involves a single striation of Pure Al stretching in the infinite bulk of the second melt, which is an Al-33%Cu eutectic alloy. The stretching rate of the striation, which represents the mixing intensity is incorporated in the model. Results show that there is significant undercooling in the Pure Al as well as at the interface of the two melts. This undercooling is a key factor for rapid nucleation, which leads to a high grain density that hinders dendritic evolution. The parameters for the calculations were selected so as to model the striations observed in section 4.3.

The methodology considers stretching and diffusion of two liquids following the methodology developed by Ranz [12]. Similar analysis has also been employed by Ohmi [13] who investigated undercooling phenomena in hypereutectic Al-Si alloys. A Lagrangian frame of reference is used. As starting condition a slab of Pure Al is considered stretching in the infinite bulk of an Al-33%Cu eutectic alloy. The problem can be described by a one dimensional diffusion equation that also incorporates the strain rate term, which accounts for turbulence.

The original formulation that describes diffusion and reaction in stretching laminae in a Lagrangian frame of reference fixed on the lamina is:

$$\frac{\partial C_a}{\partial t} + e_x x \frac{\partial C_a}{\partial x} = D_a \frac{\partial^2 C_a}{\partial x^2} \quad (5.1)$$

Where  $e_x$  is the strain rate,  $D_a$  is the diffusion coefficient of chemical species  $a$  and  $C_a$  is the concentration of the chemical species  $a$ , which in this case is the concentration in Cu.

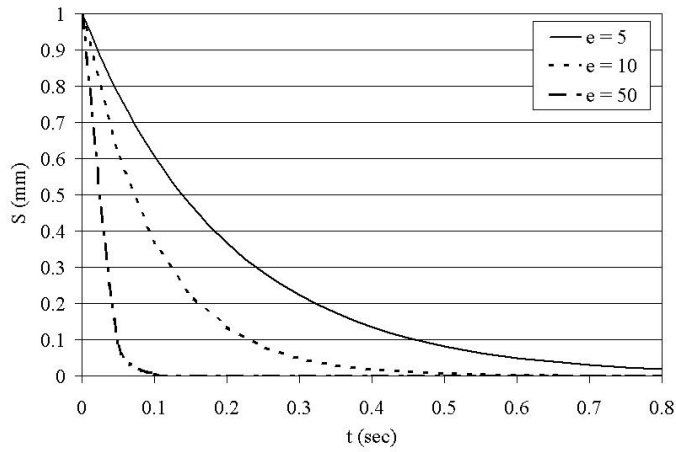


**Fig. 33: S (t) Evolution of Striation thickness S on different strain rates.**

In order to further simplify this PDE, the convection term involving  $e_x$  can disappear by introducing a warped time  $\tau$ .

$$\tau = \int_0^t S^{-2} dt' \quad (5.2)$$

and

$$\chi = \frac{x}{S} \quad (5.3)$$

In 5.3  $\chi$  is a non-dimensional space variable and  $S$  is the thickness of the striation, which is calculated by:

$$S = S_0 \exp(-e_x t) \quad (5.4)$$

$S_0$  is the initial striation thickness and  $t$  is time. Ranz by employing a warped time and a non-dimensionless space, forces space to scale to a thinning lamina thickness and time to warp in a frame of reference that moves with the fluid. So the warped time is based on the instantaneous thickness of the material filament, the diffusion and the convection. The evolution of  $S$  at different strain rates  $e_x$  can be seen in Fig. 33 for  $S_0 = 1$  mm.

The striation thickness used in this simulation was measured experimentally by the interrupted quench experiment in section 4.3. The higher the strain rate, the faster the striation stretches and its width is reduced. Following the treatment of Ohmi et al [31, 32] the solution of the system of 5.2 and 5.4 is:

$$\tau = \frac{1}{2e_x S_0^2} \{ \exp(2e_x t) - 1 \}, e_x \neq 0 \quad (5.5)$$

and

$$\tau = \frac{1}{S_0^2}, e_x = 0 \quad (5.6)$$

Introducing  $\tau$  and  $\chi$  in 3.1 the governing equation becomes:

$$\frac{\partial C_a}{\partial \tau} = D_a \frac{\partial^2 C_a}{\partial \chi^2} \quad (5.7)$$

This partial differential equation has known solutions for many boundary conditions. In this work it was numerically solved using a Crank-Nicholson (CN) scheme which is presented in Appendix III.

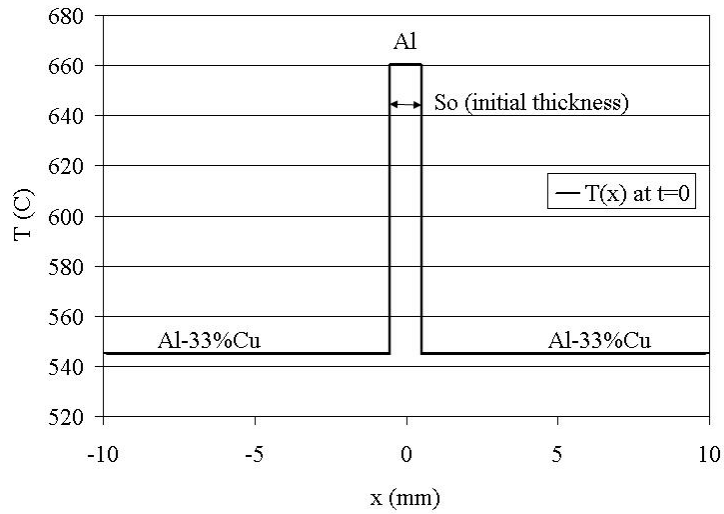


**Fig. 34: Initial temperature distribution  $T(x)$  at  $t = 0$ .  $S_0$  is the initial thickness of the Al striation.**

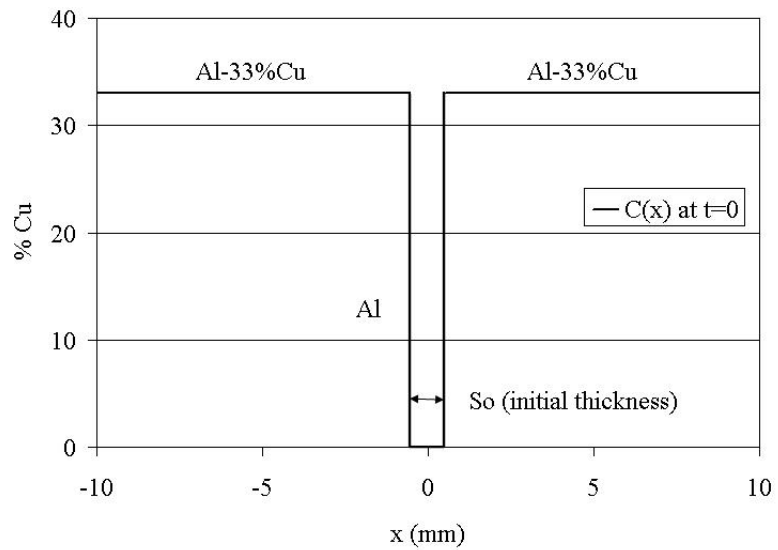


**Fig. 35: Initial composition distribution  $C(x)$  at  $t = 0$ .  $S_0$  is the initial thickness of the Al striation.**

The initial temperature distribution of the system is presented in Fig. 34 and the initial solute distribution in Fig. 35.

At  $t = 0$  both liquids are at their starting temperatures  $T_1 = 545^\circ\text{C}$  Al-33wt%Cu and  $T_2 = 660^\circ\text{C}$  Pure Al. The control of the superheat is of great importance. Experimental results in the Al-Cu system have shown that the CDS process produces globular microstructure when the Pure Al is within ten degrees of superheat [14]. In this numerical simulation both temperatures are very close to the respective liquidus lines of each melt. This gives rise to an excessive degree of undercooling; temperature diffusion is four orders of magnitude faster than solute diffusion (Cu atoms). The diffusivities are assumed to be constant. This is not a rough approximation since the scale difference between solute and temperature diffusivities is much higher, and the errors introduced are smaller in scale. The constants used in the calculations are presented in Table XI.

<b>Diffusion coefficient, <math>D</math></b>	$3.5 \cdot 10^{-9} \text{ m}^2/\text{s}$
<b>Thermal diffusivity (alloy), <math>\alpha</math></b>	$2.8 \cdot 10^{-5} \text{ m}^2/\text{s}$

**Table XI: Material constants [10].**

PDE 5.7 in the special cases of temperature and solute diffusion takes the form:

-for solute diffusion:

$$\frac{\partial C}{\partial \tau} = D \frac{\partial^2 C}{\partial \chi^2} \quad (5.8)$$

-and for heat diffusion:

$$\frac{\partial T}{\partial \tau} = a \frac{\partial^2 T}{\partial \chi^2} \quad (5.9)$$

In order to observe the undercooling phenomenon, the evolution of temperature was directly compared to the evolution of the liquidus temperature of the resulting mixture. The temperature evolution  $T(x, t)$  was extracted by numerically solving PDE 5.9. The evolution of the concentration  $C(x, t)$  was extracted from PDE 5.8. Subsequently the evolution of the liquidus temperature was extracted from the Al-Cu phase diagram by correlating it with the respective concentration at each time step. The maximum undercooling occurs right at the centre of the Al striation at  $x = 0$ . Therefore the evolution of temperature at this point compared with the respective liquidus temperatures provides insight to the undercooling conditions. Another point of interest is the undercooling that might occur at  $x = 0.55 \text{ mm}$ . Since the initial striation thickness is  $S_0 = 1 \text{ mm}$ , this is the point right next to the interface at  $t = 0$

between the two metals on the side of the eutectic. It was evident that the Pure Al would be undercooled immediately since it would find itself in a significantly lower temperature environment. What was not so evident at prima facie was that there would be undercooling also in the region of the eutectic melt. The strain rate selected for the following results was ten.

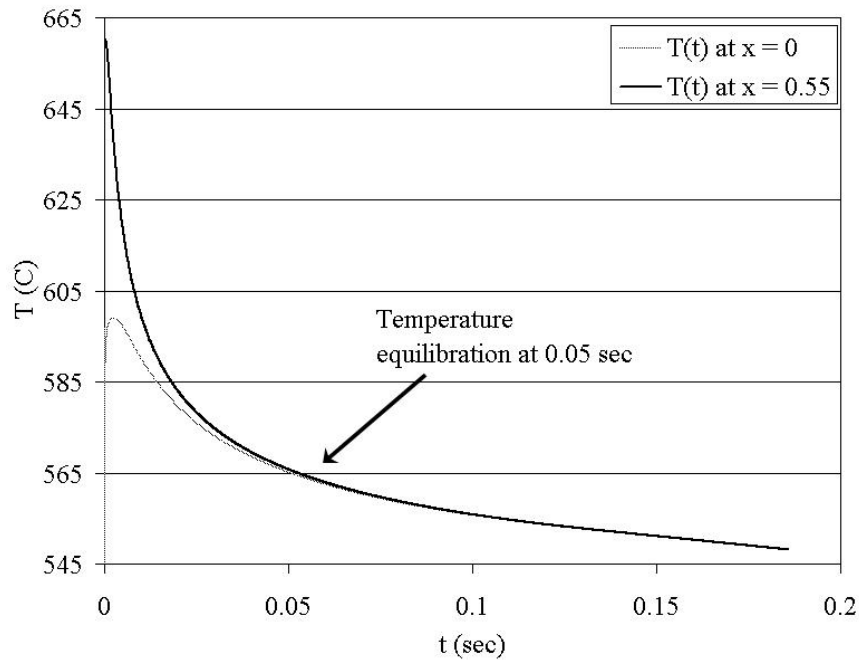


**Fig. 36: Temperature evolution at the center of the Al striation at  $x = 0$  and at  $x = 0.55$ . The equilibration of temperatures is rapid due to the high heat transfer coefficient. Equilibration is attained at 0.05sec.**

The temperature evolution at  $x = 0$  and at  $x = 0.55$  is shown in Fig. 36. The equilibration of temperature is rapid due to the high thermal diffusivity term  $\alpha$ .

Both liquids are starting from their respective initial temperatures, which are  $660^{\circ}\text{C}$  for the Pure Al and  $545^{\circ}\text{C}$  for the Al-33%Cu eutectic liquid, respectively. The temperature becomes uniform throughout the system at  $t = 0.05$  sec. The diffusion of the solute is much slower because of the low diffusion coefficient  $D$ . This means

that the actual temperatures and the respective liquidus temperatures of the two points that are tracked will follow a different path.

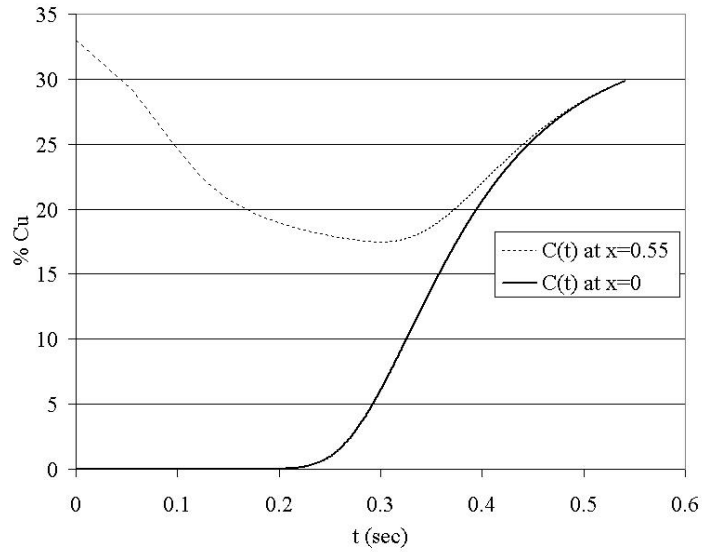


**Fig. 37: Concentration evolution at the center of the Al striation at  $x = 0$  and at  $x = 0.55$ . The equilibration of concentration is much slower than the temperature equilibration due to the lower diffusion coefficient. Equilibration is attained in 0.5sec.**

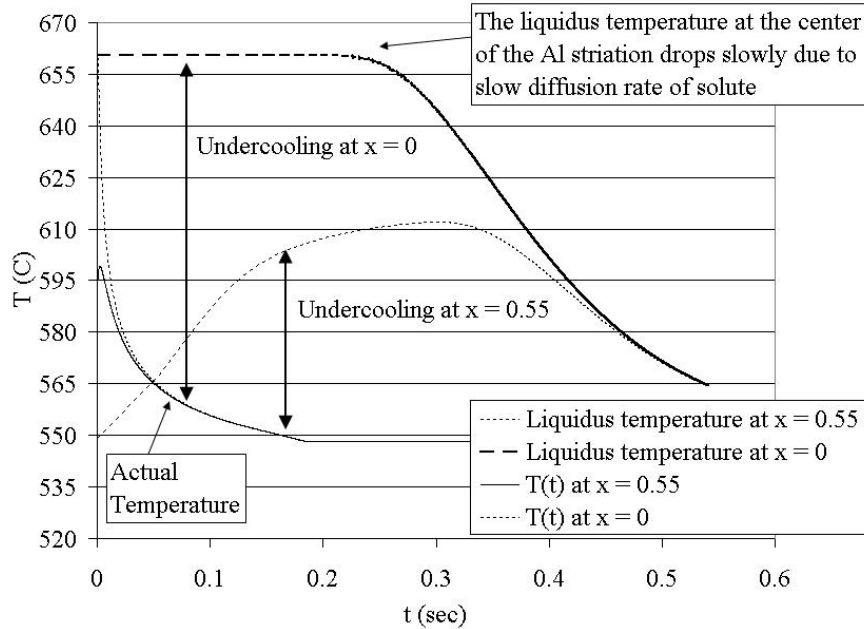


**Fig. 38: Comparison of the actual temperature at  $x = 0$  and  $x = 0.55$  and the respective liquidus temperature. The aluminum is undercooled right when the simulation begins. After a short time the solute is diffusing from  $x = 0.55$  towards the center of the aluminum striation. As a result the liquidus temperature is increasing and the melt finds itself in an undercooled state.**

The evolution of the Cu concentration at  $x = 0$  and at  $x = 0.55$  is plotted in Fig. 37.

At  $x = 0.55$  it is evident that the concentration is decreasing. Solute is being transported inside the Al striation. The solute reaches the center of the Al striation at 0.2 sec. The concentrations equilibrate close to 0.5 sec. Combining the data of Fig. 37 with the Al-Cu binary phase diagram, the evolution of the liquidus temperature was extracted. The undercooling is the difference between the liquidus temperature and the actual temperature of the alloy. Fig. 38 shows the actual temperatures plotted with the respective liquidus temperatures at  $x = 0$  and at  $x = 0.55$ .

The center of the Al striation ( $x = 0$ ) is undercooled from the beginning of the simulation. After a short time the solute is diffusing from  $x = 0.55$  towards the center

of the Al striation. As a result the liquidus temperature at  $x = 0.55$  is increasing due to the reduced concentration and the melt finds itself in an undercooled state.

The experiment presented in section 4.4 has shown that the addition of grain refiner (GR) in the Al melt before the mixing provides a much more refined globular microstructure compared to a regularly cast grain refined alloy. Addition of the GR to the eutectic liquid did not provide different results than the regularly cast alloy. The degree of undercooling in the Al melt is much higher compared to the eutectic and as such is a more efficient nucleation site.

In summary, a numerical model has been employed to investigate the undercooling during the mixing of two liquid melts with the CDS process. The simulation was performed considering the Al-Cu system and for the mixing process the model developed by Ranz was employed. The evolution of the temperature fields at the center of the Al striation and at the initial interface of the two melts was studied. Results show that the highest degree of undercooling occurs at the onset of the mixing process at the center of the Al striation. However there is also undercooling at the eutectic melt, at the position of the interface at  $x = 0.55$  due to decreasing concentration. This suggests that an increase of the number of lamella in the mixture will increase the fraction of the undercooled regions.

## 5.6 Nucleation

According to the numerical solution of the undercooling model presented in section 5.4 the undercooling occurs inside the Al striations. These results are in accord with the grain refiner experiments presented in section 4.4. This high undercooling will give rise to a high nucleation rate and a large number of nuclei. The classical nucleation theory is next after presented and the results are then used to examine the particle stability.

### 5.6.1 Classical Nucleation Theory

#### **Homogeneous nucleation**

The Nucleation is a kinetic process of great importance that can have an impact on the final microstructure and subsequently on the properties of an alloy. The classical nucleation theory [34, 35, 36] shows that the nucleation of a solid in a liquid phase does not start until the melt's temperature is lower than the melting point. Throughout the liquid, atoms come together and form small clusters, which are called embryos. These clusters can also be formed when the melt is superheated; however, they will not survive. The formation of these clusters is based on probability and thermal fluctuations. Their survival depends on two factors:

1. The free energy of the liquid to solid transformation and
2. The surface energy that is needed for the creation of the interface.

Assuming a spherical embryo the above can be expressed as:

$$\Delta G = \frac{4}{3}\pi R^3 \Delta G_v + 4\pi R^2 \gamma_{SL} \quad (5.12)$$

Where:

$\Delta G$ : Total free energy change for an embryo of radius R

R: Embryo's radius

$\Delta G_v$ : Gibbs free energy difference / unit volume between liquid and solid

$\gamma_{SL}$ : Solid-Liquid interfacial energy

The derivative at  $R=r^*$  gives an expression for the critical nuclei size:

$$r_{hom}^* = \frac{-2\gamma_{SL}}{\Delta G_v} \quad (5.13)$$

However homogeneous nucleation can never be achieved in an industrial setting. It needs specially designed experiments employing levitation and high purity metals [37-39]. The theory can be easily extended to the study of heterogeneous nucleation, which is also the case in the CDS process.

### **Heterogeneous nucleation**

In conventional casting practice nucleation occurs on the mold's wall or on solid nucleation sites that are inside the melt like impurities, oxide layers and of course on nucleation agents like  $TiB_2$  and  $TiC$  that are readily used as grain refiners. When the solid nucleates on a foreign substrate then the nucleation is characterized as heterogeneous.

## Nucleation Rate

According to the classical nucleation theory [15] the rate of homogeneous nucleation during solidification is:

$$N_{hom} = f_0 C_0 \exp \left( -\frac{16\pi\gamma_{SL}^3 T_m^2}{3L_v^2 kT\Delta T^2} \right) \quad (5.14)$$

Where:

$f_0$ : Function that depends on the vibration frequency of the atoms, the activation energy for diffusion in the liquid and the surface area of critical nuclei. It is sufficient to consider it as a constant equal to  $10^{11}$ .

$C_0$ :  $10^{29}$  Atoms/m<sup>3</sup> [15]

$\gamma_{sl}$ : interface energy.

In the above equation the nucleation rate is very sensitive to the undercooling because of the exponential term. This means that a small change in undercooling may translate in several orders of magnitude difference in the nucleation rate.

For heterogeneous nucleation the nucleation rate becomes:

$$N_{het} = f_1 C_1 \exp \left( -\frac{16\pi\gamma_{SL}^3 T_m^2 S(\theta)}{3L_v^2 kT\Delta T^2} \right) \quad (5.15)$$

Where  $f_1$  is a similar factor to  $f_0$  and  $C_1$  is the number of atoms in contact with heterogeneous sites per liquid unit volume.

## 5.6.2 Nucleation Rate in CDS

Using expression (5.15) the heterogeneous nucleation rate of Pure Al as a function of undercooling is plotted in Fig. 39. An undercooling of 35°C is easily achievable with the CDS, and it is evident that small changes in undercooling have a drastic effect on the nucleation rate. The constants for the calculations are listed in Table XII.

Quantity	Symbol	Units	Value
<b>Melting point</b>	$T_m$	$K$	933.15
<b>Density of Liquid Al at <math>T_m</math></b>	$d_L$	$gcm^{-3}$	2.39
<b>Volume change from solid to liquid at <math>T_m</math></b>	$\Delta V_m$		6.5%
<b>Density of Solid Al at <math>T_m</math></b>	$d_S$	$gcm^{-3}$	2.56
<b>Thermal conductivity of liquid Al at <math>T_m</math></b>	$k_L$	$Wm^{-1}K^{-1}$	88.18
<b>Thermal conductivity of solid Al at <math>T_m</math></b>	$k_S$	$Wm^{-1}K^{-1}$	200.03
<b>Latent heat of fusion per mole of Al</b>	$L_m$	$kJmol^{-1}$	10.7
<b>Latent heat of fusion per unit volume of Al</b>	$L_V$	$Jm^{-3}$	$4.179 \cdot 10^8$
<b>Specific heat per unit volume of liquid Al</b>	$C_V$	$Jkg^{-1}K^{-1}$	1180
		$Jm^{-3}K^{-1}$	$2.82023 \cdot 10^6$
<b>Solid-Liquid interfacial free energy of Al at <math>T_m</math></b>	$\gamma_{SL}$	$Jm^{-2}$	0.149

**Table XII: Thermochemical and physical properties of solid and liquid aluminum at  $T_m$  [10].**

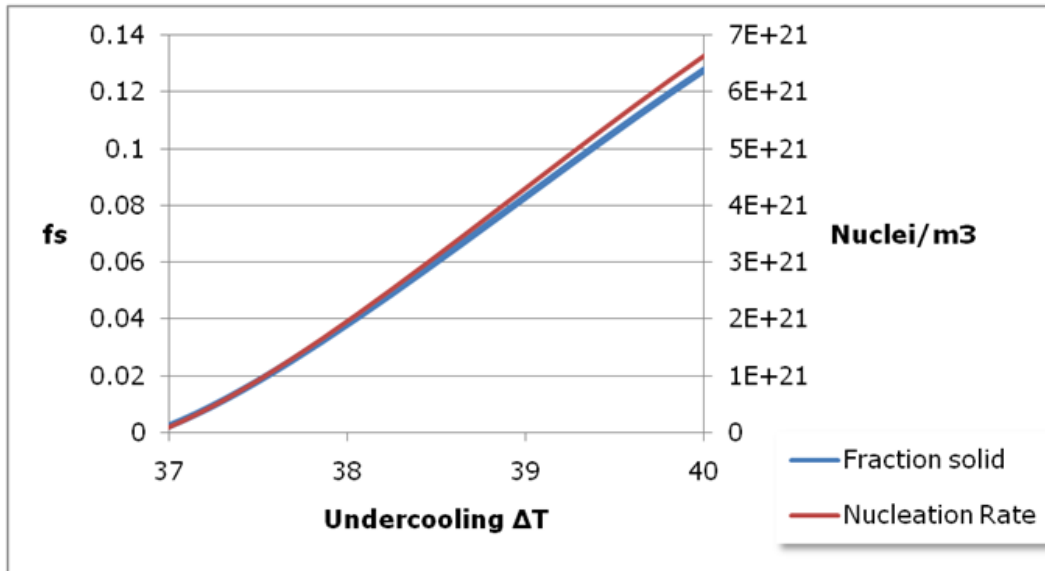


Fig. 39: Nucleation rate and fraction solid at different degrees of undercooling.

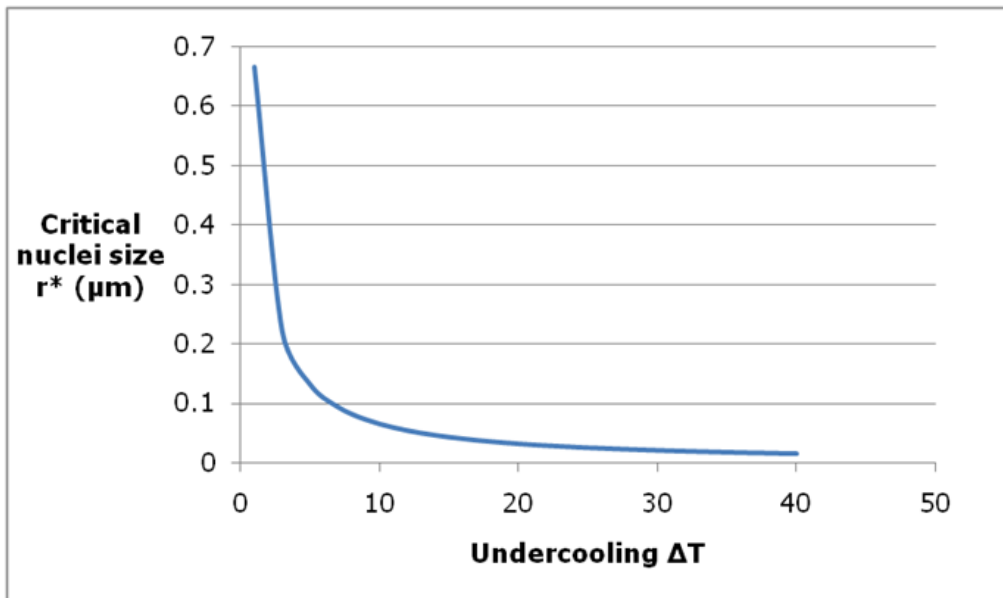


Fig. 40: Critical nuclei size of Al vs degree of undercooling.

Another important observation is that the critical nuclei size decreases dramatically as the undercooling increases according to expression (5.13). The critical nuclei size is the same for heterogeneous and homogeneous nucleation. Its variation with undercooling degree can be seen in Fig. 40.

The latter observation, that the critical size is greatly reduced with increasing undercooling, also guarantees stability of the interface at the first stage of solidification. For example an undercooling of 30 – 35°C translates to a critical nuclei size of  $\sim 0.01\mu\text{m}$ .

The relationship of the nuclei size and the stability of the planar interface will be studied by applying the Mullins and Sekerka theory for growth of a sphere under thermally controlled solidification [9]. So solidification will occur only in the Al striations and the Al nuclei will grow in the Al liquid before they get dispersed inside the superheated eutectic melt.

## 5.7 Interface Stability

In past years, a lot of academic work has been dedicated to understanding the mechanisms of globular microstructure formation [14, 40-42]. A large amount of work was aimed in understanding the principles of the various semi-solid processes, both thixocasting and rheocasting. Most of these processes include agitation, either mechanical or electromagnetic, and the proposed mechanisms consist of: dendrite fragmentation, aggregation and coalescence of fragmented crystals, and abrasion of large crystals. However these explanations cannot be directly applied to a non-agitative process like the CDS.

### **Globular stability during forced stirring**

Since the initial stage of the CDS solidification involves some convection induced by the unforced mixing of the two liquids, it is of interest to examine the theory of globular microstructure stability under stirring conditions as stirring can be supplementary to another version of the CDS.

By stirring the melt either mechanically or electromagnetically, intense convection takes place that affects the crystal morphology. The resultant microstructure is globular, and the formation mechanism was only recently understood. The proposed theory assumed dendritic arm break-up or melting at the dendrite roots. Convection then drives these fragments inside the melt where they become nuclei which ripen into spheroids. Later Zhang proved that dendritic fracture was unlikely the main mechanism and proposed a particle drift and blending compressing mechanism. This takes into account the impact of the vigorous agitation on the heat and mass transfer. Particle drift enhances heterogeneous nucleation and blending and compressing forces the crystals to grow relatively uniform in all directions.

Transparent alloy studies with succinonitrile proved that nucleation initiates directly from the liquid and not from fractured dendritic branches [16].

Today it is understood that if the initial grain density is high enough the final microstructure will be globular [10]. Martinez worked on understanding the dependence of the globular microstructure on variables such as: fraction solid, grain density and cooling rate. His work focused on the Al-4.5%Cu alloy which is of interest in the present work as well.

---

### 5.7.1 Mullins Sekerka Stability Criterion

As explained in the numerical model in paragraph 5.5 the Al striations are instantly undercooled upon contact with the cooler eutectic liquid. The concentration in the liquid does not become homogeneous until 0.5 sec. This is the time needed for the solute atoms to diffuse to the center of the Al striations. So nucleation of Al particles is assumed inside the striations. Since the nucleation occurs in a pure liquid the Mullins Sekerka criterion can be applied and demonstrate the morphological stability of the particles.

A mathematical model has been formulated by Mullins and Sekerka [9]. The M-S criterion studies the stability of globular growth in an undercooled melt.

In their work they introduce a perturbation in the surface of a sphere and examine its morphological stability while it grows in an undercooled melt. Mullins and Sekerka did certain approximations in their work. The approximations applied are the following and the reasons why they hold are stated below:

1. Isotropy
2. Thermal fields governed by Laplace's equation
3. Sharp interface (local equilibrium)

In order for approximation 2 to hold, the system must fulfill:

$$|C_V(T_m - T_\infty)/L_v| \ll 1 \quad (5.16)$$

Where:

$C_V$ : Specific heat

$L_v$ : Latent heat

$T_m$ : Melting point

$T_\infty$ : Melt temperature

Substituting the properties for aluminum from Table XII expression (5.16) becomes:

$$|0.0067(T_m - T_\infty)| \ll 1 \quad (5.17)$$

It is apparent that the above inequality holds for Aluminum since the undercooling of aluminum and its alloys is within the range of 5.17. It will even hold for higher undercoolings that can be achieved via the CDS.

In order for approximation 1 and 3 to hold:

$$T(K) = T(K = 0)(1 - \Gamma_T K) \quad (5.18)$$

Where:

$T(K)$ : Equilibrium melting temperature (mean particle curvature = K)

$T(K = 0)$ : Bulk melting temperature  $T_m$  and

$\Gamma_T = \frac{\gamma_{SL}}{L_v}$ : Where  $\gamma_{SL}$  is the crystal-melt interfacial free energy.

Equation 5.18 is used as a boundary condition for the solution of Laplace's equation.

$T(K)$  describes the temperature of the solid and the liquid at the interface.

The velocity of the front is given by:

$$v = \left( \frac{-1}{L_v} \right) \left[ k_s \left( \frac{\partial T}{\partial n} \right)_s + k_L \left( \frac{\partial T}{\partial n} \right)_L \right] \quad (5.19)$$

Where:

$k_s, k_L$  : Thermal conductivity of solid and liquid and

$\left( \frac{\partial T}{\partial n} \right)_s, \left( \frac{\partial T}{\partial n} \right)_L$  : Temperature gradient normal to the solid and liquid interface.

Another assumption is that the densities of solid and liquid are the same. In reality the difference in densities between liquid and solid aluminum is 6.7% (Table XII) so the above equation will be accepted.

In the M-S study, the critical radius of stability is derived as:

$$R_c = \frac{2\Gamma_T \left( 7 + 4 \frac{k_s}{k_l} \right)}{\left[ \frac{T_m - T_\infty}{T_m} \right]} = \left( 7 + 4 \frac{k_s}{k_l} \right) r^* \quad (5.20)$$

Where

$$r^* = \frac{2\gamma_{sl} T_m}{L_v \Delta T} \quad (5.21)$$

$r^*$  is the critical nucleus radius defined by the nucleation theory and presented in 5.6. The latter equation is the result of the M-S analysis for stability of a spherical particle in a uniformly undercooled melt. If the radius of the sphere is larger than  $R_c$  then the particle will become unstable and protrusions will survive.

Substituting the properties for Al from Table XII:

$$R_c = 16.0737 r^* = \frac{6.65}{\Delta T} (\mu m) \quad (5.22)$$

Plotting the above function of the critical radius  $R_c$  versus the undercooling  $\Delta T$  shows the dependence of the stability on  $\Delta T$ .

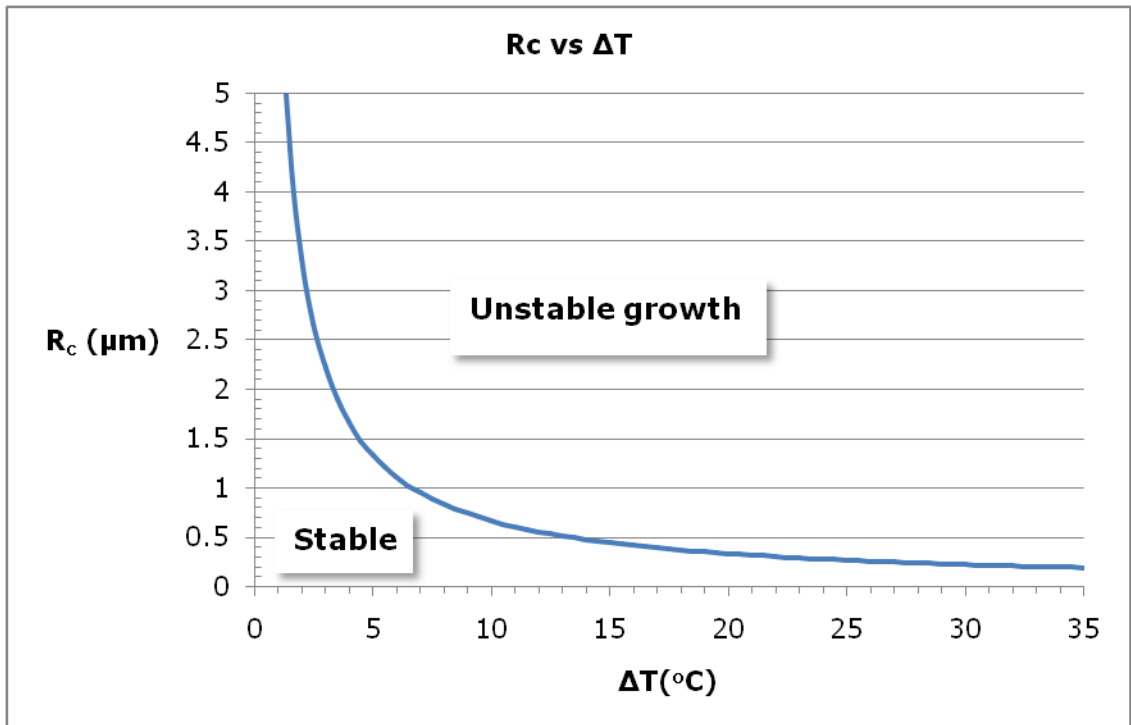


**Fig. 41: Critical radius for globular stability of an aluminum crystal related to the degree of undercooling based on the M-S stability criterion.**

Observing Fig. 41, the dependence of the stable growth to the undercooling becomes apparent. For example, when the undercooling exceeds 1 K then all spherical aluminum crystals with a size larger than 6.65  $\mu m$  will start destabilizing. But with a very low degree of undercooling (*i.e.* 0.3 K) all particles smaller than 3.33 $\mu m$  will be stable.

As was calculated before, the critical nuclei size for an undercooling of 35°C is about 0.01 μm. At this high undercooling the critical size of a globule for stability is less than 0.19μm. This means that the interface will be stable.

The M-S criterion was based on heat flow, and no further complexity was added to it. It can be applied specifically to the first step of the CDS during the nucleation of the Pure Al particles in the Al striations.

As the Al comes in contact with the lower temperature eutectic it is undercooled; the release of latent heat due to the rapid nucleation will increase the mixture temperature and some of the nuclei may remelt. The surviving nuclei will grow in a solute rich superheated melt. Since the environment is supersaturated the growth velocity of the particles will be hindered which also acts in favor of the globular stability.

The existence of excess solute dramatically changes the solidification conditions as it influences the liquidus temperature ahead of the interface and acts as solute build up in front of the solidification front.

---

### 5.7.2 Undercooling Considerations

After the nucleation event the spherical particles will keep growing and the degree of undercooling during growth is important as it will affect the interface stability. The undercooling contributing factors need to be carefully examined and understood.

In order to understand the globular stability of a particle one needs to examine the stability of the interface. The undercooling at the interface of a particle is the sum of 3 factors [17]:

$$\Delta T = \Delta T_L + \Delta T_C + \Delta T_R \quad (5.23)$$

Where  $\Delta T_L$ ,  $\Delta T_C$  and  $\Delta T_R$  are respectively the undercooling contributions; thermal, constitutional and curvature undercooling. The study of this undercooling is of utter importance as it is responsible for the cellular to dendritic transition. A low undercooling favors stability of the globular front.

The term of interest in this case is the one that can decrease the undercooling and that is the Gibbs-Thomson contribution  $\Delta T_R$ . The  $\Delta T_R$  takes into account the interface curvature, which translates to a decrease of the liquidus temperature. It works the opposite way from the temperature gradients and the constitutional differences, which increase the undercooling.

The additional molar energy of the system due to curvature is:

$$\Delta G_\gamma = \frac{2\gamma}{R} \quad (5.24)$$

Where:

- $\gamma$  is the solid/liquid interfacial energy and
- $R$  is the interface curvature

The additional free energy is equal to a temperature decrease of:

$$\Delta T_R = \frac{2\gamma}{\Delta S} \frac{1}{R} \quad (5.25)$$

Where:

- $\Delta S$  entropy difference (solid – liquid)

If spherical nuclei are assumed they are stable as long as  $R > R^*$ . If not they will dissolve.

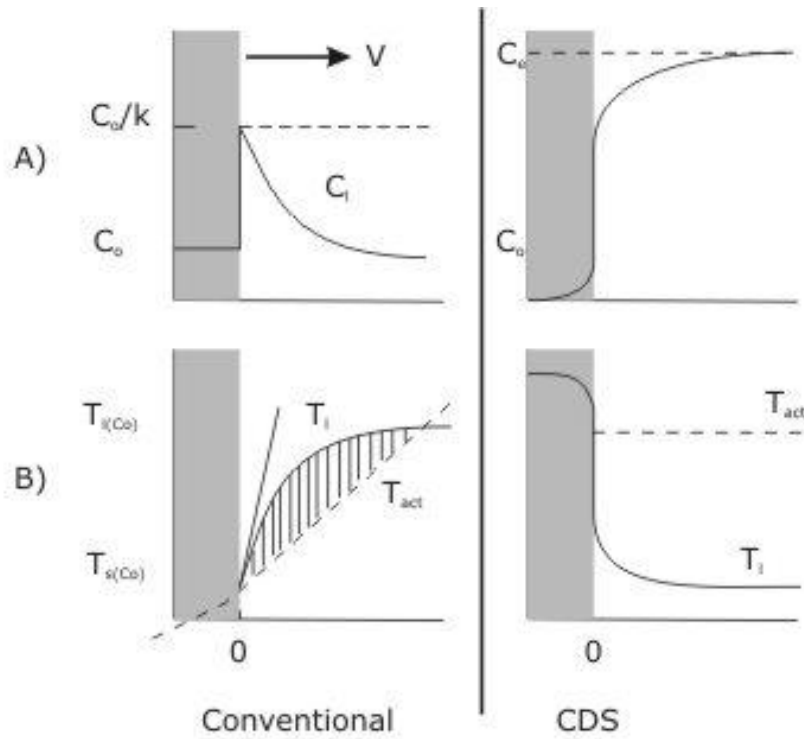


**Fig. 42: Comparison of diffusion boundary layer for growth of a particle under traditional partitioning solidification and under CDS.**

The constitutional undercooling is the main factor that causes the solidification front to break down to cellules or dendrites. Constitutional undercooling exists when the temperature of the liquid metal ahead of the solidification front is below its liquidus temperature. The CDS is a special case because as the particles grow into a solute rich melt it is unlikely that instability will occur due to constitutional undercooling. The difference between the solute fields in the CDS and a conventional casting can be observed in Fig. 42.

In conventional casting the solute profile of the solidification front can be described by the schematic representation of composition ahead of the interface as shown in Fig. 42. The concentration of the liquid decreases away from the solidification front. According to the phase diagram though, the liquidus temperature would increase. This has as a consequence that some parts of the liquid ahead of the interface may find themselves in temperatures lower than their melting point. This is the well known phenomenon of constitutional undercooling and it gives rise to the development of perturbations and thus to interface instability. The constitutional undercooling region is depicted by the cross hatched area in Fig. 42 B.

The situation in CDS is rather different. After the nucleation stage, the aluminum particles are dispersed inside a superheated eutectic liquid matrix. The composition profile is opposite the one in traditional solidification. In Fig. 42 the composition is actually increasing away from the interface. The liquidus temperature will be actually decreasing away from the interface and the constitutional undercooling will be minimal. The solidification will be diffusionally controlled.

Considerations follow with respect to the contributions of undercooling in the various stages of solidification. In the case of a planar interface or an interface with a large radius of curvature, a protrusion that will enter a constitutionally undercooled region will develop into a dendritic branch. In this case equation (5.25) becomes:

$$\Delta T = \Delta T_L + \Delta T_C \quad (5.26)$$

This assumption can only hold for protrusions with large radius  $r$  where the Gibbs Thomson contribution  $\Delta T_r$  is negligible.

On the other side, if the wavelength or radius of the protrusion is very small then  $\Delta T_R$  becomes important and in order for the thermal and constitutional undercooling to be counteracted the following should be true:

$$\Delta T_R \geq |\Delta T_L + \Delta T_C| \quad (5.27)$$

A protrusion with large  $r$  can survive at a planar or a small curvature interface. This will not happen though at an interface with high curvature. The curvature of the protrusion that is forming at a curved interface must be more pronounced:  $r \ll R$

Consider the case of a small nucleus that has reached stability i.e.  $R > R^*$ . During the initial stages of its growth only a protrusion with very small radius can be assumed with  $r \ll R^*$ . So inequality (5.27) will hold and the protrusion will melt back. So as long as (5.27) holds the nuclei will grow in a non-dendritic globular form.

As the solid sphere increases in size larger radius protrusion may form and dendrites will start forming. The importance of the  $|\Delta T_L + \Delta T_C|$  contribution increases as the sphere grows. In order to ensure stability of the globules the contributions of these two factors need to be kept to a minimum. This can be done by forced convection and by slow cooling. As shown in Fig. 42 the solute profile ahead of the solidification interface in the CDS is opposite the one in regular solidification, and constitutional undercooling is hindered.

Due to possible convection and diffusion at low cooling rates, the solute distribution in the liquid close to the solid/liquid interface is more uniform than the solute distribution in a quickly cooled melt. This leads to a lower constitutional undercooling  $\Delta T_C$  which accentuates the Gibbs-Thomson effect and increases the interface stability.

## 5.8 Globular Growth

The last step of the process is to ensure globular stability during growth. Martinez has recently developed a model of globular growth and stability that is unique in that it takes into account the effect of the overlapping of the solute fields. In short, overlapping of solute fields means that the condition of constant concentration away from the interface does not apply. Instead, as solute is rejected from neighboring particles the composition increases and growth is suppressed. This leads to slow growth which is favorable for globular stability.

In the CDS process the nucleated particles find themselves in a similar solute rich matrix. This is favorable for stability, but the effect of the cooling rate also needs to be examined. Increased cooling rate leads to instability of the interface as shown in the experiments in Chapter 4. There is a certain processing window that is left to be determined.

### **Effect of solute fields overlap**

Martinez developed a model that studies the growth of a spherical particle that takes into account the solute field overlap from its neighboring particles.

The model was specifically solved for a particle that undergoes growth with a slow cooling rate of  $0.28\text{ }^{\circ}\text{C}/\text{s}$  up to a  $20\mu\text{m}$  radius and then the cooling rate is increased to  $375\text{ }^{\circ}\text{C}/\text{s}$ . The particle is growing in a spherical field of  $R_T = 50\mu\text{m}$ .  $R_T$  is the spherical volume that occupies the same volume with the solidified grain. So solute is contained within the volume of  $R_T$  and the model can examine the effect of the solute fields overlap on particle growth velocity. This is of great interest as when the fields overlap the growth velocity drops and that in turn favors globular stability.

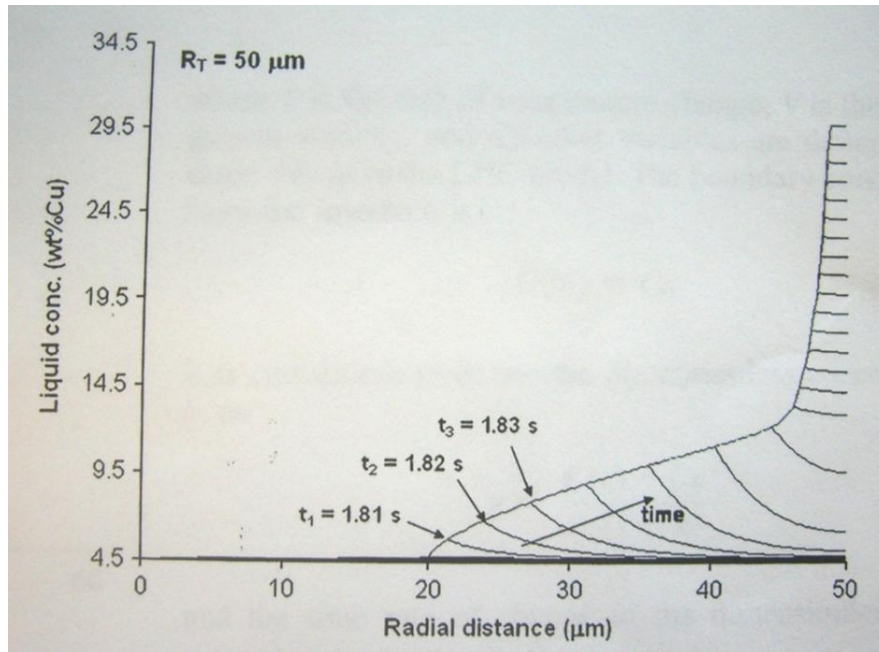


**Fig. 43: Liquid composition vs. radial distance. When the cooling rate increases at  $r = 20\mu\text{m}$  the solute starts to build up at the interface. But when  $r = 40\mu\text{m}$  the solute concentration at  $r = 50\mu\text{m}$  starts increasing and this marks the onset of solute field overlap. Martinez [10].**

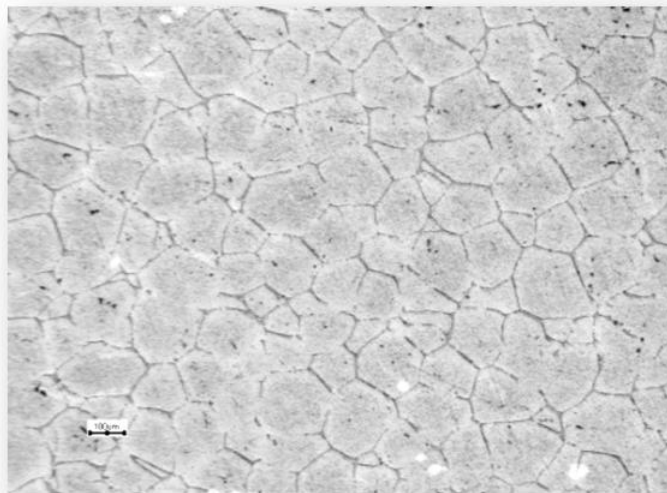


**Fig. 44: Typical Al-4.5wt%Cu microstructure cast via CDS.**

Fig. 43 shows that as soon as the solute fields overlap which means that there is a solute build up at  $r = 50\mu m$  the growth velocity decreases dramatically. That is the case with the CDS. The Al crystals after nucleation are situated in a liquid with excess solute. Therefore, solidification speed will be very slow, which is favorable for the globular stability. In CDS the solute composition of the liquid can be approximated if we know the size and density of the particles. As was shown in the numerical simulations in section 5.4 only the Al striations become undercooled, so it can be assumed that no further nucleation events occur outside of the striations. The size of the Al-particles can be approximated by the composition profile in solute across the grain as shown in Fig. 22. Observing the solute profile, a solute depleted region in the center of the grain is clearly distinguishable. This region represents the Al-particle the moment it gets dispersed in the solute rich matrix and has an average diameter of 40  $\mu m$ . The grain density can be measured from typical CDS microstructures like the one in Fig. 44. The grain density was measured to be 512 grains/ $mm^3$  by ASTM standard E112.

From the above data the composition of the liquid was calculated for different grain densities and Al-grain size.

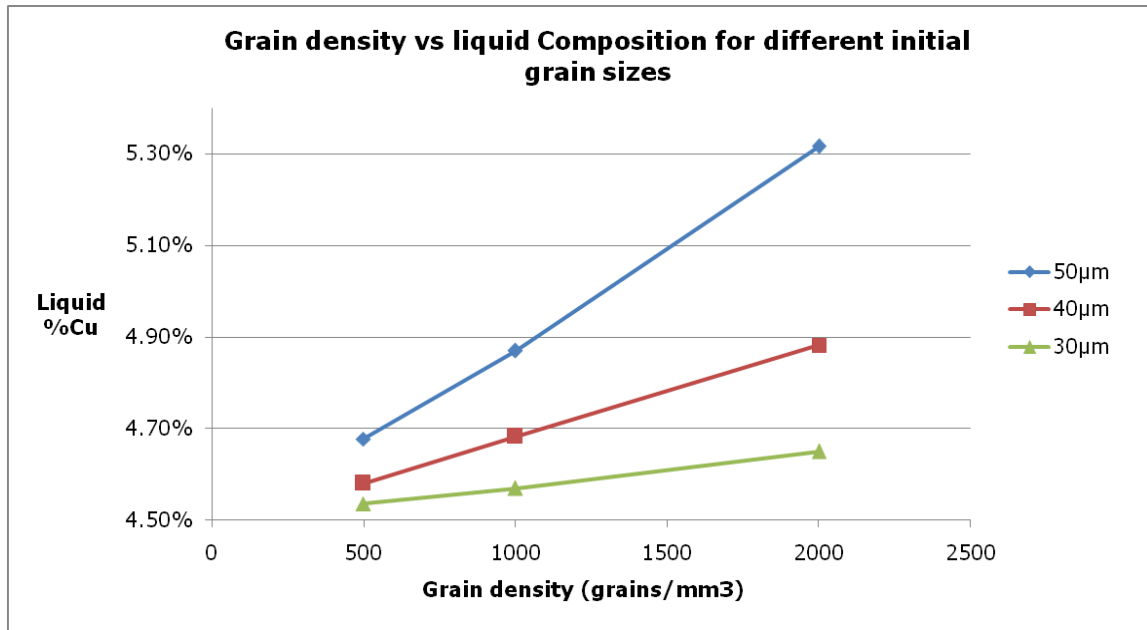


**Fig. 45: Liquid composition and grain density vs initial grain size.**

With the present experimental conditions the CDS refers to a grain size of about 500gr/mm<sup>3</sup> and there is only a small difference in the liquid concentration regarding different initial grain sizes. A smaller grain size translates in a faster dispersion of the Al-particles formed in the striations in the liquid solute-rich matrix which means a faster mixing mechanism as represented by the strain rate  $e_x$  in section 5.5.

### 5.8.1 Globular Stability Analysis

Martinez [10] also developed a model that relates the initial solid fraction in semisolid slurry with the maximum cooling rate, so that a stable spherical front will be maintained. He employs the basic globular stability theory developed by M-S that was presented in the previous paragraphs. While in the M-S study the particle was growing in an infinite field, that is not the case here, as the overlapping of the diffusion field is an added factor. The model is fitted to the experimental data from section 4.5.

The model calculates the maximum cooling rate for a certain grain density and a given fraction solid.

$$f_s = \left[ 1 - C \left( \frac{4\pi N}{3} \right)^{1/3} \left[ \frac{(D_L)^3 \Gamma [m_L C_0 (k - 1)]^2}{(\dot{T}_{max})^3} \right]^{1/7} \right]^3 \quad (5.28)$$

Where:

$f_s$ : Initial fraction solid

C: Prefactor

N: Number of particles per unit volume

$D_L$ : Diffusion coefficient in the liquid

$\Gamma$ : Gibbs Thomson coefficient (interface energy)

$m_L$ : Liquidus slope

$C_0$ : Alloy concentration

$k$ : Alloy partition coefficient

$\dot{T}_{max}$ : Maximum process cooling rate

Data used for the calculations is given in Table XIII.

Quantity	Symbol	Units	Value
Solute diffusivity in liquid phase	$D_L$	$m^2 s^{-1}$	$3 \cdot 10^{-9}$
Slope of liquidus line	$m_L$	$^{\circ}C wt\% Cu^{-1}$	-3.4
Alloy partition coefficient	$k$		0.19
Bulk solute concentration	$C_0$	$wt\% Cu$	4.5
Gibbs-Thomson coefficient	$\Gamma$	$mC^{\circ}$	$2.4 \cdot 10^{-9}$

**Table XIII: Thermochemical and physical properties of Al-4.5%Cu alloy.**

Experimental results in Chapter 4 exhibited similar behavior. Increase in cooling rate leads to a breakdown of the interface to dendritic as shown in Fig. 24. By fitting the

model to the experimental results Fig. 46 is obtained. In order to apply the process to CDS a prefactor of 1.2 is added to (5.28).

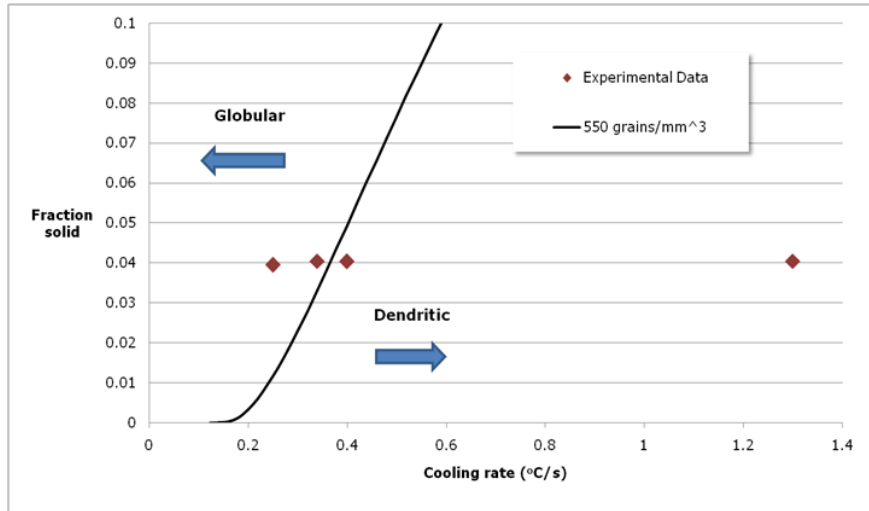


**Fig. 46:** The graph shows the stability region for an Al-4.5wt%Cu alloy under cast via CDS under different cooling rates. The left of the curve denotes stability and the right indicates instability of the front. From the above graph the combinations of fraction solid and maximum cooling rate can be extracted that ensure stable globular growth.

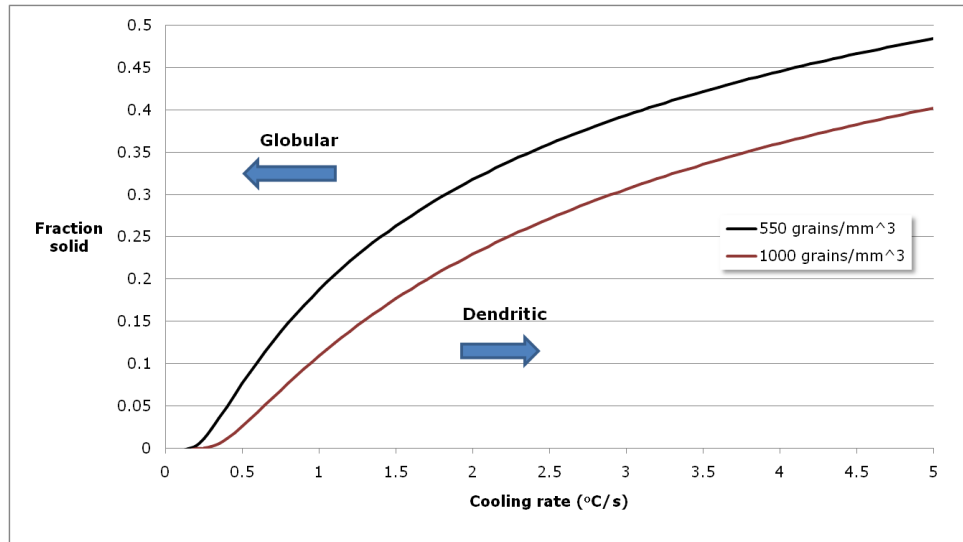


**Fig. 47:** The graph compares the stability region of the Al-4.5wt%Cu alloy for different fraction solid and cooling rate combinations. The higher the solid fraction and the grain density, the higher the maximum cooling rate is.

Martinez model is applied to semisolid processing. In that case the alloy was held isothermally and allowed to reach equilibrium in the semisolid state. Then a cooling rate was applied and the microstructure was examined for stability. The difference in CDS is that the alloy is not at equilibrium. There will be a small increase in solute in the liquid since the Pure Al particles consume part of the total Al. Therefore the  $c_0$  is also modified to be the concentration of the liquid after mixing, taking into account the solidified Al particles. The liquid concentration can be calculated by approximating the total weight of the pure Al particles. In Fig. 46 the average grain size of all experiments is 550 grains/mm<sup>3</sup>, typical of a CDS casting. The fraction solid represents the solidified Pure-Al particles. On the left of the curve are the favorable combinations of cooling rate and fraction solid for stability, while the right of the curve denotes instability of the front. It is obvious that stability is favored by high particle density, high fraction solid and low cooling rates. From this graph casting parameters may be extracted that ensure globular microstructure.

Another important point that should be stated is that the operating window of the CDS may be affected by the casting technique. For example for gravity casting the fraction solid should be less than 20% solid. The max cooling rate of 0.4°C/s is close to the limits of sand casting. Fig. 47 shows that a higher grain density will enable faster cooling rates. Thus the addition of grain refiner may be necessary. For higher fraction solid a shear force may need to be applied to fill the mold similar to semi-solid casting processes. As shown in Fig. 47 a higher fraction solid will also allow for higher cooling rates.

## 5.8.2 Discussion

From the preceding analysis it can be seen that the formation of spherical primary aluminum particles is a result of the combined effects of rapid nucleation and absence of constitutional undercooling at the latter stages of solidification. It should be pointed out that when an aluminum alloy is cast via the CDS, precipitation of Aluminum particles occurs in the Pure Al melt before the Cu diffuses and the liquid becomes homogeneous. If these in situ formed aluminum precipitates become large in size before the end of mixing, they can increase the solute concentration in the liquid.

For example an Al-4.5wt%Cu alloy was cast with the CDS. The initial liquids were Pure Al and the Al-33wt%Cu eutectic. Since this is a simple system there are not many possible configurations for the initial liquids compositions. However the selection follows the guideline that there should be a high  $\Delta T$  between the two liquidus lines and both the liquids should be close to their respective liquidus temperatures upon mixing. The two liquids  $\Delta T$  ensures high undercoolings, which provide a high nucleation potential. By employing the thermal-solute mixing model in section 5.5, the nucleation potential can be calculated. Due to the configuration of the initial liquids, only Pure Al particles nucleate. The particles grow in the Pure Al until the solute diffuses inside the Al striations as shown in section 4.3. With the present experimental setup the solute reaches the center of the striations at 0.5 sec. After that point the mixture is considered homogeneous and is comprised of pure Al particles in a solute rich matrix. Note that the liquid composition in solute is now higher than the target alloy since the Aluminum in the alloy is "consumed" by the Al particles. The size of the Al particles can be approximated by an EDX line scan across a grain. As is shown in Chapter 4 the pure Al particles have a size between 30-40 $\mu\text{m}$ . This increases the solute concentration in the liquid by 0.2% and decreased the

liquidus of the liquid. This in combination with a slow cooling rate ensures absence of constitutional supercooling which is the main factor for the breakdown of a planar front to dendritic. The max cooling rate for globular stability can be approximated with the modified stability model. Experiments presented in Chapter 4 show that the max cooling rate for an Al-4.5wt%Cu alloy is 0.4°C/sec. These cooling rates are representative of sand castings, and investment castings. It is here that the CDS can have an impact since these processes are limited to casting alloys. Hot-tearing prone alloys should be reconsidered since CDS has the ability to reduce the hot-tearing tendency as shown experimentally for a hot-tearing prone alloy in Chapter 4.

The guidelines of this Thesis are confirmed to a high degree by the results of casting experiments. Following is a case study of wrought alloy 2014.

### **Casting of 2014 Alloy via CDS**

In order to demonstrate the applicability of the CDS method to casting wrought alloys that belong to the 2xxx system, the CDS method was used to cast 2014 alloy having the nominal composition shown in Table XIV. Note that 2014 is very close in composition with the Al-4.5wt%Cu alloy that was the main focus of the experimental work in the present thesis. 2014 is an important alloy, as it exhibits very high strength and good machinability among other heat-treatable alloys. It is mainly used in forgings. As a wrought alloy it is plagued by a high hot tearing tendency. Following the guidelines of this thesis the successful casting and reduction in hot tearing tendency of 2014 is demonstrated.

Element	Weight %
Al	93.5
Si	0.8
Cu	4.4
Mg	0.5

**Table XIV: 2014 Chemical composition.**

When the alloys become more complicated there are more possibilities of forming the initial composition of the two liquids. The main guideline is to create a high  $\Delta T$  between the liquidus of the two liquids that will ensure a high undercooling. In the present case study the liquidus difference of the two alloys is  $98^{\circ}\text{C}$ . Assuming the Liquidus difference was smaller, then the high temperature liquid wouldn't be partially quenched during mixing and would follow the alloying path described and demonstrated in Chapter 4. Also if grain refiner is to be used as in Chapter 4 it should be included in the high temperature liquid since it would enhance the nucleation. In the present casting no grain refiner was added. It should also be pointed out that in order to obey the modified stability criterion the mold was preheated at  $300^{\circ}\text{C}$ .

Attempting to directly cast a 2014 alloy in an intricate shape is a real challenge. This can be clearly seen in Fig. 48 and Fig. 49. The ring mold setup that was described in Chapter 4 enforces hoop stresses due to shrinkage during solidification. A dendritic microstructure renders the casting prone to hot-tearing. Casting via the CDS method provides dramatically reduced hot-tearing tendency. Alloy #1 and alloy #2 were mixed following the procedures described in Chapter 4. Their respective composition is listed in Table XV. The hot tearing-free casting is shown in Fig. 50.

<b>Chemical analysis:</b>	<b>Alloy #1</b>	<b>Alloy #2</b>
Al (weight gr)	720	51
Cu (weight gr)	0	36.73
Si (weight gr)	0	6.61
Mg (weight gr)	0	4.24
Liquidus temperature (°C)	660	562
Mixing Temperature (°C)	665	570
Liquidus temperature of 2014 alloy (°C)	641	

**Table XV: Chemical Analysis, Weight Fraction, and Temperature of the Initial Alloys Used in Casting 2014 Alloy via CDS.**



**Fig. 48: 2014 - Regularly cast - Hairline Hot Tear.**



**Fig. 49: 2014 – Regularly cast – Moderate crack.**



**Fig. 50: 2014 – Cast via CDS – No crack.**

## 6. Conclusions

The CDS process is a novel means of casting an alloy of a given composition by mixing two liquid entities of different compositions (and thus different solute amounts) as well as two different volumes of the two liquids. The process allows one to alleviate the casting issues that are encountered when casting alloys that have hot tearing tendencies – i.e., wrought Al alloys.

The following conclusions can be made from this work:

1. The governing mechanism of the Controlled Diffusion Solidification casting process was investigated and verified with experimental results. The nucleation mechanism was identified to occur in the undercooled Al-striations. The parameters for interface stability were also identified and investigated experimentally and theoretically.
2. The underlying mechanism is explained on the basis of mixing considerations, initial conditions and evolution of thermal and solute fields. Specifically, in order for the solid phase to nucleate and grow in a globular morphology, the two precursor alloys need to be mixed in suitable conditions that will follow the reaction-mixing mode. The reaction mixing mode requires that the mixture's temperature is in the semi-solid region of the phase diagram. This forces rapid nucleation due to the high degree of undercooling in the Al-striations.
3. The underlying mechanism and the knowledge of the CDS process can be extended to other alloying systems. From a commercial perspective, foundries can take advantage of the hot-tearing free castings produced via CDS with shorter solidification times and cast wrought alloys without the hot-tearing issues.
4. CDS can be readily applied in sand and investment castings. The application in higher cooling rate casting processes may require the addition of grain refiners.

5. The operating window of the process was established to be 10°C, and the maximum cooling rate 0.4°C/sec. Higher cooling rates may be achieved by allowing a higher fraction solid before casting. In fraction solids above 20% external force should be applied to fill the cavity.

6. Successful casting of alloys via the CDS was demonstrated. Al alloys 206 and 2014 exhibited globular microstructure and the hot-tearing reduction was demonstrated in both alloys.

## 7. Suggestions for Future Work

The present work has provided fundamental understanding of the CDS's governing mechanisms. Future work should focus in direct implementation of the process in an industrial setting.

Proposed work:

- Establish mechanical properties of alloys cast via the CDS.
- Design of a dedicated CDS casting apparatus. The apparatus should include two separate furnaces and volumetric control for the flow. The volumetric mixing is important so that the developed model can be more accurately applied.
- While the Al-Cu system has been the main focus of this dissertation, other systems should be examined as well. The most favorable systems would be the ones with high temperature differences between the pure and the eutectic liquid and high eutectic content. Such systems are: Al-Si, Al-Mg, Al-Zn.
- In this dissertation, the reduction in hot tearing of alloys cast via CDS has been confirmed. However, extensive work needs to be done in that field to further understand the effect of the microstructure on hot-tearing tendency.

## 8. References

- [1] D Apelian, G Langford. *Rapid Cycle Casting of Steel*. 1977.
  
- [2] Massalski, T.B. Binary Alloy Phase Diagrams. *Binary Alloy Phase Diagrams*. 1990.
  
- [3] D Saha, S Shankar, D Apelian, MM Makhlof. Metallurgical and Materials Transactions A, 2004.
  
- [4] D Saha, S Shankar, D Apelian, MM Makhlof. *Casting of aluminum based wrought alloys and aluminum based cast alloys via controlled diffusion solidification*. Dec 2, 2004.
  
- [5] Lin, S, Aliravci, C and Pekguleryuz, M O. Metallurgical and Materials Transactions, 2007.
  
- [6] Suyitno, D.G. Eskin, , and L. Katgermana. Materials Science and Engineering A , 2006.
  
- [7] D.G. Eskin a, Suyitno, L. Katgerman. Progress in Materials Science , 2004, Vol. 49.
  
- [8] M.Rappaz, P. Grasso, V. Mathier, J. Drezet, A. Jacot. TMS, 2004, Vols. p. 179-90.

- [9] Joseph R. Davis, J. R. Davis & Associates, ASM International Handbook Committee. *Aluminum and Aluminum Alloys*. ASM International, 1993.
- [10] M.Rappaz, J Drezet, M Grameaud. *Metallurgical and Materials Transactions A*, 1999, Vol. 30A.
- [11] Ottino, J. M. *The Kinematics of Mixing*.
- [12] Diran Apelian, Qingyue Pan, Makhlof M. Makhlof. *Low Cost and Energy Efficient Methods for the Manufacture of Semi-Solid*. D.O.E., 2005.
- [13] William J. Bernard, III. *The Continuous Rheoconversion Process*. W.P.I., 2005.
- [14] Uggowitzzer, P. J. Kaufmann, H. *Steel Research International*, 2004, Vol. 75.
- [15] R. A. Martinez, A. Karma, M.C. Flemings. *Metallurgical and Materials Transactions A*, 2005, Vol. 37.
- [16] G. Sigworth, T. Kuhn. 1, *International Journal of Metalcasting*, Fall 2007, Vol. 1.
- [17] Davies, V. de L. *The British Foundryman*, 1970, Vol. 63.
- [18] DeHart, G. Sigworth F. *AFS Transactions*, 2003.
- [19] W.A.Schneider, T.E. Quested, A.L. Greer, P.S. Cooper. *LMT*, 2003.

- [20] Wannasin J, Schwam D., Yurko J.A, Rohloff C., Woycik G. Solid state phenomena Part B, 2006, Vols. 116-17.
- [21] Pantelakis, N.D. Alexopoulos Sp. G. Springer NY, 2007, Vol. 12.
- [22] Novikov II, Grushko OE. 926, Mater Sci Technol, 1995, Vol. 11.
- [23] Singer ARE, Jennings PH. 197, J. Inst. Met., 1947, Vol. 73.
- [24] J-M, Drezet. 53, Journal de Physique IV, 1999, Vol. 9.
- [25] WW Mullins, RF Sekerka. Journal of Applied Physics, 1963, Vol. 34.
- [26] Danckwerts, Peter V. Appl. Sci. Re, 1952.
- [27] S. Rogers, L. Katgerman, P. G. Enright and N. A. Darby. 1, Applied Scientific Research, 1987, Vol. 44.
- [28] P. G. Enright, L. Katgerman, J. C. Ludwig, S. Rogers. 1, International Journal for Numerical Methods in Engineering, 1986, Vol. 24.
- [29] Ranz, WE. 9, AIChE, 1979, Vol. 25.
- [30] Ohmi, K Matsuura, M Kudoh, Y Itoh. 1, JJILM , 1998, Vol. 48.
- [31] Y., OHMI T. MATSUURA K. KUDOH M. ITOH. 2, 1997 , Vol. 47.

- [32] Y., OHMI T. MATSUURA K. KUDOH M. ITOH. 12, 1998, Vol. 48.
- [33] K. Symeonidis D.Apelian, M.M.Makhlouf. LMT, Vol. 2006.
- [34] Christian, JW. *The Theory of Transformations in Metals and Alloys: An Advanced Textbook in Physical Metallurgy*. Pergamon, 1975.
- [35] Turnbull, D. J. Appl. Phys, 1950.
- [36] Turnbull, D. 198, J. Chem. Phys., 1950, Vol. 18.
- [37] Herlach, D M. Annual Review of Materials Science, Vol. 21.
- [38] Flemings, G. J. Abbaschian and M. C., Metallurgical and Materials Transactions A, 1982 , Vol. Volume 14.
- [39] Oxtoby, D.W. 38, Journal of Physic: Condensed Matter, 1992, Vol. 4.
- [40] Qian, Ma. Acta Materialia, 2006, Vol. 54.
- [41] Xia K, Tausig G. 1, Mater Sci Eng A , 1998, Vol. 246.
- [42] Wang H, Davidson CJ, StJohn DH. In: Chiarmetta GL, Rosso M. Turin, Italy; : Proceedings of the 6th international conference on semi-solid, 2000.
- [43] Zhang JX, Zhang K, Liu GJ, Xu J, Shi LK. Chinese J Nonferrous, 2000, Vol. 10.

- [44] WW Mullins, RF Sekerka. *Journal of Applied Physics*, 1964, Vol. 35.
- [45] Woodruff, D.P. *The solid-liquid interface*. Cambridge : Cambridge University Press, 1973. p. 85.
- [46] Lawley, A. *J. of Metals*, 1981, Vol. 33.
- [47] G Langford, D Apelian. *J. of Metals*, 1980, Vol. 32.
- [48] Sreshta, Harry. *Diffusion Solidification Kinetics and Casting Machine Design*.
- [49] Herlach, Dieter M. *Materials Science and Engineering*, 1997.
- [50] Flemings, MC. *Solidification processing*. Metallurgical and Materials Transactions B, 1974 .
- [51] Coriell, S. 1, *Journal of Crystal Growth*, 1976, Vol. 32.
- [52] Suyitno, D.G. Eskin, L. Katgerman. *Materials Science and Engineering A*, 2006.
- [53] G Langford, RE Cunningham. *Metallurgical and Materials Transactions B*, 1978 .
- [54] JJ, Hyott. 65, *Phys Rev B*, 2002.

## 9. Appendices

### 9.1 Appendix I: Published Work

- A. K. Symeonidis, D. Apelian, M. M. Makhlof, "Controlled Diffusion Solidification: Application to Metal Casting", *La Metallurgia Italiana*, March 2009 (*in press*)
- B. K. Symeonidis, D. Apelian, M.M. Makhlof, "Study of Undercooling Mechanism in the Al-Cu Alloy System Cast via Controlled Diffusion Solidification (CDS) Process", *NADCA Transactions*; published by NADCA, Cast Expo, May 2008.
- C. K. Symeonidis, D. Apelian, M. M. Makhlof, "Controlled Diffusion Solidification: Application to Metal Casting", *Proceedings of the 4<sup>th</sup> International High Tech Die Casting Conference (HTDC 2008 Brescia, Italy, April 2008) – Paper #39 (Invited Paper)*
- D. K. Symeonidis, D. Apelian, M. M. Makhlof, "Controlled Diffusion Solidification", *International Foundry Research/Giessereiforschung* 60 (2008) No. 1 pp. 2 - 8
- E. K. Symeonidis, D. Apelian, M. M. Makhlof, "Controlled Diffusion Solidification: Application to Metal Casting", *Metallurgical Science & Technology*, Vol. 26-1, pp 30-36, 2008.
- F. K. Symeonidis, D. Apelian and M.M. Makhlof, "Controlled Diffusion Solidification", in the *Proceedings of LMT – Light Metals Technology 2007*, September 2007, Saint-Sauveur, Québec, CA, published by CANMET.

# Controlled Diffusion Solidification

**K. Symeonidis, D. Apelian, and M. M. Makhoulf**

Advanced Casting Research Center  
Metal Processing Institute, WPI, Worcester (USA)

## ABSTRACT

Wrought aluminum-based alloys exhibit superior physical and mechanical properties compared to conventional shape casting alloys. However, wrought alloys cannot be cast into near net shapes because they develop hot tears and hot cracks during solidification. For this reason, these alloys are typically cast into ingots and are subsequently brought to final shape by mechanical processes such as rolling, extrusion, drawing and forging. These processes significantly increase the cost of the manufactured component. **Controlled Diffusion Solidification** (CDS) is a novel process that allows casting of wrought alloys directly into final shapes that are free of hot tears, thus CDS eliminates the added cost of machining. The process follows a different route from conventional casting methods. In CDS two liquid alloys of predetermined composition and temperature are mixed together so that upon solidification the resultant alloy has a globular rather than a dendritic microstructure. The hot tearing tendency of wrought alloys originates from the inadequate permeability of their dendritic network, which obstructs the flow of interdendritic liquid and hinders compensation for shrinkage. The nondendritic microstructure made possible by CDS minimizes hot-tearing thus enabling wrought alloys to be cast directly.

**Keywords:** *wrought Al alloys, cast alloys, hot tearing, diffusion solidification*

## INTRODUCTION

Controlled Diffusion solidification (CDS), a concept that was first introduced by Apelian and Langford in 1980 [1], and further developed by Shankar et al [2] is a process that provides alloys with globular microstructure by mixing two liquid alloys. Previous work utilizing CDS has been shown to provide globular microstructures in various alloy systems [2] but the underlying principles that govern formation of the globular microstructure are yet to be understood. The present study is intended to quantify the effect of various process variables on the formation and the stability of the globular morphology and specifically to establish an operational window for the process. Work on the mechanism and the theoretical framework is ongoing at WPI.

In separate sets of experiments the effect of superheat of the liquid aluminum (which is mixed with a lower temperature liquid alloy), the effect of cooling rate, and the effect of adding grain refiner additions to the melt were investigated.

## BACKGROUND

The challenge we face in the CDS process is the mixing of two melts that are both near their respective liquidus temperatures. Experimentally, we have verified with various different Al based systems that through this reaction-mixing process we can obtain globular microstructures.

In most casting processes the master alloy is melted in the furnace and alloying elements are added subsequently. Upon stirring, either mechanically or through Lorentz forces the liquid melt becomes homogeneous and is then poured. In the CDS process we start with a relatively pure liquid metal near its melting point, and pour it into a second alloy melt, which is near its liquidus. Figure 1 illustrates the CDS process; in this case, commercial grade Pure Al is mixed with Al-33%Cu.

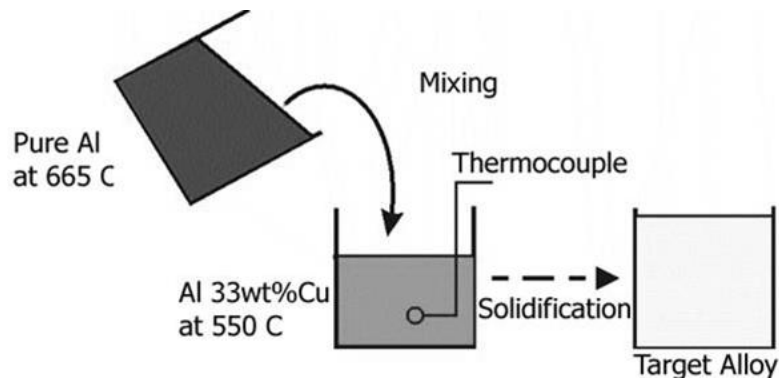


**Figure 1:** Schematic illustration of the CDS process applied. Pure Al is poured into a eutectic Al-33wt%Cu melt. The process temperature is monitored by means of a thermocouple that is submerged in the eutectic melt. Melting points: Al: 659°C; Al-33wt%Cu: 545 °C.

The reason why this process is different from the traditional mixing of the alloying elements in a furnace is that in CDS solidification and liquid diffusion are coupled as soon as the two liquids come into contact. Specifically, let us explore what happens upon contact of the two liquid masses. Assuming a hypothetical binary phase diagram with a eutectic point as in Figure 2.  $C_e$  is the eutectic concentration and  $C_o$  is the target alloy composition. There are three ways by which the two liquid melts may mix depending on their temperature and relative weights.

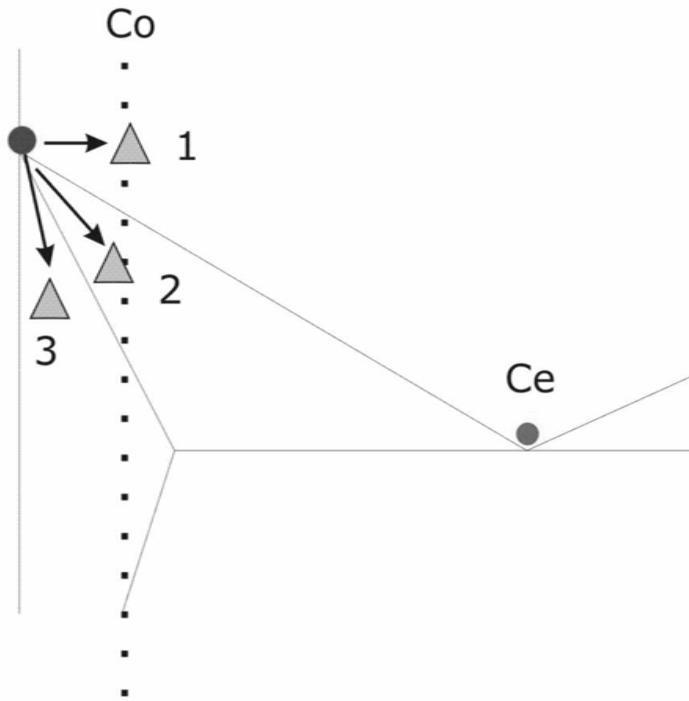


**Figure 2:** Hypothetical phase diagram with initial two compositions pure element (i.e., Al) and Ce (eutectic composition) showing three possible mixing paths; namely, ( 1 ) alloying , ( 2 ) reaction mixing, and ( 3 ) quenching.

*Path 1: Alloying in the liquid state*

If the two melts have enough superheat, they will form a homogeneous liquid melt with the target composition Co. This liquid melt will solidify with a dendritic microstructure.

*Path 2: Reaction Mixing – CDS*

If the superheats are controlled, such that the resulting alloy is in the two-phase region and reaction mixing will occur giving rise to a globular microstructure.

*Path 3: Quenching*

If the eutectic liquid mass is substantially larger than the pure liquid mass, then the pure liquid mass will be partially quenched, resulting in segregation.

Experiments were conducted to establish processing conditions that lead to *Path 2*. In brief, it has been determined that the two respective superheats of two melts and the ratio of the thermal masses are key factors that provide the limiting values for globular microstructure formation.

In general, when two alloy melts of controlled composition and temperature are brought together, two events occur: (1) thermal equilibration by the redistribution of thermal energy in the resulting alloy *via* conduction and convection, and (2) chemical equilibration by mass diffusion across the liquid interfaces. Figure 3 illustrates that once the solid has nucleated from the liquid, the absence of constitutional

undercooling during the early stages of growth and convection leads to the development of a planar interface, and thus a globular primary phase [3].

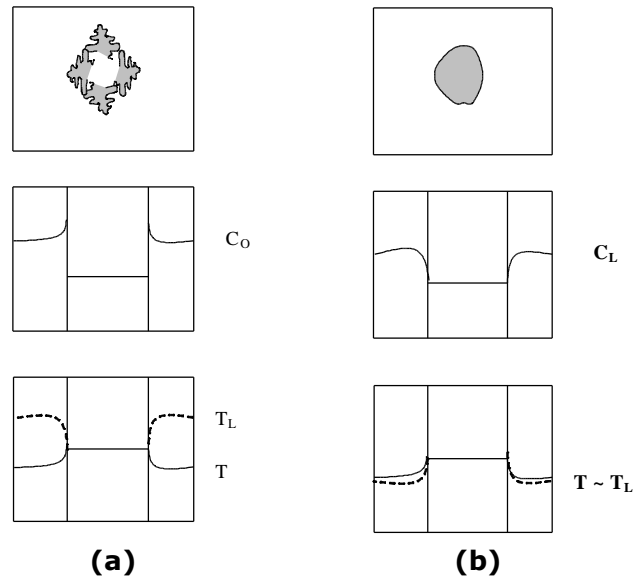


**Figure 3:** **a)** Schematic showing constitutional undercooling in a free growing dendrite in an under-cooled melt. The alloy has an initial composition of  $C_0$ , the solute is rejected across the interface, leading to a drop in the liquidus temperature ( $T_L$ ) ahead of the interface. The region between the actual temperature of the liquid ( $T$ ) and  $T_L$  leads to the breakdown of a planar interface into a dendritic structure; **b)** Schematic showing the condition when a liquid of composition  $C_L$  (i.e., Al-33%Cu) is mixed with Pure Al. Clearly, growth of the structure follows the liquidus line, leading to minimal or no constitutional undercooling, and leading to a non-dendritic structure [3].

In Figure 4 micrographs are presented of samples, which were prepared following the three paths shown in Figure 2. The system is Al - Al-33wt%Cu; Pure Al being one melt, and the eutectic composition being the other melt.

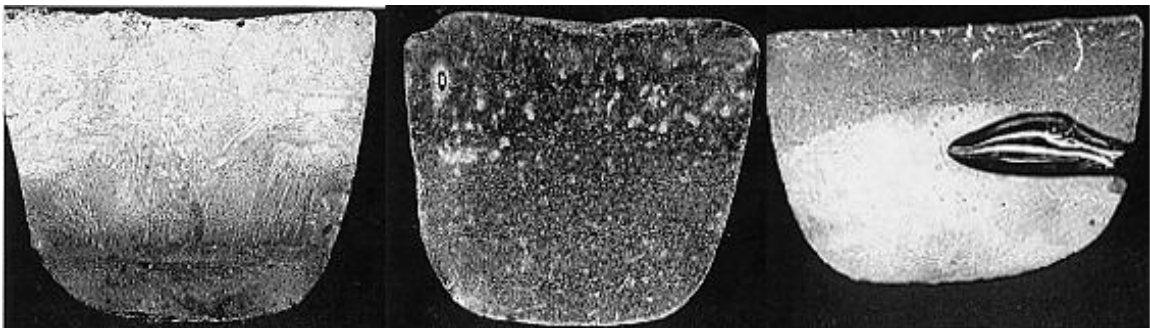


**Figure 4:** From left to right - 1) Homogeneous liquid solidifying, 2) Reaction mixing, and 3) Quenching.

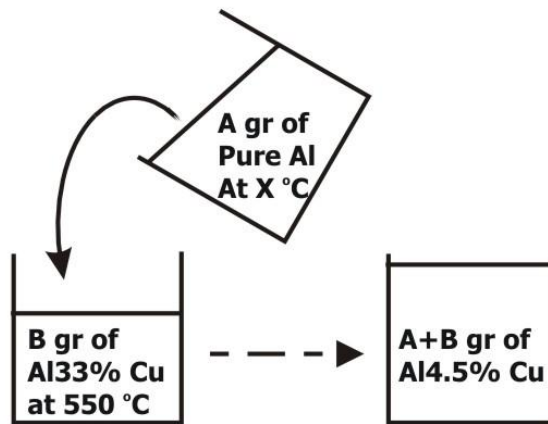
The first sample (far left in Figure 4) was mixed with high superheats for both melts and the mixture was left to solidify. Mixing the melts with high superheats leads to the creation of a homogeneous liquid alloy with target concentration  $C_0$ . As shown in

Figure 4, the microstructure is dendritic and some segregation is evident because the copper is heavier and settles.

The second sample (center of Figure 4) followed the reaction-mixing path and two areas can clearly be distinguished. On the top is the dendritic region and on the bottom the globular region. The dendritic zone is most likely due to settling of the globular grains. Similar results have been reported in the literature regarding grain settling but with a different grain refining method [4].

The third sample (far right, Figure 4) was produced by mixing a small quantity of liquid aluminum with a larger quantity of eutectic melt. The result was immediate quenching of the Al as it entered the crucible and minimum mixing between the two liquids. Air entrapment is due to rapid solidification that occurred.

As shown in Figure 5, 300g of Pure Al liquid is kept at a controlled temperature in the resistance furnace. A thermocouple placed in the center of the melt monitors the melt temperature. In the Induction furnace, 50gr of Liquid Al-33wt%Cu is maintained at 650-700°C. The liquid Al-33wt%Cu is taken out of the furnace and placed on a refractory material. A thermocouple is inserted at the center of the melt and the temperature is monitored. When the Temperature drops to 550°C the Pure Al is poured in the Al-33wt%Cu crucible (Figure 5). The alloy is left to solidify at room temperature or with forced convection. Thermal curves are recorded and analyzed and micrographs are taken from various cross-sections.



**Figure 5:** Schematic diagram of mixing process.

#### **SAMPLE PREPARATION FOR MICROSTRUCTURE EVALUATION**

Samples were cut vertically in half with a SiC cutting wheel and one side was ground and polished with Struers SiC papers using water as a coolant. Subsequently, the samples were etched using Keller's Reagent (2.5 % HNO<sub>3</sub>, 1.5 % HCl, 0.5 % HF, balance H<sub>2</sub>O) for approximately 7-8 sec. Micrographs were taken from the bulk of the sample.

## SENSITIVITY OF PROCESSING VARIABLES

### Effect of Superheat

The effect of superheat of the Pure Al melt was investigated in these experiments. Three levels of superheat were evaluated, each differing by 10 °C – see Table I, below. The results show that at the higher superheat value of 682 °C the microstructure is composed of rosettes, while at lower superheats it is globular. The maximum superheat that provides globular microstructure defines the operational window. A large operational window is vital for the process, because tighter processing parameters mean reduced flexibility and increased cost in controlling the process.

**Table I:** Mixing parameters and data from thermal curves.

Al Pouring T (°C)	Al-33wt%Cu T(°C)
<b>662</b>	549
<b>671</b>	549
<b>682</b>	550

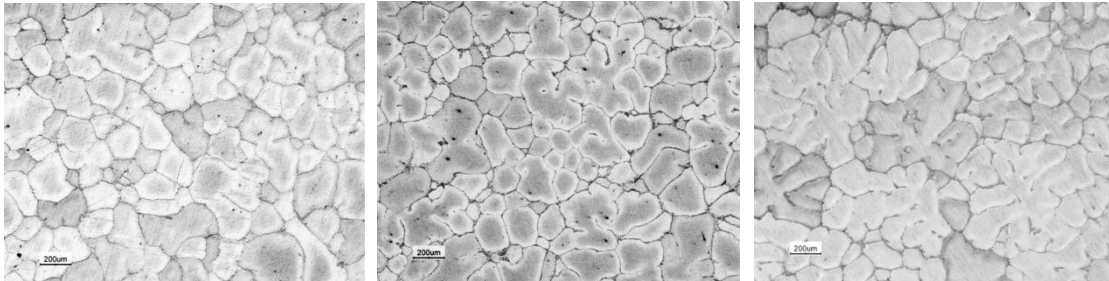


**Figure 6:** Representative microstructures from the center of the samples. Left: Al Superheat: 662 °C, middle: 671 °C, right: 682 °C.

### Effect of Cooling Rate

In order to achieve globular microstructures a high nucleation rate should be followed by a slow cooling rate. At high cooling rates the evolving globular grains become unstable and become dendritic. No grain refiners were added to the system. The addition of a grain refiner would enhance the nucleation and globular stability could be attained at even higher cooling rates.

The same experimental setup is employed as above; after the melts have been mixed, three different cooling rates were imposed. The experimental results confirm the hypothesis – see Figure 7. Increased cooling rate leads to instability of the globular phase and the resulting microstructure becomes dendritic. The lower the

cooling rate the more uniform and globular the microstructure is as more time is allowed for diffusion.

This result may seem to constrain the CDS process only to casting processes with a slow cooling rate. However the above results are without the presence of any alloying elements. With the presence of a grain refiner higher cooling rates should be achievable.

**Table II:** Cooling rates and mixing temperatures.

Cooling Rate °C/sec	Al Temp (°C)	Al-33wt% Cu Temp (°C)
<b>0.25</b>	660	547
<b>0.4</b>	660	552
<b>1.3</b>	660	548

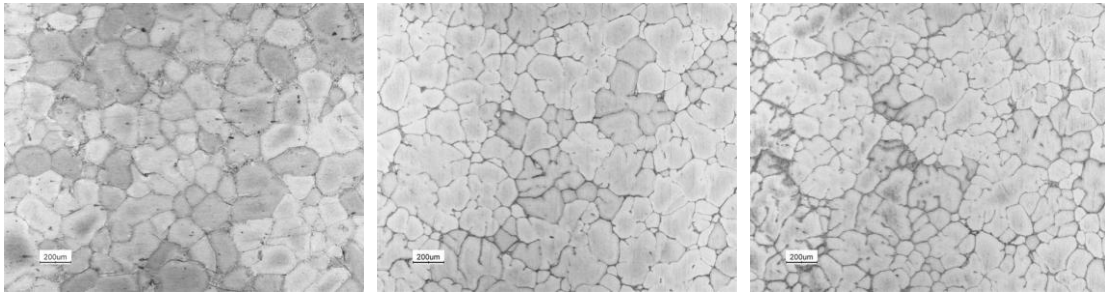


**Figure 7:** Representative microstructures from the center of the samples. Cooling rates: left: 0.25 °C/sec, middle: 0.4 °C/sec, right 1.3 °C/sec. Lower cooling rates favor globular microstructure.

### **Effect of Grain Refiner Addition**

When the liquid Al comes into contact with the eutectic melt it cools rapidly and nucleation commences. To investigate the effect of grain refiners added to the melt (additional nuclei), two experiments were carried out. In the first, the grain refiner Al-5wt%Ti-1wt%B was added to the Pure Al prior to mixing. In the second, the GR was added to the eutectic Al-33wt%Cu prior to mixing. Finally an alloy with the target composition with grain refiner was conventionally cast.

As can be seen in Figure 8, the degree of grain refinement is much higher when the grain refiner is added in the Pure Al. Grain size is smaller and the grains are uniform throughout the sample. In the other two cases there does not appear to be significant difference in grain size.

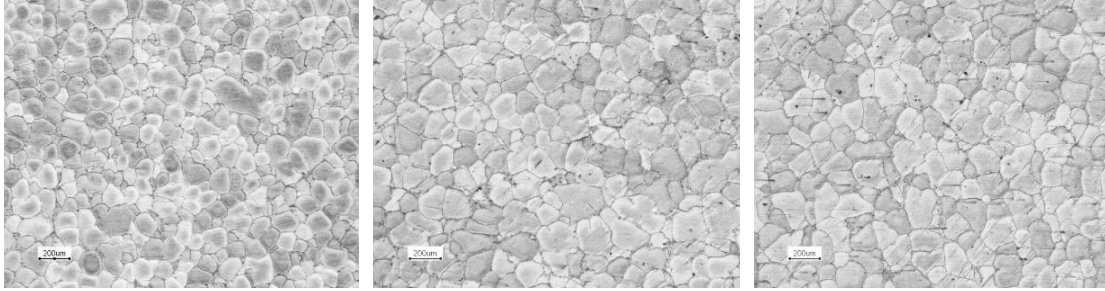


**Figure 8:** Representative microstructures from the center of the samples. Left: Grain refiner Al-5wt%Ti-1wt%B added to the Pure Al; middle: Grain refiner added to the eutectic melt; right: Al-4.5wt%Cu grain refined and traditionally cast.

### **EFFECT OF EXPERIMENTAL VARIABLES - CONCLUSIONS**

Following conclusions are drawn:

- Globular microstructure is attainable with Al superheat up to 10 °C.
- Lower cooling rates favor the stability of globular growth
- Presence of grain refiner (GR) eliminates the dendritic zone due to increased nucleation
- Nucleation rate and microstructure quality increases significantly when the GR is added to the Pure Al melt.
- Processing variables are such that the operating window for CDS is commercially viable.

Globular microstructures and reduced grain size should minimize hot-tearing tendency of difficult to cast alloys. The binary alloy systems that should be more flexible and more efficient in obtaining globular microstructure are the ones with higher eutectic points, and the ones that have a large temperature difference between the eutectic and the pure phase. The high composition difference ensures higher diffusion rates, and the temperature difference provides a larger operational window.

### **APPLICATION OF CDS FOR COMMERCIAL ALLOYS**

Two sets of experiments were performed in order to illustrate the preceding principles for formation of a solid phase with a globular microstructure by mixing two liquids. The materials used in the experiments are commercially Pure Aluminum, Al-33% Cu, and Al-12.8%Si [constituted from commercially Pure Aluminum (99.9% Purity) and pure Si (99.99%)]. The chemical composition of the starting materials as well as the Al-32.3 %Cu and Al-12.8%Si alloys were determined using spark emission spectrometry<sup>5,6</sup>, and are given in Table III.

<sup>5</sup> Model Spectro Lab-Max LMXM3, Spectro Analytical Instruments, Fitchburg, MA, USA.

<sup>6</sup> Accuracy of the spark transmission spectrometer is Si  $\pm 0.3$ , Fe  $\pm 0.0003$  when Fe < 0.01, and  $\pm 0.0022$  when Fe > 0.1. Other relevant elements show negligible measurement errors.

**Table III:** Chemical Composition of Materials Used.

	Si	Cu	Fe	Mg	Mn
Commercially Pure Al	0.5-0.8		0.5-0.8	0.2 max.	0.2 max.
Al-32.3 %Cu master alloy	0.07	33	0.11		
Al-12.8%Si	12.5	<0.05	0.05	< 0.05	<0.05

In the first set of experiments, 350 grams of commercially Pure Aluminum at 665°C (*i.e.*, 5°C superheat) was poured into a crucible that contained 50 grams of Al-32.3%Cu at 550°C (*i.e.*, at 5°C superheat) and allowed to mix naturally while cooling in ambient environment at room temperature. A type K thermocouple was inserted near the center of the crucible and connected to a data acquisition system<sup>7</sup> in order to record the thermal history of the liquid as it cooled. In similar experiments, the resultant alloy was quenched in water when its temperature reached 646°C, 641°C, and 635°C in order to track the evolution of microstructure as the alloy cooled. After every experiment, the composition of the resultant solid ingot was measured using spark emission spectroscopy and the ingot was sectioned into two halves. One half was used to produce specimens for microstructure characterization, while the second half was re-melted at 700°C (*i.e.*, at 50°C superheat), conventionally cast in a second crucible, and allowed to cool in room temperature air, then sectioned to produce specimens for microstructure characterization.

In the second set of experiments, 200 grams of commercially Pure Aluminum at 665°C (*i.e.*, at 5°C superheat) was poured into a crucible that contained 300 grams of Al-12.8%Si at 580°C (*i.e.*, at 2-5°C superheat) and allowed to mix naturally while cooling in room temperature air. A type K thermocouple was inserted near the center of the crucible and connected to a data acquisition system in order to record the thermal history of the liquid as it cooled. Upon solidification, the composition of the resultant ingot was measured using spark emission spectroscopy and the ingot was sectioned into two halves. One half was used to produce specimens for microstructure characterization, while the second half was re-melted at 700°C (*i.e.*, at ~50°C superheat), conventionally cast in a second crucible, and allowed to cool in room temperature air, then sectioned to produce specimens for microstructure characterization.

In addition, the following procedures were performed in order to demonstrate the applicability of the CDS method to casting alloys from the 2xxx, 4xxx, 5xxx, and 7xxx systems.

<sup>7</sup> DasyLab Version 5.6

**CASTING OF 2014 ALLOY USING CDS**

In order to demonstrate the applicability of the CDS method to casting wrought alloys that belong to the 2xxx system, the CDS method was used to cast 2014 alloy having the following nominal composition,

Cu (wt.%)	Minor elements <sup>8</sup>	Al
4.4	2.0	Remainder

**Table IV:** Chemical Analyses, Weight Fraction, and Temperature of the Precursor Alloys Used in Casting 2014 Alloy *via* CDS.

Chemical analysis:	Precursor Alloy #1	Precursor Alloy #2
Cu (wt.%)	33	-
Al (wt.%)	67	~ 98
Liquidus temperature (°C)	548	660
Weight fraction	~ 0.14	~ 0.86
Temperature (°C)	550	665
Liquidus temperature of 2014 alloy (°C)	648	
Maximum temperature of resultant alloy (°C)	646	

Precursor alloy #1 and precursor alloy #2 were poured in a crucible and allowed to mix naturally while they air-cooled – see Table IV.

The measured chemistry of the resultant alloy was as follows:

Cu (wt.%)	Minor elements <sup>9</sup>	Al
4.57	1.5	Balance

The globular microstructure is shown in Figure 9.

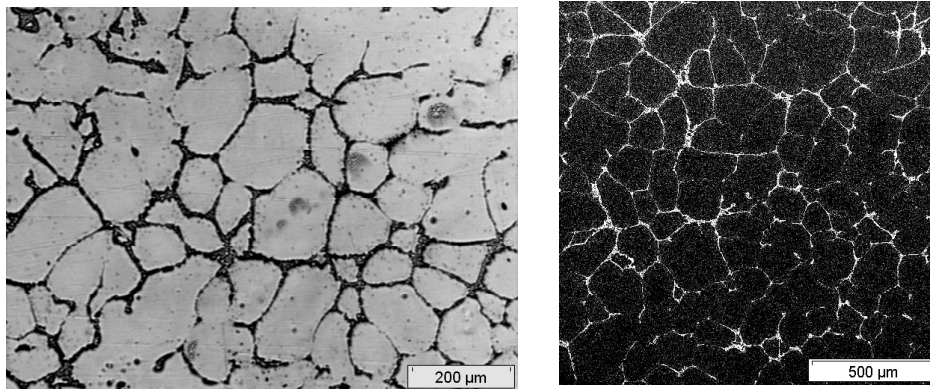


**Figure 9:** Micrographs of a 2024 Al-Cu alloy cast by mixing Pure Al and Al-33%Cu; (a) optical image of the final solidified structure, (b) back scattered SEM image of the final solidified structure.

<sup>8</sup> Predominantly Si, Mg, and Mn.

<sup>9</sup> Predominantly Si, Mg, and Mn from commercially Pure Aluminum.

**CASTING OF 4145 ALLOY USING CDS**

In order to demonstrate the applicability of the CDS method to casting wrought alloys that belong to the 4xxx system, the CDS method was used to cast 4145 alloy having the following nominal composition:

Si (wt.%)	Cu (%)	Al
10	4	Remainder

Table V shows the chemical analyses, weight fraction, and temperature of the precursor alloys.

**Table V:** Precursor Alloys’ Chemical Analyses, Weight Fractions, and Temperatures for Casting of 4145 alloy

Chemical Analysis	Precursor Alloy #1	Precursor Alloy #2
Cu	~ 33 wt.%	-
Si	-	~ 12.7 wt.%
Al	67 wt.%	Balance
Liquidus temperature (°C)	548	578
Weight fraction	~ 0.14	~ 0.86
Temperature (°C)	550	585
Liquidus temperature of 4145 alloy (°C)		580
Maximum temp. of resultant alloy on mixing(°C)		578

The measured chemistry of the alloy produced *via* CDS was as follows; the resultant structure is shown in Figure 10:

Si (wt.%)	Cu (wt.%)	Al
10.37	4.7	Remainder

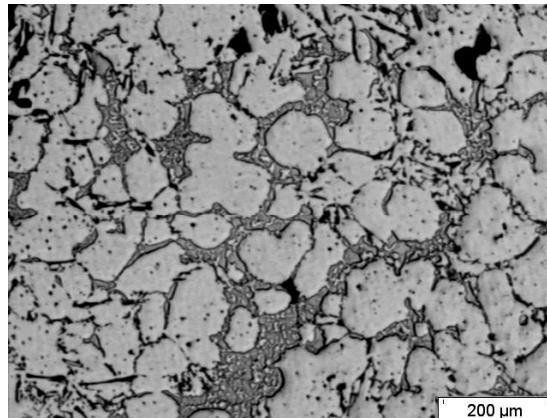


**Figure 10:** Microstructure obtained by mixing eutectic Al-Cu and eutectic Al-Si (Table V) to produce a 4145 Al-Si-Cu wrought alloy.

**CASTING OF 5056 ALLOY USING CDS**

In order to demonstrate the applicability of the CDS method to casting wrought alloys that belong to the 5xxx system, the CDS method was used to cast 5056 alloy, which has the following nominal composition:

Mg (wt.%)	Mn (wt.%)	Cr (wt.%)	Al
5.0	0.12	0.12	Balance

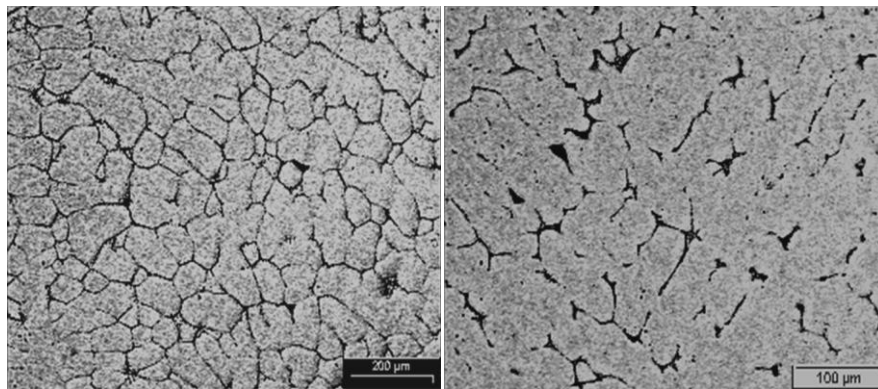
Table VI shows the chemical analyses, weight fraction, and temperature of the precursor alloys.

**Table VI:** Chemical Analyses, Weight Fraction, and Temperature of the Precursor Alloys Used in Casting 5056 Alloy *via* CDS.

Chemical analysis:	Precursor Alloy #1	Precursor Alloy #2
Mg (wt.%)	35	-
Al (wt.%)	65	~ 98
Liquidus temperature (°C)	451	660.7
Weight fraction	~ 0.14	~ 0.86
Temperature (°C)	445	665
Liquidus temperature of 5056 alloy (°C)	636.8	
Maximum temperature of resultant alloy (°C)	638	

The measured chemistry of the alloy produced *via* CDS was as follows; Figure 11 shows the structure of the resultant cast sample:

Mg (wt.%)	Mn (wt.%)	Cr (wt.%)	Al
4.8	0.15	0.02	Balance



(a)

(b)

**Figure 11:** (a) Microstructures obtained by mixing Al- 35% Mg and Pure Al (Table VI) and air cooled in crucible, (b) the same crucible reheated with a 15°C superheat and air cooled in crucible. Notice the presence of dendrites in regular casting.

**CASTING OF 7050 ALLOY USING CDS**

In order to demonstrate the applicability of the CDS method to casting wrought alloys that belong to the 7xxx system, the CDS method was used to cast 7050 alloy, which has the following nominal composition:

Zn (wt.%)	Mg (wt.%)	Cu (wt.%)	Al
6.2	2.2	2.3	Balance

Compared to 2014, and 5056, alloy 7050 is a complex one with several alloying elements, and thus there are many possibilities for precursor alloys that can yield 7050 alloy. Table VII shows one possible set of chemical analysis, weight fraction, and temperature of precursor alloys.

**Table VII:** Chemical Analysis, Weight Fraction, and Temperature of the Precursor Alloys Used in Casting 7050 Alloy via CDS.

Chemical Analysis	Precursor Alloy #1	Precursor Alloy #2
Cu (wt.%)	~ 24	-
Mg (wt.%)	-	~ 2.65
Zn (wt.%)	-	~ 7
Al	76	Balance
Liquidus temperature (°C)	589	634
Weight fraction	~ 0.10	~ 0.89
Temperature (°C)	592	640
Liquidus temperature of 7050 (°C)	630	
Maximum temperature of resultant alloy (°C)	628	

The measured chemistry of the resultant alloy was as follows:

Zn (wt.%)	Mg (wt.%)	Cu (wt.%)	Al
6.7	2.2	2.5	Balance

Specimens for microstructure characterization were mounted in Bakelite, polished using standard metallographic techniques. The specimens were observed using optical<sup>10</sup> and scanning electron microscopy (SEM)<sup>11</sup>. Figure 12 shows the resultant microstructure.

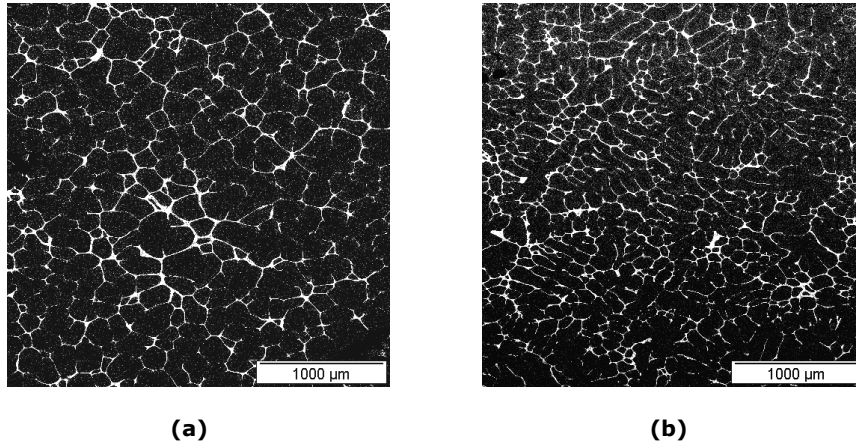


**Figure 12:** (a) Microstructures obtained by mixing Al-Mg-Zn and Al-Cu liquids (Table VII) via and air cooled in crucible, (b) the same crucible reheated with a 15°C superheat and air cooled in crucible. Notice the presence of dendrites in regular casting.

## **SUMMARY**

A novel and easy to employ method has recently been devised to allow casting of wrought alloys. The method, which is referred to as *Controlled Diffusion Solidification (CDS)* relies on mixing two precursor liquid alloys of precisely controlled chemistry and temperature in order to produce a predetermined alloy composition. The final temperature of the resultant alloy is aimed at a temperature that is a few degrees below the alloy's liquidus temperature, and therefore contains some fraction solid that allows fast, copious nucleation of the solid phase from the liquid phase. Consequently, the resultant alloy solidifies over a short temperature range and has a non-dendritic microstructure that minimizes its tendency towards hot tearing and makes it more amenable to casting operations, rather than the predominantly dendritic microstructure that is typical of conventionally cast alloys. In this publication, the process variables are explored and an operational window is established. In addition, the applicability of the CDS is demonstrated for commercial alloys.

---

<sup>10</sup> Nikon Epiphot

<sup>11</sup> Jeol 840

## **REFERENCES**

- [1] D. Apelian, G. Langford, "Rapid Cycle Casting of Steel", 1980.
- [2] Sumanth Shankar, Deepak Saha, Makhoulf M. Makhoulf, Diran Apelian, Die Casting Engineer, March 2004, 52.
- [3] D. Apelian, D. Saha, "Novel and Advanced Solidification Processes for the Manufacture of High Integrity Aluminum Cast Components", in the Proceedings of Second Intl. Light Metals Technology 2005, St. Wolfgang, Austria, published by LKR, pp 203-208 (2005).
- [4] J.Wannasin, R.A. Martinez, M.C. Flemings, Scripta Materialia 55 (2006) 115-118.
-

## 9.2 Appendix II: Diffusion Solidification

### **Introduction**

The first application of the CDS is on the development of a rapid-cycle casting process for steel [1]. Solidification takes place by carbon redistribution between iron-saturated high-carbon liquid iron and low carbon pre-existing solid iron in a refractory mold. Since no heat need be rejected to the surroundings during this process, the solidification time is shorter and the economic scaling law is less dependent on the size of the casting than in conventional casting processes. By utilizing CDS, many metals, including steel can be cast at still lower temperatures than rheocasting. Liquid iron, having high carbon content, is brought into contact with a low carbon solid iron isothermally, and the liquid solidifies by rejecting carbon to the surrounding solid iron. The mold is first filled with uniform-sized low carbon steel shot, then heated and subsequently infiltrated with liquid cast iron (2 to 4%) under moderate pressure.

Considering the simple binary diagram in Figure 1, conventional casting, Rheocasting and CDS paths are directly compared. In the Rheocasting process solidification occurs by manipulation of temperature on an iso-composition line, whereas the diffusion solidification process is carried out isothermally by manipulation of composition, *i.e.* by solute rejection from the liquid phase. In steels more specifically, carbon diffuses into the preheated spherical low carbon steel particles out of the high carbon liquid under essentially isothermal conditions. The average carbon content of the mixture is within the all-austenite portion of the iron carbon phase diagram so complete solidification can take place. The process has practical utility because the large solubility of carbon in face-centered cubic austenite permits the solid particles to absorb the excess carbon from a large amount of liquid.

## **Process Advantages**

In conventional casting solidification occurs via heat transport over a temperature range and the final structure is dendritic; in CDS castings solidification occurs via mass transport, the process is iso-thermal and the liquid-solid front is planar. Other advantages of the CDS process are that casting takes place at a lower temperature – reduced by 150-200 °C – and that the process can be carried out isothermally to cause 100% solidification and to obtain complete homogenization of the resulting casting, all without rejecting any heat to the mold.

Solidification time in conventional casting processes is dependent on casting dimensions and mold characteristics. In CDS castings, the solidification time is essentially independent of casting dimensions and is controlled by the infiltrable shot size. Furthermore, the mold characteristics do not control the solidification time in CDS castings. In brief solidification time and mold filling time are shorter when compared to conventional castings.

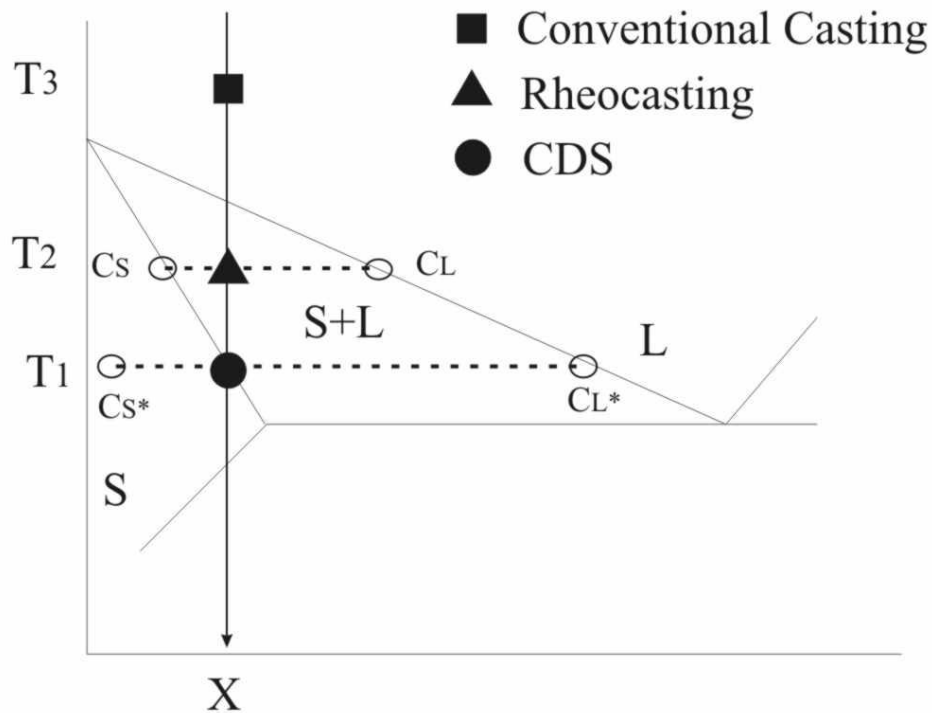


**Fig. 51: Paths of conventional casting, Rheocasting and of CDS. In Rheocasting alloy X is cooled to T2 and isothermally agitated. The solid – liquid mixture consists of liquid phase of composition CL and solid phase of composition CS. In CDS fs amount of solid particles of composition CS\* and at temperature T1 are infiltrated by fL amount of liquid of composition CL\* such that  $f_sCS^* + f_LCL^* = X$ .**

- In conventional castings,  $t_s$ , time for solidification is proportional to  $\ell^2$  where  $\ell$  is the dimensional term, length. (Chorinov’s Rule) [18]
- In CDS casting on the other hand,  $t_{c_{ds}}$  is proportional to  $\left( \frac{\ell^{6/5}}{p^{2/5}} \right)$ ; where  $p$  is the infiltration pressure available [19].

The weaker dependence of solidification time on workpiece dimensions can be advantageous when considering the CDS process for automation. Cycle times comparable to die casting ought to be achievable with the CDS process. There is much less of a problem of thermal shock to the “die” (mold), and the microstructure

of the resultant casting is homogeneous with respect to carbon because of its rapid diffusion over these short distances. In CDS the preheated solid particles occupy approximately 5/8 of the final volume of the casting prior to infiltration of the liquid phase; therefore, solidification shrinkage and heat of solidification to be accommodated are at least proportionately reduced. Although in conventional castings a riser is needed and the solidification shrinkage is concentrated in the last liquid to freeze, no riser is needed in diffusionally solidified castings and the solidification shrinkage is isolated, uniformly distributed and smaller in amount if the workpiece will be subsequently worked out or hot isostatically pressed [20].

### **Metallurgy of CDS**

Diffusion solidification as a casting technique produces unique properties and microstructures without resort to extreme pressures, and it may therefore compete favorably with hot isostatic pressing as a way of consolidating atomized metal powder (shot). The atomized shot has the benefits of rapid solidification (because of the small size of individual particles) and of the controlled melting and solidification environments and the infiltrating liquid has the benefits of vacuum melting and of filtration by the particle valve. The distribution and magnitude of shrinkage cavitation are controlled by the particle size distribution of the shot and by the content of inclusions (such as aluminum oxide or silicates in steel). Steel castings have been made by CDS with more than 99% of theoretical density, for example [1].

Since solidification proceeds simultaneously throughout the casting during CDS, hot tearing and macrosegregation of impurities and alloying elements are decreased. The microstructure of diffusion-solidified steels is more like that of wrought steel than of cast steels - there is no columnar zone. The grain size and grain orientation of the diffusionally solidified casting is instead controlled by the grains in the initially solid

portion of the charge. It is possible to produce completely homogeneous microstructures free of microsegregation by CDS since the particle size is chosen to minimize the freezing time by minimizing the diffusion distance consistent with successful forced infiltration under a reasonable external pressure. Most alloy systems to which SD can be applied are nearly completely homogenized soon after the completion of freezing. It has been discovered that it may even be possible to achieve relatively good homogenization with respect to third alloying elements (i.e. those not taking part in the basic SD mechanism, such as silicon and manganese in plain Fe-C-Mn-Si steel). Manganese, for example, can have positive microsegregation (more Mn in the last metal to freeze), and negative or even neutral microsegregation depending on whether the shot has low, high, or the same manganese concentration as the liquid. Apparently, the sharp carbon differential [1] at the solid-liquid interface and elastic interaction due to the difference in size of Fe and X atoms act to defeat the mechanism usually leading to microsegregation (slow diffusion in the solid, rapid mixing in the liquid). This is not necessarily a general phenomenon in CDS, it is only a possibility. Presumably, the liquid-state and solid-state concentrations of the third alloying elements can be made to be nearly identical at the solid-liquid interface, thus defeating the usual ternary distribution coefficient given by the ratio of the solid and liquid solubilities of that element in the alloy system. Bear in mind that CDS occurs isothermally and is a transient phenomenon between initially out-of-equilibrium components: the original solid and the infiltrant liquid.

There are other advantages for CDS castings. Pieces with small surface to volume ratios or those with drastic changes in cross-section can easily be produced because the casting solidifies without rejecting heat to the surroundings. Also, the casting will be free of laps and cold shuts because the mold is heated prior to infiltration.

Excellent ductility of CDS steel castings can be obtained if they are adequately infiltrated and if metallurgical bonding is achieved at the original solid-liquid interface. Surface and subsurface scales such as silicates are especially harmful and lead to dotted-line fractures along the particles outlining the original shot surface. All that is necessary to correct this fault is to leave sufficient carbon in the original shot to reduce the silicates during heating to the process temperature [1]. It is even possible to reduce the shrinkage cavitation below the theoretical amount if the total number of remaining inclusions is substantially less than the number of intershot interstices [1].

### 9.3 Appendix III: Numerical Simulation Algorithm

#### NUMERICAL CODE

The MATLAB code used to calculate the evolution of Temperature is presented. Similarly the diffusion of solute was simulated.

```
function T = heat_cn(h,r)

%%%%%%%%%%%%%%%%%%%%%%%%%%%%%%%%%%%%%%%%%%%%%%%%%%%%%%%%%%%%%%%%%%%%%%%%

% heat_cn.m

% this program calculates the Heat equation by the Crank Nicholson method

% for 0 <= x <= 1

%    0 <= t <= 0.6

%%%%%%%%%%%%%%%%%%%%%%%%%%%%%%%%%%%%%%%%%%%%%%%%%%%%%%%%%%%%%%%%%%%%%%%%

% Setup attributes

T1actual = 545;    %low Temperature (K)

T2actual = 660;    %high Temperature (K)

T1=0;            %normalized T

T2 = T2actual - T1actual; %normalized T

eps = 10;        %Strain rate

S0 = 1;          %Initial Striation thickness

e = 2.71828183; %e
```

```

a = 28;           %Thermal diffusivity

h = 0.05;        %step size in x dimension

dt = 0.001;      %step size in the t dimension

r=a*dt/(h^2);

T0 = 2;          % time interval over which we calculate T

TN = ceil(T0/dt); % number of steps in the t-interval

X0 = 21;         % the x interval over which we calculate T

XN = ceil(X0/h); % the number of steps in the x-interval

T= zeros(XN+1, TN+1); %setup an array of zeros

%%%%%%%%%%%%%%%%%%%%%%%%%%%%%%%%%%%%%%%%%%%%%%%%%%%%%%%%%%%%%%%%%%%%%%%%

% Initial Conditions

%%%%%%%%%%%%%%%%%%%%%%%%%%%%%%%%%%%%%%%%%%%%%%%%%%%%%%%%%%%%%%%%%%%%%%%%

for x=0:(XN/2-10)

    T(x+1 ,1)=T1;

for x=(XN/2-10):(XN/2+10)

    T(x+1,1)=T2;

for x=(XN/2+10):XN

    T(x+1,1)=T1;

end;

```

```

end;

end;

% All other values in the matrix T are 0 so the rest of the Boundary
% conditions are all set.

%%%%%%%%%%%%%%%%%%%%%%%%%%%%%%%%%%%%%%%%%%%%%%%%%%%%%%%%%%%%%%%%%%%%%%%%

% CRANK NICHOLSON

%%%%%%%%%%%%%%%%%%%%%%%%%%%%%%%%%%%%%%%%%%%%%%%%%%%%%%%%%%%%%%%%%%%%%%%%

% 1 - define repeatedly calculated constants

cnA = 2 + (2 * r);

cnB = 2 - (2 * r);

% 2 - Build a XN-1 x XN-1 matrix containing the coefficients

Coeffs = zeros(XN-1,XN-1);

% 3 - Build first and last rows

Coeffs(1,1) = cnA;    Coeffs(2,1) = -r;

Coeffs(XN-2,XN-1) = -r; Coeffs(XN-1,XN-1) = cnA;

% populate the rest automatically:

for row = 2 : XN - 2

    Coeffs(row - 1 , row) = -r;

    Coeffs(row,    row) = cnA;

```

```

        Coeffs(row + 1, row) = -r;

end;

% find the inverse of the coefficients:

invCoeffs = inv(Coeffs);

% set up a matrix of values for the right-hand-side of the C/N eqn..

RHS = zeros(1,XN-1);

for t = 1 : TN

    for x = 2 : XN

        % calculate the RHS first:

        RHS(x - 1) = cnB * T(x,t) + r * (T(x+1,t) + T(x-1,t));

    end;

% the C/N method yields us a system of equations of the form:

%         Coeffs * Y = RHS

%

% where:

%         o Y is a vector of unknowns

%         o Coeffs is a matrix of the Coefficients relevant to X

%         o RHS (Right Hand Side of the equation)is a vector

%         containing calculated constant values.

```

```

%

% We can solve this system of equation by first finding the

% inverse of the matrix of Coefficients (above), and then

% multiplying the inverse across both sides of the equation

% gives us our solutions:

% |

% |i.e.    Coeffs * Y = RHS

% |       => Coeffs^-1 * Coeffs * Y = Coeffs^-1 * RHS

% |       (Coeffs^-1 is the inverse of Coeffs)

% |       => I * Y = Coeffs^-1 * RHS      (I is the Identity Matrix)

% |       => Y = Coeffs^-1 * RHS

% |

%

Y = invCoeffs * RHS';

% assign the vector of solutions to the relevant time-row:

T(2:YN,t+1) = Y;

```

End